Dpto. Sistemas físicos, químicos y naturales

Dpto. Nanotecnología de superficies

Development of photonic gas sensors based on porphyrin/metal oxide nanostructured thin films obtained by glancing angle deposition

Desarrollo de sensores fotónicos de gases basados en láminas delgadas nanoestructuradas de porfirina/óxido metálico obtenidas mediante deposición en ángulo rasante

Tesis doctoral

Pedro Castillero Durán

Noviembre 2014

Development of photonic gas sensors based on porphyrin/metal oxide nanostructured thin films obtained by glancing angle deposition

A dissertation submitted to obtain the degree of

Doctor of Philosophy

Pablo de Olavide University

Directed by

Dr. José María Pedrosa Poyato

Associate professor

University of Pablo de Olavide (UPO)

Physical, Chemical and Natural Systems

Dr. Ángel Barranco Quero

Tenured scientist

National Research Council (CSIC)

Materials Science Institute of Seville

CSIC-US

Fdo.: Ldo. **Pedro Castillero Durán**

Degree in Physics

Seville, November 2015

This Doctoral Thesis has been carried out thanks to the collaboration between Nanotechnologies and Surfaces group of the Materials Science Institute of Seville (CSIC-University of Seville) and the department of Physical, Chemical and Natural Systems of the Pablo de Olavide University under the direction of the doctors D. José María Pedrosa Poyato and D. Angel Barranco Quero.

During the period of this thesis it has been developed the next articles:

- "Anchoring effect on (tetra)carboxyphenyl porphyrin/TiO_2 composite films for VOC optical detection", Roales J., Pedrosa J.M., Cano M., Guillen M., Lopes-Costa T., Castillero P., Barranco A. and Gonzalez-Elipe A.R.,RSC ADVANCES, vol 4, (2014), p.1974-1981
- "*Differences in n-type doping efficiency between Al- and Ga-ZnO films*", Gabas, M., Landa-Canovas, A., Costa-Kramer, J.L., Agullo-Rueda, F., Gonzalez-Elipe, A.R., Diaz-Carrasco, P., Hernandez-Moro, J., Lorite, I., Herrero, P., Castillero, P., and Ramos-Barrado, J.R., Journal of Applied Physics, vol 113, (2013), 163709
- "*Selective detection of volatile organic compounds by spectral imaging of porphyrin derivatives bound to TiO_2 porous film* ", Roales J., Pedrosa J.M., Castillero P., Cano M. and Richardson T.H., Applied Material and Interfaces, vol 4, no 10, (2012), p. 5147-54.
- "*Improving the training and data processing of an electronic olfactory system for the classification of virgin olive oil into quality categories*", Cano M., Castillero P., Roales J., Mendoza P., Calero A.M., Jimenez-Ot C. and Pedrosa J.M., vol 160, no 1, (2011), p. 916-922.
- "*Optimization of mixed Langmuir–Blodgett films of a water insoluble porphyrin in a calixarene matrix for optical gas sensing*", Roales J., Pedrosa J.M., Castillero P., Cano M. and Richardson T.H., Thin Solid Films, vol 519, (2011), p. 2025-2030.
- "*A transparent TMPyP/TiO_2 composite thin film as an HCl sensitive optochemical gas sensor*", Cano M., Castillero P., Roales J., Pedrosa J.M., Brittle S., Richardson T.H., Gonzalez-Elipe A.R. and Barranco A., Sensor and Actuator B: Chemical, vol 150, (2010), p. 764-769.

- "*Active and optically transparent tetracationic porphyrin_TiO_2 composite thin films*", Castillero P., Sanchez-Valencia J.R., Cano M., Pedrosa J.M., Roales J., Barranco A. and Gonzalez-Elipe A.R., Applied Material and Interfaces, vol 2, no3, (2009), p. 712-721.

And the next patent:

- *"Procedimiento de fabricación de un sensor de detección de hidrógeno y sensor así fabricado"* Nº solicitud: 201300896

A Pedro y Carmen

A mi familia

Contents

Resumen de tesis

Development of photonic gas sensors based on porphyrin/metal oxide nanostructured thin films obtained by glancing angle deposition

Desarrollo de sensores fotónicos de gases basados en láminas delgadas nanoestructuradas de porfirina/óxido metálico obtenidas mediante deposición en ángulo rasante

1. INTRODUCCIÓN

Hoy en día existe un gran interés tecnológico y científico por el estudio y desarrollo de nuevos materiales nanoestructurados en los que podemos predecir y controlar sus propiedades para su uso en una aplicación tecnológica. Un ejemplo muy interesante de materiales compuestos nanoestructurados o "nanocomposites" son aquellos fabricados mediante una estrategia denominada "host-guest" (huésped-anfitrión) compuestos de matrices de óxidos en los cuales se incorpora el material activo para obtener la funcionalidad requerida, ya sean nanopartículas metálicas, colorantes orgánicos, puntos cuánticos, etc, a escala nanométrica. Esto materiales presentan grandes posibilidades de aplicación en campos tales como microelectrónica, sensórica, ingeniería química y bioquímica, etc.

Materiales híbridos son aquellos que se componen de dos sustancias, normalmente una orgánica y otra inorgánica. Estos materiales híbridos son muy versátiles en cuanto a su composición, procesado y propiedades ópticas y mecánicas.

De las interacciones superficiales entre las matrices de óxido y el material incorporado se derivan características singulares que dependen en gran medida de la presencia de defectos, gradientes composicionales, rugosidad y microestructura, que juegan un papel vital en la funcionalidad de estos nuevos materiales.

El hecho de poder fabricar materiales nanoestructurados altamente porosos supone maximizar el área superficial accesible, lo que conduce a la posibilidad de poder incorporar materiales activos en el interior de los poros. Esta propiedad ha sido muy útil en catálisis, absorción, purificación y almacenamiento de gases, en el desarrollo de materiales aislantes en la industria de los semiconductores y en aplicaciones ópticas.

Dentro de la gran cantidad de las aplicaciones que dan lugar estos materiales híbridos nanoestructurados, el presente trabajo se centra en el desarrollo de sensores de gases fotónicos basados en una matriz porosa de óxido metálico, donde los poros están abiertos, que actúa de material anfitrión o matriz y un material huésped activo que se incorpora a los poros de la matriz.

2. OBJETIVOS

El objetivo general de esta tesis consiste en fabricar películas delgadas con buena calidad óptica capaces de detectar la presencia de gases. Estas películas son sistemas soportados que pueden implementarse en dispositivos ópticos y fotónicos.

Las películas delgadas estudiadas están compuestas de dióxido de titánio (TiO_2), óxido de wolframio(VI) (WO_3) u óxido mixto de wolframio y Silicio (WO_3/SiO_2) nanoestructurados a las que se les introduce un material activo que, según el gas de reconocimiento, es un colorante orgánico o una partícula metálica.

Mediante el control en los parámetros más importantes del crecimiento de las matrices de óxidos hemos obtenido películas con buena calidad óptica. Esto ha permitido controlar la porosidad y espesor de las películas, lo que le confiere dos características muy importantes para objetivo perseguido. La primera es la posibilidad de incorporar la cantidad de material activo deseada, con lo que optimizamos la respuesta sensora. La segunda es que el material activo incorporado está, por un lado, en contacto íntimo con la atmósfera que le rodea y el por otro lado con la matriz, por lo que la respuesta será rápida tanto si la detección del gas se produce mediante el material incorporado como si sirve de catalizador para la matriz de óxido.

Debido a estas características, se propone en la memoria el desarrollo de materiales compuestos nanoestructurados como sensor de gases de alta velocidad de respuesta y bajo límite de detección.

Los objetivos principales del trabajo son:

- Síntesis y caracterización de las películas delgadas columnares preparadas por Physical Vapour Deposition (PVD) o deposición física en fase vapor y Magnetron Sputtering o pulverización catódica en condiciones de ángulo rasante.
- Control de la incorporación del material activo y optimización de sus características funcionales.
- Estudio de la respuesta sensora a distintos gases (reproducibilidad, repetitividad, reversibilidad, tiempo de respuesta…).
- Evolución y estabilidad de las películas delgadas nanocompuestos.

3. METODOLOGÍA

3.1 Fabricación de la matriz de óxido

Las películas delgadas matrices de óxido se prepararán mediante técnicas de Evaporación Electrónica a Ángulos Rasantes (PVD) o Magnetron Sputtering en la configuración Ángulo Rasante. Estas dos técnicas de fabricación de películas micrométricas de alto vacío permiten la obtención de capas delgadas nanoestructuradas de espesor controlado.

La deposición a ángulos rasantes o *glancing angle deposition* (GLAD) es un tipo de deposición que permite fabricar películas delgadas con una morfología nanocolumnar. Mediante esta técnica se han llegado a producir nanoestructuras columnares de gran complejidad, como nanofibras periódicas, perforadas, o de porosidad gradual para el uso en aplicaciones desde sensores, filtros ópticos, microfluídica o catálisis.

Estas películas poseen una propiedad muy importante para la aplicación defendida en esta memoria: son capas extremadamente porosas. Esta propiedad hace que tengan aplicaciones en el campo de los supercondensadores, celdas solares, sensores de gases de alta velocidad, recubrimientos de barrera térmica, etc.

El crecimiento columnar direccional es el resultado de un mecanismo de sombreado (shadowing) que ocurre en la superficie del sustrato, tal y como se muestra en la Figura 1. Durante el estadío inicial del crecimiento, se condensan átomos o agregados en el sustrato y forman islas separadas individualmente o “núcleos”. Cuando el sustrato está inclinado se produce un aporte a ángulos oblicuos, de manera que la topografía del material adsorbido proyecta un cono de sombra sobre el sustrato, impidiendo la deposición allí, por lo que se evita la coalescencia de los núcleos y la formación de una capa continua. Es más, como el núcleo inicial captura los átomos incidentes que deberían depositarse en las zonas con sombra, se forman columnas que crecen en la dirección de aporte del vapor.

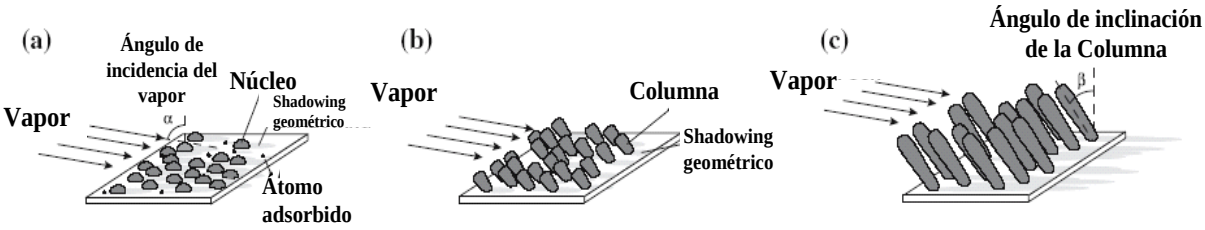

Figura 1.- Mecanismo de crecimiento columnar. En las primeras etapas de crecimiento (a), se condensan átomos y forman núcleos que proyectan sombra en distintas regiones, impidiendo el crecimiento en ellas (b). La película resultante se compone de columnas crecidas a partir de los núcleos, inclinadas en la dirección de aporte de material.

3.2 Incorporación del material activo a las películas

Una vez preparadas las películas según se ha indicado anteriormente se procede a la incorporación de un determinado material activo. Los materiales activos que se estudiaran en esta tesis son: moléculas orgánicas de la familia de las porfirinas y [redacted]

3.2.1 Colorante

Para la realización de esta tesis se ha utilizado porfirinas como moléculas activas (figura 2). A las porfirinas se les llama las moléculas de la vida ya que tiene un papel fundamental en dos procesos fundamentales: la fotosíntesis y la respiración aeróbica. Es por esto que las porfirinas son uno de los colorantes más estudiados.

Las porfirinas son moléculas orgánicas con una estructura hidrocarbonada en forma de anillo tetrapirrólico y en cuyo centro se puede acoplar un metal. Esta molécula cuenta con un sistema de electrones π fuertemente conjugado, lo que proporciona una fuerte absorción en la zona del espectro. De la interacción entre esta nube electrónica y los distintos gases se pueden producir importantes cambios espectrales, lo que supone la base para la detección de gases.

Las porfirinas se han introducido en las películas delgadas columnares por vía líquida. Se han utilizado porfirinas catiónicas capaces de anclarse en la matriz de óxido mediante enlaces electrostáticos a grupos cargados de la superficie del óxido.

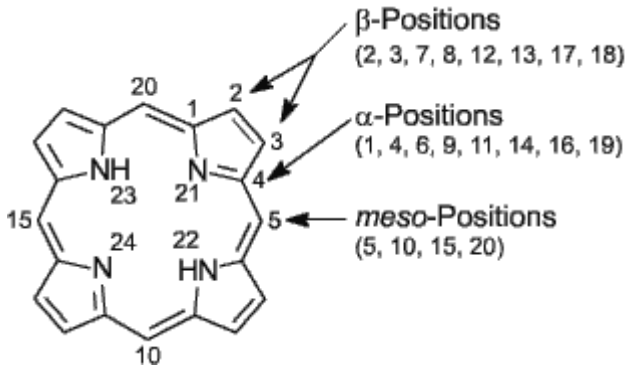

Figura 2.- Estructura de la molécula de la porfirina. Existen numerosas moléculas derivadas de la porfirina según sus sustituyentes y la posición de dichos sustituyentes.

Las porfirinas presentan una fuerte coloración con una intensa banda de absorción, denominada banda Soret, en la región con longitudes de onda entre 380-500 nm seguidas de otras bandas de absorción, denominadas bandas Q, más débiles en intensidad entre 500-750 nm. Este espectro característico hace que podamos medir mediante espectroscopia UV-Vis su estado inicial y su estado después de exponerse a un gas. Por ejemplo, los dos átomos libres del nitrógeno de la porfirina pueden ser protonados fácilmente con ácidos formando un di-ácido mientras que las bases fuertes pueden quitar los dos protones a los átomos internos del nitrógeno de una porfirina para formar un di-anión.

Por otra parte, la porfirina puede ser una molécula fluorescente, por lo que mediante espectroscopia de fluorescencia es posible estudiar cómo se comporta la molécula frente a la exposición a vapores. Las porfirinas presentan dos bandas de emisión de diferente intensidad siendo la primera más intensa que la segunda. Se encuentran situadas en 600-750 nm. Por ejemplo, la porfirina TMPyP en estado natural es fluorescente mientras que en su estado protonado pierde la fluorescencia detectándose con ello la presencia de una ambiente ácido.

Mediante la combinación de la absorción UV-Vis y fluorescencia podemos estudiar la respuesta sensora de las porfirina a distintos gases.

[redacted]

[redacted]

3.3 Detección de gases

Una vez fabricada la película constituida por una matriz de óxido y un colorante orgánico o nanopartículas en su interior se ha estudiado su respuesta a distintos gases.

La detección de gases y vapores se ha realizado en una cámara donde se puede medir simultáneamente, en dos muestras distintas, los espectros UV-visible y fluorescencia. En la figura 3 podemos ver una foto de la cámara usada para los distintos experimentos de reconocimiento de gases. La cámara está fabricada en el taller mecánico del Instituto de Ciencias Materiales de Sevilla diseñada para contener el menor volumen de gas posible de manera que las muestras respondan rápidamente al gas al que se enfrentan.

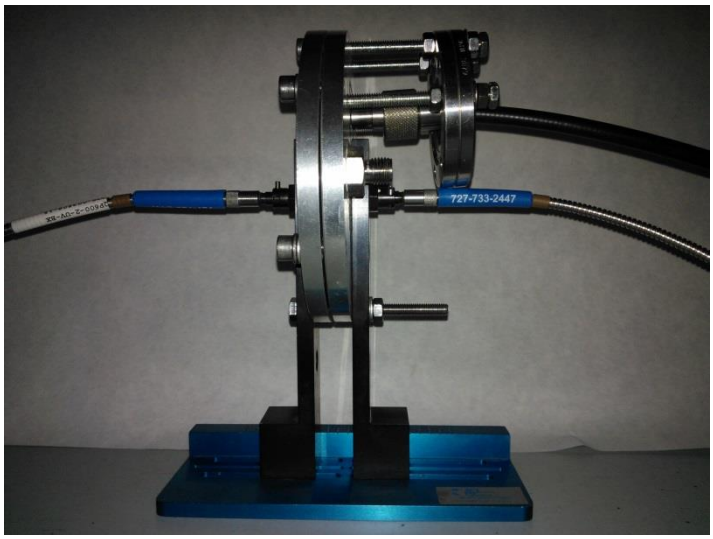

Figura 3.- Cámara sensora de gases donde podemos ver la colocación de las fibras ópticas para medir simultáneamente espectroscopias UV-Vis y de fluorescencia.

Se han estudiado distintos vapores según el tipo de muestra. Se ha enfrentado moléculas de porfirina a vapores ácidos y básicos estudiando la protonación y desprotonación de la porfirina.

[redacted]

Se han estudiado las características propias de un sensor como son la reproducibilidad, sensibilidad, estabilidad, límites de detección…

4. ESQUEMA DE TESIS

Esta memoria corresponde al diseño y caracterización de películas delgadas con la funcionalidad de detectar gases ópticamente. Para la obtención de éstas películas se ha utilizado el modelo de preparación anfitrión-huésped (host-guest), basado en la incorporación de un determinado material activo (huésped) en una película delgada porosa (anfitrión) como se ha indicado antes.

Los capítulos del cuerpo principal de la tesis vienen determinados por la incorporación del colorante en la matriz y por el tipo de película utilizada usada para detectar el gas:

- Capítulo 3: Active and optically transparent TMPyP/TiO_2 composite thin films

  Películas delgadas ópticamente activa y transparentes del compuesto TMPyP/TiO_2.

En este capítulo se hace una caracterización de las películas delgadas de TiO_2 y se estudia el proceso de incorporación de una porfirina tetracatiónica a la matriz de TiO_2.

Las películas anfitrionas de TiO_2 están fabricadas mediante la técnica de alto vacío de deposición física en fase vapor donde los sustratos están colocados formado un determinado ángulo respecto a la dirección del aporte de material. Debido a esta configuración geométrica la microestructura crecida está compuesta de nanocolumnas inclinadas. La microestructura de TiO_2 crecida tiene buena calidad óptica debido a que presentado bajo índice de refracción y alta transparencia, además son películas altamente porosas, propiedad muy importante para la aplicación que se persigue.

La porfirina tetracatiónica se ha anclado a la película de TiO_2 mediante inmersión simple de la capa nanoporosa en una disolución acuosa controlada de porfirina. Se ha estudiado los distintos parámetros que condicionan la infiltración de moléculas como concentración, tiempo de infiltración o pH y se ha verificado que se anclan mediante la interacción de fuerzas electrostáticas presentando una fuerte dependencia con el pH.

En este capítulo no solo se ha desarrollado un nuevo sistema de películas nanocompuestas ópticamente activas sino que se ha demostrado su potencialidad para desarrollar sensores de gases. Dicho sistema parece óptimo para poner implementarse en un sistema fotónico.

- Capítulo 4: A transparent TMPyP/TiO_2 composite thin film as an HCl sensitive optochemical gas sensor

  Película delgada transparente compuesta de composición TMPyP/TiO_2 usada como un sensor de gas sensible optoquímico de HCl.

En el capítulo 4 se ha probado el nuevo sistema desarrollado en el capítulo anterior como sensor de ácido clorhídrico (HCl).

Para ello se ha estudiado el comportamiento de la porfirina en disolución acuosa frente a la incorporación de cantidades controladas de HCl y se ha verificado su cambio espectral tanto en absorción UV-Vis como en fluorescencia. Posteriormente se ha infiltrado la porfirina tetracatiónica en una matriz de TiO_2 según el procedimiento descrito en el capítulo 3 y la película de TMPyP/TiO_2 ha sido expuesta a vapores de HCl y se ha verificado que el comportamiento espectroscópico de la porfirina en la matriz de TMPyP es similar al comportamiento de la disolución.

Por otro lado, se han infiltrado dos concdentraciones distintas de moléculas y se han comparado sus respuestas sensoras concluyendo que el compuesto con menor concentración de moléculas de porfirina presenta un límite de detección (0,1 ppm) menor que la más concentrada.

Este capítulo defiende el desarrollo de un nuevo sistema de películas compuestas soportadas como sensor de HCl. El sensor presenta una rápida respuesta y una gran estabilidad con poca concentración de moléculas sensoras comparadas con las reportadas previamente en otros sistemas por otros investigadores.

- Capítulo 5: Gas sensing ammonia and amines based on protonated porphyrin/TiO2 composite thin films.

  Sensor de amoniaco y aminas en estado gaseoso basado en películas delgadas compuestas de porfirina protonada/TiO_2.

En este capítulo de ha utilizado el sistema expuesto en el capítulo 4 y se ha usado para la detección de aminas en estado gaseoso. Es un sensor que para la detección de las aminas volátiles las moléculas de porfirina de la película compuesta deben estar en estado protonado.

Se han estudiado dos moleculas de porfirinas similares donde la única diferencia es que MMPyP es una porfirina con una sola carga positiva mientras que TMPyP presenta 4 cargas positivas. Ambas porfirinas han sido ancladas electrostáticamente a una matriz de TiO_2 (MMPyP/TiO_2 y TMPyP/TiO_2). Tanto en disolución como soportada en la matriz porosa se ha protonado indicándose sus cambios espectrales en la región UV-Vis, fluorescencia y tiempo de vida, mediante la adición de HCl en disolución o la exposición a vapores de HCl en el caso de los compuestos soportados de porfirina/TiO_2. El estado protonado de las porfirinas de los compuestos soportados es el punto de partida del sensor.

El sensor se ha expuesto a vapores de amoniaco y aminas para estudiar la respuesta sensora mediante espectroscopia de fluorescencia. Con la exposición de los compuestos sensores a vapores de amoniaco se ha estudiado el tiempo de respuesta y el límite de detección (0.05 ppm para MMPyP/TiO_2 y 0.16 ppm para TMPyP/TiO_2), concluyéndose que el compuesto MMPyP/TiO_2 es más rápido en responder y presenta un menor límite de detección que el compuesto TMPyP/TiO_2. Este comportamiento se atribuye a que la molécula MMPyP tiene un solo punto de enlace entre la porfirina y la matriz de TiO_2. Así, esta molécula está más expuesta a la atmósfera que le rodea presentando una mayor accesibilidad de los analítos a la porfirina, y por consiguiente, provocando cambios espectrales más importantes.

Se ha verificado que la intensidad de la emisión de fluorescencia disminuye a lo largo de los ciclos de protonación con HCl y recuperación con amoniaco o aminas. Esta pérdida de intensidad se ha estudiado mediante espectroscopia infrarroja observándose que el cloruro amónico queda recluido en el interior del compuesto provocando la disminución de la intensidad de fluorescencia.

Como resumen del capítulo se puede indicar que se ha desarrollado un nuevo sistema de detección de amoniaco y aminas basado en cambios espectrales de

fluorescencia. El sensor presenta una rápida respuesta frente a los analitos y tiene un bajo límite de detección.

- Capítulo 6: Optical hydrogen gas sensor hand in nanocomposites films deposited by GLAD

  Sensor óptico de hidrógeno soportado en películas nanocompuestas depositadas mediante GLAD

Este capítulo se ha desarrollado en el marco de un proyecto industrial y está sujeto a compromiso de confidencialidad.

Objectives of the Thesis

The present work deals with the development and study of novel nanostructured functional thin films. *The main objective of this thesis is to develop active optical sensing elements with the ability of detecting certain vapors by measuring the change of thin films optical properties. Thus, these thin films will be the optically active layers of photonic gas/vapor sensing devices.*

1.- Development of nanoporous optical films as host for the fabrication of photonic sensing films by glancing angle deposition.

The nanostructured films have been prepared in two differentiated steps based following a host – guest synthetic strategy. The critical parameters in each step have been identified and optimized. The first step consists in the fabrication of a thin film that will act as the **host material**. The main characteristics of these host films are:

- High optical quality
    - Controlled and reproducible refractive index (n).
    - Extremely low extinction coefficients (k) reaching values lower than 10^{-5} in the visible region.
- Well defined and reproducible nanoporous nanostructure accessible to gas/vapors and to molecules in solution.

The host materials in the form of thin films have been prepared by Physical Vapour Deposition (PVD) using two different thin film deposition techniques:

- Nanostructured Titanium dioxide (TiO_2) films have been prepared by e-beam evaporation in glancing angle (GLAD).
- Nanostructured Tungsten oxide films (WO_3) and mixed tungsten-silicon oxide films (WO_3/SiO_2) have been prepared by Direct Current (DC) Magnetron Sputtering in glancing angle conditions.

The films prepared by the two techniques are formed by vertical or tilted porous nanocolums. Both techniques allow the control of critical parameters determining the

thin films composition, nanostructure (nanocolumnar structure, tilted angle, etc.) and optical properties in a wide range. Thus, for the fabrication process of a host material it is critical to control very important parameters like thickness, composition, density, nanostructure, porosity (pore distribution, percentage of porosity, percentage of open porosity etc.), thickness and chemical composition and, hence, its optical properties. Furthermore, these films present a very low light dispersion coefficient which it is a critical requirement for photonic applications.

In this thesis, the host materials are transparent nanostructured metal oxides with a dielectric or semiconductor behavior (TiO_2, WO_3, WO_3 / SiO_2). The thin films have been deposited on different kind of substrates like glass, fused silica and doped and intrinsic silicon (Si(100)) wafers. These substrates are chosen according to the requirements of the different thin film characterization techniques utilized.

The high porosity of the studied host materials has two important advantages: firstly, their high specific surface can incorporate a large number of molecules and, secondly, the high open porosity in the nanocolumns and the large spacing between columns permits the anchored active molecules to be in intimate contact with the atmosphere surrounding the film.

2.- Development of a methodology of infiltration of guest porphyrin molecules into nanoporous optical thin films.

Hybrid materials are composites consisting of two organic and inorganic constituents. In our case, the host is inorganic and the guest component is an organic functional molecule bond to the inner nanoporous surface of the host film. Thus, after the fabrication of the nanoporous host films, the second synthetic step is the incorporation of the active component. These guest components for the fabrication of optical sensor can be of different nature (i.e., organic molecules, metallic nanoparticles…) and depend on the gas/vapor to be detected and the specific optical response that is going to be measured. In this thesis, luminescent organic molecules of the family of porphyrins have been incorporated as active elements.

It is important to indicate the development of new versatile luminescent materials for their integration in photonic devices as active elements is objective of great technological interest. Our research group has previous experience in the

incorporation of luminescent organic molecules like rhodamine dyes [1] in nanoporous TiO_2 and SiO_2 thin films fabricated by e-beam evaporation in GLAD conditions. On the other hand, the characterization of such nanoporous films has been also the object of several recent doctoral thesis [1-3]. In this thesis we introduce the study of porphyrin dye molecules as guest elements and WO_3 and WO_3/SiO_2 nanocolumnar host films deposited by DC magnetron sputtering for the fabrication of different types of gas sensing films.

3. Optimization of the porphyrins/TiO_2 nanocomposites for optical vapor sensing.

Porphyrins molecules play important roles in the nature due to their special absorption, emission, charge transfer and complexing properties as a result of their characteristic ring structure of conjugated double bonds[4]. Furthermore, metal ions can be incorporate into the porphyrin to form metalloporphyrins that play key roles in several biochemical processes like in photosynthesis, oxygen transport in blood, etc.[5] In this thesis we use porphyrins as guest molecules incorporated in the host nanoporous films. The most important feature of the porphyrins dyes studied is that they experience a change in their optical absorption and emission properties depending on the state of aggregation, the geometrical configuration the chemical interaction with the oxide surface and the presence of certain gases in the atmosphere surrounding the composite film. The host film nanoporous structure and the porphyrins infiltration process control the optical properties of the porphyrin molecules in the solid state.

The porphyrins/TiO_2 films are exposed to different gases in order to study its optical properties under controlled atmosphere. These vapors are chloride acid, ammonium and several amines.

[redacted]

REFERENCES

1. Sánchez-Valencia, J.R., *Tesis doctoral: Fabricación de Láminas Delgadas Mixtas Nanoestructuradas con Funcionalidad Óptica y Fotónica*. 2010, Sevilla: US-CSIC.
2. Gil-Rostra, J., *Tesis doctoral: Láminas Delgadas de Óxidos Mixtos con Aplicaciones Ópticas y Funcionales Obtenidas Mediante Magnetron Sputtering*. 2013, Sevilla: US-CSIC.
3. Rico, V., *Tesis Doctoral: Láminas Delgadas de Óxidos Fotoactivos para el Aprovechamiento de Energía Solar*. 2010, Sevilla: US-CSIC.
4. Dolphin, D., *The Porphyrins*. 1978, Academic, New York.
5. Milgrom, L.R., *The Colours of Life*. 1997, OUP, Oxford.
6. Gil-Rostra, J., et al., *Electrochromic Behavior of $W_xSi_yO_z$ Thin Films Prepared by Reactive Magnetron Sputtering at Normal and Glancing Angles.* ACS Applied Materials & Interfaces, 2011. **4**(2): p. 628-638.
7. Sermon, P.A. and G.C. Bond, *Studies of hydrogen spillover. Part 1.-Study of the rate, extent and products of hydrogen spillover from platinum to the trioxides of tungsten and molybdenum.* Journal of the Chemical Society, Faraday Transactions 1: Physical Chemistry in Condensed Phases, 1976. **72**(0): p. 730-744.

Chapter 1

Introduction

1.- Introduction to host-guest functional materials

Functional Materials

Nowadays, the development of new material systems pursues the fabrication of materials with predicted and controlled properties, for its use in well predetermined technological applications.

The term "functional" is often used in combination with new materials to indicate their potential for specific applications. These materials are the basis for the construction or improvement of devices. Indeed, the definition "functional material" has already been applied to a large number of different compounds, ranging from liquid crystals[1], organo-gels[2], biomaterials[3, 4], block copolymer nanocomposites[5, 6], and inorganic–organic hybrids[7] to silicas and zeolites[8], metal oxides[9, 10] semiconductors[11], and metals[12].

To be "functional", a material must possess a certain chemical or physical functionality. Examples of the former are acidity/basicity or the ability to coordinate to metals, while typical examples of physical functions are electrical and optical properties. It should, furthermore, be noted that many materials display their function only when they exist or are assembled into a certain structure or morphology. Two important examples are liquid crystals and semiconductor nanoparticles ("quantum dots").

One of the greatest challenges for modern science and technology of materials is the synthesis of nanostructured materials considering the final application and expected performance, in response to the technological demand. The correct selection of a specific material for a required application is a challenge in material science which needs to be compatible with industrial scale in order to advance in the development of specific devices. Many of the requirements are associated to a predetermined functionality, and the materials engineers are prepared to develop nanostructured materials with the combination of physical and chemical methods, following the modus operandi of molecular engineering procedures.

Hybrid materials

Many of the well-established materials, such as metals, ceramics or plastics cannot fulfill all technological desires for new applications. Scientists and engineers realized early on that mixtures of materials can show superior properties compared with

respect to their pure counterparts. For example, encapsulation of organic pigments inside inorganic matrices can be used to extend the coloration lifetime by reducing its oxidation close to zero. This strategy was used by Maya civilization in the 8th century, which paintings have survived more than twelve centuries in a harsh jungle environment. This hybrid pigment can resist acids, alkalis and organic solvents[13]. This pigment called "Maya blue" is a perfect example of the importance of hybrid materials.

Figure 1.1.- Mayan wall paintings show a good preservation of the blue colour twelve centuries after its creation. This is due to the utilization of the pigment "Mayan blue" which is a hybrid material formed by the indigo pigment encapsulated inside a palygorskite clay mineral.

Hybrid materials are defined as composites consisting of two constituents of different nature at the nanometer or molecular level. Commonly one of these compounds is inorganic and the other one is organic[14]. One characteristic example of hybrid materials are those formed by the incorporation of a basic structural material into a second substance.

The Nature shows many examples of hybrid materials. In most cases, the inorganic part provides mechanical strength and an overall structure to the natural objects while the organic part delivers bonding between the inorganic building blocks and/or the soft tissue. Typical examples of such materials are bone, or nacre.

Many materials now are based on the look for technological solutions inspired in the designs of the nature, known as biomimetism and bioinspiration[15]. Diatomaceous are a characteristic example of hybrid materials. Diatomaceous are an abundant group of unicellular algae in the ocean that have a shell composed of silica

and an organic material containing mainly carbohydrates and glycoproteins[16]. This organic material is anchored to the silicic acid (present in the water), and produces the polycondensation of the silica, followed by a self-assembly phenomenon, leading to periodic nanostructures. This silica shell, called frustule, contains a large amount of tiny holes in its structure causing multiple reflections of light and shows an amazing range of colors depending on their orientation. The formation of this shell does not require high pressures and temperatures, and overcomes the molecular engineering capabilities today. Diatomaceous are a perfect example of hybrid porous biomaterial, and taken as a reference in the design of hybrid materials[16].

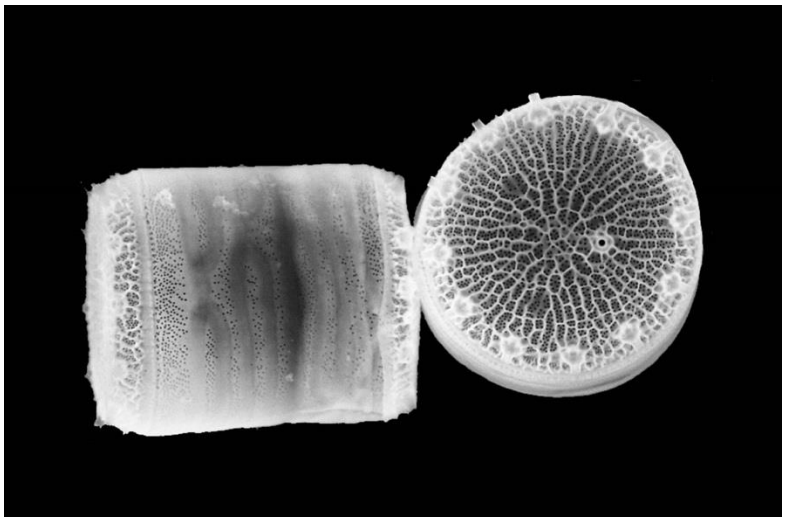

Figure 1.2.-SEM image of frustules of Diatomaceous algae.

The organic-inorganic hybrid materials are not only a creative alternative to design new materials, but their properties allow the development of innovative applications in the industrial sector[17]. Nowadays, most of the hybrid materials that have been introduced in the market, have been synthesized and processed using conventional chemical routes developed in the 80´s[14, 17]. These processes include: a) organosilanes polymerization, macro monomers and metal alkoxides, b) encapsulation of organic components by sol-gel processes of metal oxides or silica derivatives, c) the organic functionalization of nanoclays and other compounds with laminar structures. All of these strategies allow the assembly of a wide variety of nano-objects into organized-hierarchically architectures.

Chronologically, the first organic-inorganic materials were intercalation compounds, resulting from the inclusion of cations of organic molecules inside laminar

aluminosilicate (clays). Typically, these materials are formed by two tetrahedral sheets of SiO_4 making a sandwich with a central layer of AlO_6^{-3} octahedral.

The laminar aluminosilicates may have a degree of isomorphic substitution of cations of Al by Si in the tetrahedral layer, or Mg or Al in the octahedral layer, maintaining the stability of the structure. These substitutions are characteristic of smectite (montmorillonite, hectorite, beidellite, etc.), and lead to a deficiency of positive charge in the network. This charge deficiency is balanced by the presence of various cations (Na +, K +, Fe +3, Al +3, etc.), located in the interlaminar space and held there by electrostatic attraction forces. This makes them easily interchangeable by other cations from the medium, for example, by immersing the clay in concentrated salt solutions. These systems have been extensively studied in the field of hybrid materials, but have several limitations, such as steric impediments due to the 2D geometry of the host materials.

Host-Guest Hybrid functional materials

The study and development of new functional nanostructured materials has received a great interest in recent years, due to significant advances in fields such as microelectronics, chemical engineering and biochemistry, etc. The use of highly porous materials with the goal to enhance its accessible surface area is a common approach to enhance their functionality and can lead to a high number of applications. Porous materials are, for example, used as catalysts or catalyst supports[18-20], for the sorption, purification, and storage of gases, [16,17] for electrodes[21, 22], as insulating materials for the semiconductor industry (low dielectrics constant)[23], and for optical applications[24].

A large number of functional nanostructured materials are based on porous inorganic oxide matrices (host) where a second material is incorporated into the pores (guest). This latter material, commonly called active material, can be inorganic (metal, semiconductor, etc.) or organic (isolated molecules, molecular aggregates, polymers, etc.)[25].

The method of synthesis of organic-inorganic hybrid materials employed in this thesis consist in the utilization of highly porous thin films (host) and the subsequent incorporation of the active material (guest) to introduce the desired functionality. This methodology possesses similarities with the incorporation of organic molecules to

laminar clays, although there are important differences between them. The first, is the three dimensional nature of our system; the inorganic thin films used in this thesis as host, have pores throughout its thickness, where the active material can be accommodated. The second is that this host material does not have net charge for being balanced by exchangeable cations, so the mechanism of incorporation and anchoring of the organic material is different from the laminar clay. Therefore, the functional properties of the final material which are largely determined by the nature of the interaction between the matrix and the active material can be substantially different. The third difference is around the final application of functional materials: the thin films used in this thesis have a high open porosity with a separation between columns of tens of nanometers, which are easily permeable by liquids or gases. Due to this property, these films are postulated as chemical sensors in gas phase and in liquid media.

The synthesis method used in this thesis presents a remarkable advantage over wet processes like sol-gel in which the synthesis of the host material and the inclusion of the active material occur simultaneously. In the method used in the memory, the inorganic host films are previously prepared by Physical Vapor Deposition technique, where it critical parameters of the preparation as thickness, refractive index, composition, etc. can independently controlled. Then, in a second step, the active material is incorporated from the solution, without altering significantly the physicochemical properties of the inorganic material. . This methodology has been used to fabricate photonic sensors in gas and liquid phase.

Photonic gas sensors

Chemical sensors have an extreme importance in our lives: the air we breathe or the water we drink are perfect examples of the value of knowing the exact chemical composition of gases and liquids. Sensors devices fulfil this need by detecting changes in the chemical or physical environment[26-28]. The global market for sensors and related technologies is expanding significantly during the last decade, and it is foreseen that the investment will rise to more than 154 billion dollars in 2020, with a yearly growth rate of 10.1% (source www.bccresearch.com). The expected investment in

sensors from 2013 to 2020 is shown in Figure 1.3, where it can be noted a remarkable increase.

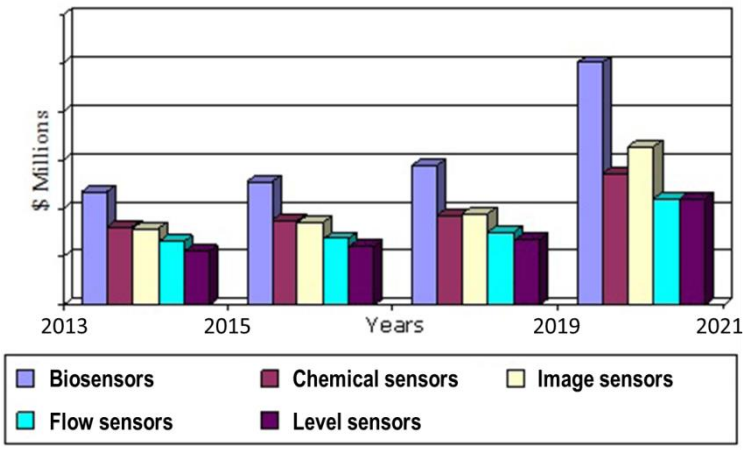

Figure 1.3.- Expected global market for sensors from 2013 to 2020 (source www.bccresearch.com).

The development of new devices for specific and more effective detection and monitoring (e. g. humidity, pH, temperature, gases, volatile compounds, UV…) is a very important field of research, with multiple applications in the industrial sector such as process control, environmental pollution monitoring, security food and medicine [29, 30].

There are many different types of sensors: acoustic, vibration, chemical, electric, magnetic, humidity, flow, radiation, position, pressure, density, level, temperature, etc[26, 27]. An ideal sensor should present: 1) specificity to a target agent (chemical or physical) in the presence of a mixture, usually referred as selectivity, 2) a clear and intense detectable response, usually referred as sensitivity and 3) a very fast response, therefore the sensing material needs to be in intimate contact with the environment (high open porosity). Usually the points 2) and 3) are linked, since materials with increased porosity and surface area present faster and more intense responses. In addition, the response of a sensor (transduction) can be of different nature as electrical, optical, electrochemical, etc.[31, 32]

The selectivity of most of the sensors is often a concern. For example, SnO_2 is a common and widely used material in many commercial solid state semiconductor sensors,[33] but different gases often produce similar responses. For example, ethanol, methanol or carbon monoxide usually produce indistinguishable electrical changes in

SnO_2 sensors[33, 34]. Commercially available techniques to improve the selectivity of the sensors include sensor operating temperature, filters or catalysts[27, 28, 33]. But usually these techniques tend to reduce drastically the sensor sensitivity or response speed (for example the use of filters decreases the diffusion speed of the target gas or liquid).

Gas detection has an important impact for a wide range of applications. Early markets have included the process and petrochemical industries, where sensors are used to ensure safety (e. g. via detection of toxic or flammable gases), monitor feedstocks and measure key species in products and processes[35]. Use of high sensitivity gas detectors is widespread in atmospheric science, to measure and understand the profile and pathways of different gas species including greenhouse gases[36]. Various potential biomarker gases are also under study for use in breath diagnostics, including nitric oxide (NO), ethane, ammonia (NH_3), and many others[37].

Quantitative detection of gases is traditionally dominated by laboratory analytical equipment such as gas chromatographs, with sampling that precludes real-time data[38], or small ultra-low-cost devices such as pellistors, semiconductor gas sensors or electrochemical devices. Pellistors are robust devices that respond to combustion on a catalyst bead[38]; they perform well in detecting flammable gases close to the lower explosive limit, however suffer from zero drift at parts per million (ppm) levels.

Semiconductor gas sensors can be highly sensitive at the low ppm level[39] , they change their conductivity when are exposed to certain compounds. Semiconductor gas sensors have been proposed as ideals of the new environmental detection technology to be developed in the coming years, because of their small size and high sensibility[40, 41]. However these also suffer from drift and cross-respond to other gases and changing humidity levels. On the other hand, these devices have some drawbacks like, for instance, their high operating temperatures (between 200 and 400 º C) or the use of electrical current to work. Electrochemical gas sensors can be relatively specific to individual gases and sensitive at ppm or ppb levels[39], however they have limited lifetimes and also suffer from some known cross response, e g to humidity.

In contrast, gas sensors based in changes in the optical properties (refractive index, light absorption, luminescent emission ...) or photonic sensors, usually offer fast

responses (below 1 second are possible), minimal drift and high gas selectivity, with zero cross response to other gases as long as their design is carefully considered[28, 42]. Measurements can be made in real time and *in situ* without disturbing the gas sample, which can be especially important in process control[43]. The transduction mechanism offer a direct measurement of the physical properties of a molecule or material (e. g. its absorption at a specific wavelength), drift is reduced and, measurements are self-referenced, making them inherently reliable.

Gas sensors using fluorescence-intensity changes organic dyes adsorbed in porous materials are also very promising. Usually, fluorescence provides higher sensitivity than sensors based in absorption of light (since single molecule fluorescence can be measured[44]). Moreover, the emission of fluorescent molecules is strongly affected by their aggregation state. Sensors based on fluorescent molecules with different aggregation states are also reported in literature[45, 46]. Further information about the aggregation of porphyrins dye can be found in section 3.

Gas detection applications can cover a very wide range of gas concentrations. Since most gases at standard temperature and pressure behave as ideal gases, the fraction volume concentration is proportional to the molar concentration in the matrix. Concentrations are usually expressed as % vol (% by volume), ppm (parts per million by volume; 1 part in 10^6), ppb (parts per billion by volume; 1 part in 10^9) or ppt (parts per trillion by volume, 1 part in 10^{12}).

The development of photonic sensors are an interesting alternative to solid state sensors based in electrical responses [47]. The main advantages of these detectors are the absence of electrical contacts, capability of working at room temperature and remote monitoring by using optical fibers[48]. All of these properties make them ideal candidates for the detection of flammable compounds and their use in explosive or toxic environments, especially, in situations where it is impossible to measure electric currents[49, 50]. Other advantages of photonic sensors are high sensitivity, no electromagnetic interference and the possibility of using internal references.

A large number of photonic sensors are based on nanocomposite materials incorporating dyes that respond to the presence of specific gases and volatiles changing its absorption spectrum and/or luminescent emission[47, 51-53]. For instance, the fluorescent emission of numerous organic compounds (such as pyrene and its

derivatives) or organometallic (metalloporphyrins and numerous compounds of iridium and ruthenium) are deactivated in the presence of O_2 [51-53]. This property is the operating principle of many photonic oxygen sensors [47]. This strategy of synthesis and the wide variety of sensitive compounds to the presence of gases, allows to design new materials for photonic sensors applications.

In this thesis, photonic sensors for different gases have been developed. Usually, the photonic sensor is part of a larger integrated system in a measuring device with a source of light, a light guiding system, a detector of light and the sensor itself. Figure 4.1 shows a scheme of a photonic sensor. One of the features of a photonic sensor is its ability to measure changes from one or more light beams, by monitoring alterations in the intensity of the light at different wavelengths.

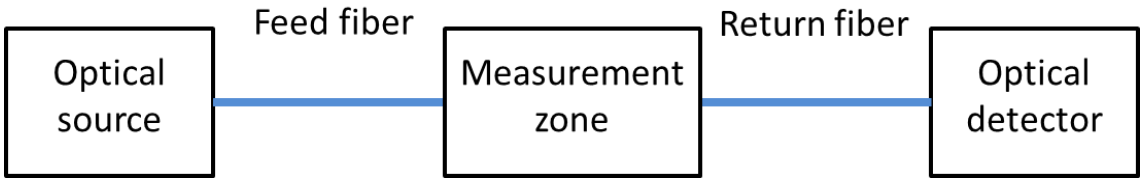

Figure 1.4.- Scheme of a photonic sensor

1.2.- Host material: Thin Film Deposition Processes and Characterization Techniques

Introduction to Thin Films

The continuous advances in materials science have changed the modern society and the microtechnology field is not left behind. Modern technology requires thin films for many different applications[54]. For example, the current microelectronics devices are fabricated with thin film technologies and its development during the last decade has been crucial. It is widely accepted that the thickness range of thin films is between tenths of nanometer to several micrometers.

Thin film studies have directly or indirectly contributed to the progress of many areas of research such as solid state physics and chemistry and are the key elements of many technological advances made in the fields of optoelectronic, photonic, and magnetic devices. The processing of materials into thin films allows easy integration into many types of devices for example in microelectronics and integrated optics applications where they are widely used [54]. Figure 2.1 shows some examples of thin film for flexible microelectronic device (a) and optical filters (b).

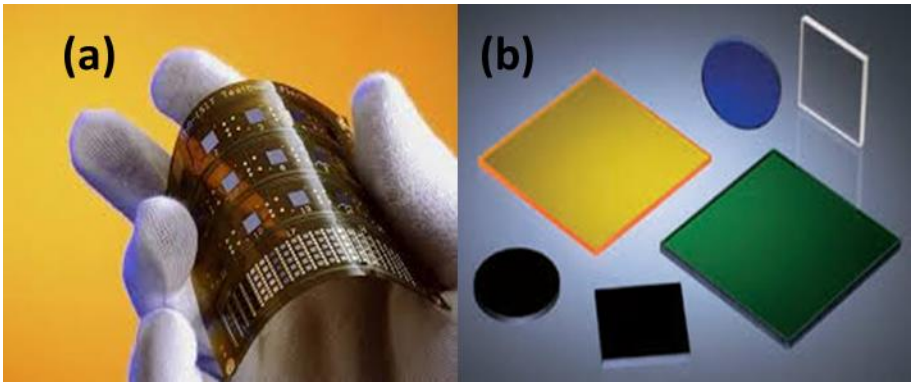

Figure 2.1.- Some examples of applications in microelectronics and integrated optics: (a) flexible electronic integrated circuit (b) optical filters.

Most of the functional materials are based in thin film due to their specific electrical, magnetic, optical or mechanical properties. Some examples of functional materials based in thin films are microelectronic devices, magnetic thin films in recording devices, magnetic sensors, gas sensors, anti-reflective coatings,

photoconductors, IR detectors, interference filters, solar cells, polarizers, temperature controllers in satellites, superconducting films, anticorrosive and decorative coatings.

Applications of Thin Films

Nanometric coatings are used to change significantly the properties of the substrate where they are deposited. Change in theirs properties that can be exploited in well required technological applications.

Although the study of thin film phenomena dates back well over a century, it has been over the last four decades where they have been used in real devices. The requirements of micro and nano miniaturization make the use of thin films imperative. Many thin film devices have been developed for a specific application mainly imposed by the market. The current devices are a direct result of the last decades of research above the physical properties of thin films.

On the other hand, as well as generating ideas for new devices, fundamental research has led to a dramatic improvement in the understanding of thin films and surfaces. This in turn has resulted in a greater ability to fabricate devices with predictable, controllable and reproducible properties. The cleanliness and nature of the substrate, the deposition conditions, post deposition treatment and passivation are vital process variables for thin film fabrication. Therefore, before the understanding of thin films, it has not really been possible to apply them to real devices.

Moreover, most of the budget for early thin film research originated from space and defence programs in which the device cost is less important than other specific properties. The major applications of thin film technology are not now exclusive in these areas but rather often lay in the domestic sector in which low cost is essential[54, 55].

Thin film materials are currently used in semiconductor devices, telecommunications, integrated circuits, rectifiers, transistors, solar cells, light-emitting diodes, photoconductors, light crystal displays, magneto-optic memories, smart windows, micro electromechanical systems (MEMS), and multifunctional emerging coatings, as well as cutting tools as well as sensors.

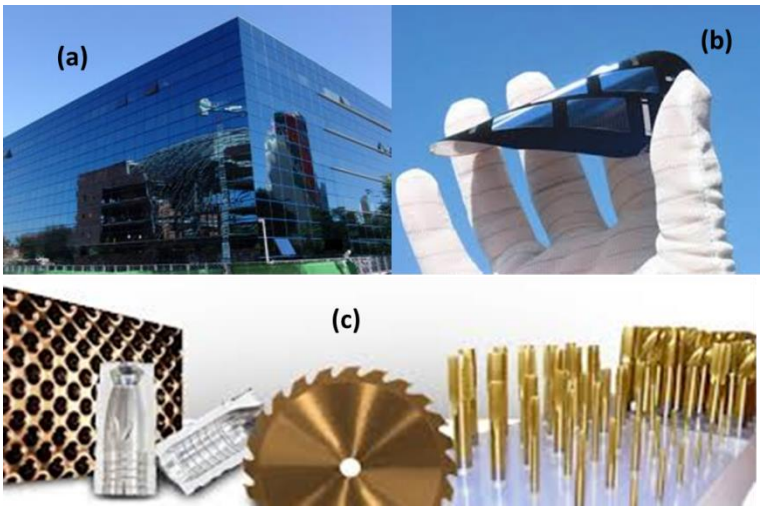

Figure 2.2.- Some examples of the industrial application. (a) Bluenet building located in La Cartuja, Seville, (b) flexible solar cell or (c) cutting tools.

Advancements in micro-technology and the evolution of new materials and devices play a key role in the development of very accurate and reliable thin films sensors technology. The technology of integrated sensors has been developed tremendously in the last few years. The fabrication and miniaturized devices capable of molecular level imaging and monitoring of pathological samples and macromolecules is recently the focus of attention of the scientific community, due to the increasing need for environmental safety and health monitoring.

Gas sensing devices have been developed in past years that operate under different principles, among which the resistive metal oxide sensors thin films are the most used. However, these sensing elements typically operate at elevated temperatures for optimum performance, and therefore possess high power consumption. Nowadays, room temperature gas sensor as optical thin film sensors are attracting and growing interest for many applications.

Thin Films Deposition Techniques

The choice of the proper deposition technique is crucial for the final application of the thin film. Factors like the nature of the substrate, coating, temperature, crystallinity, etc… will determine the most suitable deposition technique. On the other hand, the compatibility of the technique with industrial scale is extremely important to achieve a real commercial device.

The techniques used to fabricate thin films are divided in Physical and Chemical methods[54, 55].

In the physical methods the required material is sublimed or ejected from a source, i.e. evaporation or sputtering, whereas chemical methods a chemical reaction of the source material is required.

The thin films developed within this thesis have been fabricated by Physical Vapour Deposition (PVD), where the target material has been sublimed by electron beam heating and by Magnetron Sputtering (MS) techniques. The main aspects of both techniques are described in the next section.

Physical Vapour Deposition (PVD)

The term Physical Vapour Deposition (PVD) originally appeared in the 1966 book Vapor Deposition by C. F. Powell, J. H. Oxley and J. M. Blocher Jr., but Michael Faraday was using PVD to deposit coatings as far back as 1838.

PVD is a process based on the vaporization of the required material and the following condensation on a specific substrate under vacuum conditions. To achieve this goal, the material in solid state is heated until its evaporation (thermal evaporation) or is "sputtered" by an intense bombardment with ions (sputtering). In this latter case, the ions are generated by an electrical discharge between two electrodes producing the ionization of a certain gas (plasma). These methods are widely used to deposit different type of material, mainly metal or metallic oxide materials.

PVD has some advantages like very easy assembly and the possibility to evaporate materials in a simple form (dust, pellets,..).

Electron beam evaporation

Electron Beam Physical Vapour Deposition or EBPVD is widely used for the preparation of thin layers. Figure 2.3 shows a scheme of an EBPVD system which consists in an incandescent filament, usually of tungsten, (cathode) which emits an electron beam by thermo-ionic emission. These electrons are accelerated toward the anode which is polarized at a high voltage (kilovolts).

The electrons are directed to the target material, which is heated and subsequently sublimed. These evaporated atoms condense on the required substrates. A magnetic field is usually included in the setup in order to deflect the electrons keeping

the filament away from the deposited material and then reducing the contamination of the filament and increasing its lifetime.

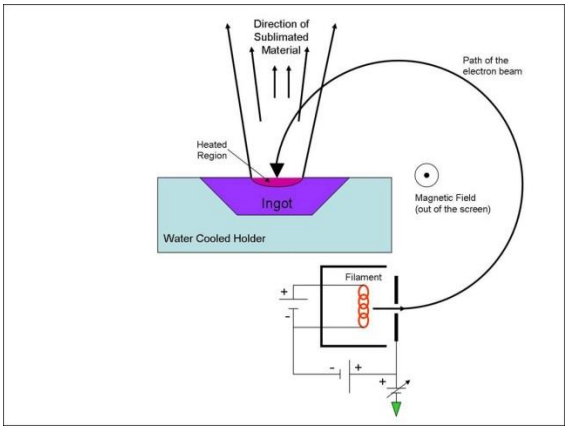

Figure 2.3 .- Scheme of the setup of an Electron Beam Physical Vapour Deposition system.

EBPVD is a deposition technique mainly used for high melting point materials such as nitrides or oxides. Vacuum condition is required for electron beam evaporation (electrons collide with the gases at higher pressures), which also avoids the contamination of the target, and keep the directionality of the sublimed material, which is mandatory for Glancing Angle Deposition as it will be seen in next section. The evaporator and the crucible are usually refrigerated to avoid contamination problems associated to thermal outgassing[56].

Magnetron Sputtering

MS is one of the most used PVD methods which are widespread in the industrial sector. Sputtering is a process whereby atoms are ejected from a solid material due to bombardment of the target by energetic particles. It only occurs whenever any particle strikes a surface with enough energy to dislodge an atom from the surface, i. e., when the kinetic energy of the incoming particles is much higher than conventional thermal energies ($\gg$ 1 eV). Sputtering can occur for any incident species, including atoms, ions, electrons, photons and neutrons as well as molecules and molecular ions. For most of practical cases, sputtering utilizes ion bombardment, either with inert gas ions such as Ar^+ and Kr^+, or small molecular ions such as N_2^+ or O_2^+. Physically, sputtering relies on the transfer of physical momentum and kinetic energy from the incident particle to the surface atoms, and this is independent of the particle's charge. Sputtering is usually

practiced by means of plasmas which generate charged particles which can be accelerated towards the surface electrically.

The sputtering process is shown in figure 2.4. The incident particles impact on the surface or near-surface atoms of the solid with enough energy to break bonds and dislodge atoms. If, during this process, one or more atoms are removed from the solid, they are considered to be sputtered atoms.

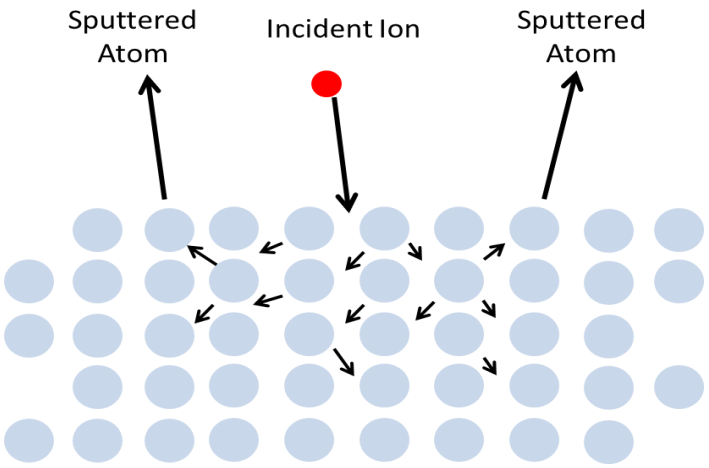

Figure 2.4.- Schematic of physical sputtering process

Depending on the target material radio-frequency (RF) or direct current (DC) sources may be used. If the target material is a conductor, a constant voltage (DC) source can be used to accelerate the ions to the desired bombarding velocity. As the ions strike the surface, the resulting charges can be drained to prevent any charge build-up. However, if the material is an insulator, the conduction bands will not allow free charge movement. As the ions strike the surface, their charge will remain localized and after a certain time, the charge will build up, preventing further bombardment of the surface. In order to prevent this, alternating current (RF) source at high frequency is used. The heavy ions cannot follow the fast switching and only electrons feel the oscilation field and hit the surface to neutralize the charge[57].

Glancing Angle Deposition (GLAD)

It is well known that the properties of a thin layer can be very different from the bulk material. This behaviour, apparently anomalous, is due to the peculiar structure of the thin layers which, in turn, is determined by different processes that take place in the initial stages of growth.

In fact, the process of condensation of a gas on a solid surface to obtain a thin layer is a complex thermodynamic phenomenon in where different microscopic stages are taking place, from the arrival of the vapour atoms on the surface in growth to the formation of small sorted or disordered structures of atoms that ultimately determine the morphology and crystallinity of the film growth.

During these processes, each atom that reaches the surface interacts locally with individual atoms or nuclei already formed in theirs environment by complex mechanisms of energy exchange. Thus, the atoms diffuse into the surface and desorb or adsorb in their final positions waiting for the adsorption of other atoms. It is obvious that the variables that determine each of these stages are related, so it is very difficult to separate each of these events of accommodation of the atoms, and only in ideal cases is possible to model the process.

"Vapour-surface" is itself a complex system in which coexist numerous variables such as: the nature of the gas, pressure and temperature, surface condition, the rate of arrival of atoms, presence of impurities, the geometry of the system, etc.[56].

PVD is a high vacuum deposition technique (pressure < 10^{-3} mbar) and it is a "line of sight" technique, i. e., it is a directional method in which the vapours follow a linear trajectory that is not altered by collisions with other species.

A variant of PVD involves placing the substrates at oblique and glancing angles, so the vapours flow at certain angle with the normal of the substrates. This technique is called *Oblique and Glancing Angle Deposition* (OAD and GLAD) depending if the angles is lower or higher than 80º respectively [58-64].

The use of the GLAD produces extremely porous films with a very open and tilted columnar morphology. Figure 2.5 shows some examples of thin films prepared by GLAD. Different microstructures can be obtained by changing the orientation of the substrate and therefore the direction of arrival of vapour flow. This can be used to design the columnar growth and the nanostructure of the thin film[65].

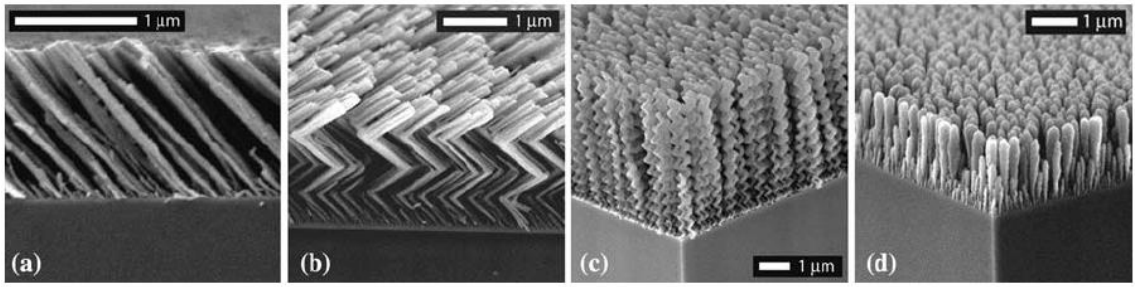

Figure 2.5.-Examples of nanostructured thin films prepared by GLAD-PVD. The thin film a) shows a columnar structure grown at an oblique angle, and b) the same kind of deposition,but rotating the sample 180º at regular time intervals. The samples c) and d) are growth by rotating the sample at a constant speed, c) spirals obtained at low speed while isolated columns perpendicular to each other are formed at high rotation speed.

Figure 2.6 shows a schematic representation of GLAD-PVD evaporation system. During deposition, the vapour incidence angle (α) and rotation angle (ϕ) are adjusted according to a predefined motion, designed to obtain a given nanostructure of the thin film.

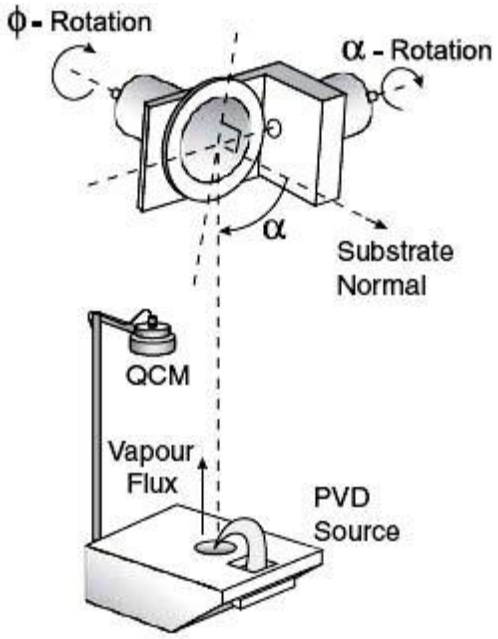

Figure 2.6.- Scheme of an electron beam physical vapour deposition in glancing angle configuration. The design of the nanostructure of the thin film is obtained by adjusting of the angles α and ϕ during deposition.

GLAD technique started in 1994, when Robbie and Brett fabricated porous thin films with an amazing zig-zag columnar microstructure[65]. The microstructure was achieved by the periodically change of the flow of material, suggesting that a large degree of microstructural control can be obtained by changing geometrical parameters like vapour incident angle or rotation angle. A year later, Robbie et al. [66] built the first anisotropic helical thin film medium. To achieve this, they grew helices shaped columns having dimensions comparable to the wavelength of visible light. Nowadays, this technique has produced columnar nanostructures of great complexity, as regular

nanofibers, perforated, or gradual porosity, which have applications in sensors, microfluidics , catalysis , optics, etc.[67].

Columnar growth in GLAD configuration. Shadowing effect

As detailed previously, the deposition from vapour phase involves the transformation of the material from its solid state to a gaseous state[56, 57, 68]. Therefore, when the atoms or molecules reach the substrate surface, different processes according to the energy and the type of interaction between the vapour and the substrate can occur. Volmer-Weber model describes the formation of three-dimensional nuclei as a result of energetically more favourable interaction between the atoms or molecules of vapour with the substrate surface[56, 57].

An important factor that determines the growth of the layers prepared by PVD is surface diffusion. This process is associated with the substrate temperature among others[68]. A rule of thumb for films grown at low temperature is that, below 0.3 times the melting temperature of the source material[56], the effect of diffusion is minimized and a directional growth of the film is obtained, leading to a tilted columnar structure as shown in figure 2.5.

The directional columnar growth is the result of a process called "shadowing" that occurs on the surface of the substrate. This mechanism is outlined in figure 2.7. During the initial stage of growth, atoms and atomic aggregates condense on the substrate forming individual seeds or nuclei according to Volmer-Weber tridimensional model. When the substrate is inclined and the material arrives at glancing angles, the nuclei produce a geometric shadowing effect on its back region, preventing the arrival of new material to this zone, which inhibit the coalescence between nuclei and the formation of a continuous film. Moreover, the nuclei capture incidents atoms that should be deposited in shaded areas, forming columns that grow in the direction of the vapour source.

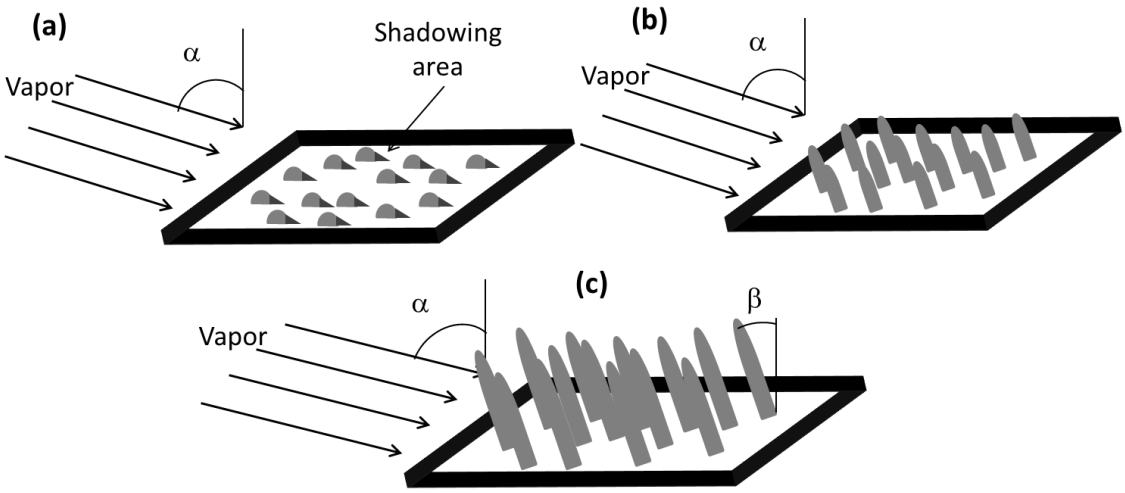

Figure 2.7.- Scheme of Columnar growth mechanism in GLAD configuration. In the first stages of growth (a) atoms condense and form nuclei that produce a shadowing effect in different regions (b). The final film is composed by columns which grow from nuclei and are inclined in the direction of the vapour source (c). The main geometrical parameters have been indicated: the angle of the vapour incident (α) and the angle of the tilted column (β).

The films grown in this thesis have been deposited by keeping α (vapour incidence angle) and ϕ (rotation angle) constants. The fabrication of more exotic structures (as zig-zag or helicoidal) are out of the scope if this work since they are not necessary for the gas sensor applications and it is easier to implement in the industrial sector.

It is important to emphasize that this type of columnar growth is possible only from a directional vapour source of steam, with a small angular distribution, to maintain the shadowing at an atomic level. The vapour source may be achieved by techniques such as thermal evaporation deposition, by electron bombardment or by sputtering at low pressures[65, 69-71].

This type of layers possess a very important property for the applications defended in this thesis: the porosity can be tuned by controlling geometrical parameters. Such layers have micro and mesopores (according to IUPAC, pores with diameters below and above 2 nm, respectively)[72], which can be controlled by adjusting the deposition parameters. Its high porosity makes them ideal candidates for the incorporation of active materials as host films.

1.3.- Guest material: Porphyrins.

Spectra of porphyrins

Porphyrins are a group of aromatic macrocycle organic compounds composed of carbon, nitrogen, and hydrogen that are found in many biological processes and play a very important role in the metabolism of living organisms. The name porphyrin is derived from the Greek “porphura” meaning purple[73]. Examples of porphyrins and its importance are the iron-containing porphyrins found as heme (of haemoglobin) and the magnesium-containing reduced porphyrin (or chlorine) found in chlorophyll (figure 3.1). The knowledge of porphyrins and their electronic excited states is essential in understanding a wide variety of biological processes, including oxygen binding, electron transfer, catalysis, and the initial photochemical step in photosynthesis.

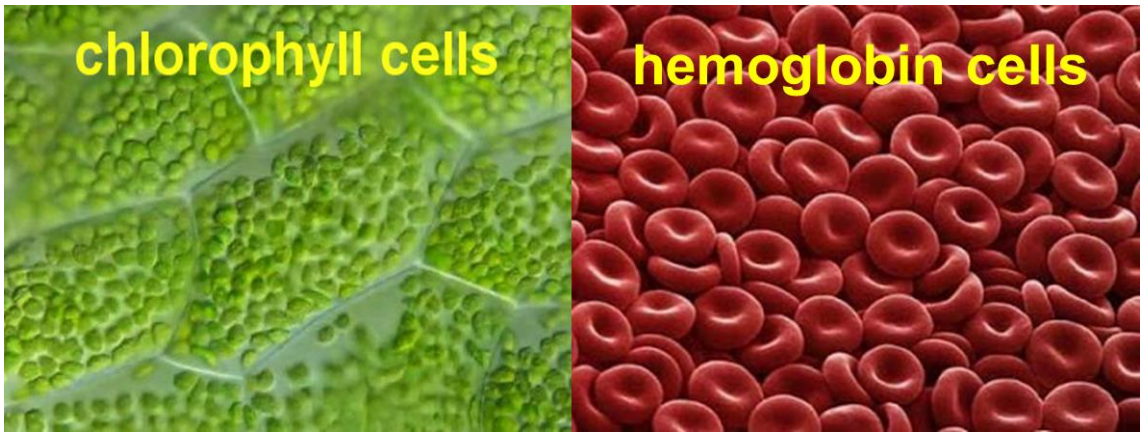

Figure 3.1.-Left, chlorophyll cells. Chlorophyll is an extremely important biomolecule, critical in photosynthesis, which allows plants to absorb energy from light. The basic structure of a chlorophyll molecule is a porphyrin ring coordinated to a magnesium atom in the center of the ring. Right, hemoglobin cells. Hemoglobin make possible for red cells to transport oxygen within the body. The basic structure of a hemoglobin molecule is a porphyrin ring coordinated to an iron atom in the center of the ring.

Figure 3.2 shows the most basic porphyrin called porphyne. They are in fact a large class of deeply colored pigment, of natural or synthetic origin, composed of four modified pyrrole subunits interconnected at their α carbon atoms via methine bridges (=CH−) [74, 75]. Its structure supports a highly stable configuration of single and double bonds with aromatic characteristics.

Figure 3.2.- Atomic structure of porphyrins

The porphyrins play important roles in the nature, due to their special absorption, emission, charge transfer and complexing properties as a result their highly conjugated systems[75].

Thus, they typically have very intense absorption bands in the visible region. The absorption spectrum present Soret band or B-bands in the 380–500 nm range with molar extinction coefficients of 10^5 M^{-1} cm^{-1}. Moreover, at longer wavelengths, in the 500–750-nm range, their spectra contain a set of weaker, but still considerably intense Q bands with molar extinction coefficients of 10^4 M^{-1} cm^{-1}.

The studies of the wavelength shift of their adsorption band and the absorbance changes as function of pH, temperature, solvent change, reaction with metal ions and other parameters permits to obtained accurate information about equilibrium, complexation, kinetic and aggregation of porphyrins.

Porphyrins have diverse applications, such as energy storage devices, sensors, switches, solar energy devices, and electrochromic displays among others. Because of their unique blend of photoactivity and ability to transport electrons, porphyrins and related macrocyclic compounds are playing an important part in these exciting developments.

The porphyrin macrocycle is a highly-conjugated molecule containing 22 π-electrons, but only 18 of them are delocalized according to the Hückel's rule of aromaticity (4n+2 delocalized π-electrons, where n = 4).

Differing substituents on the macrocycle have a clear impact on optical properties such as the position and number of absorption and fluorescence bands. There are two different sites on the porphyrins macrocycle, where electrophylic substitution can take place with different reactivity[75]: i) positions 5, 10, 15 and 20, in the methine bridge, called meso and, ii) positions 2, 3, 7, 8, 12, 13, 17 and 18, called β-pyrrole positions. The pyrrole positions next to nitrogen atoms are called α-carbons (figure 3.3), according to the International Union of Pure and Applied Chemistry (IUPAC) and International Union of Biochemistry (IUB).

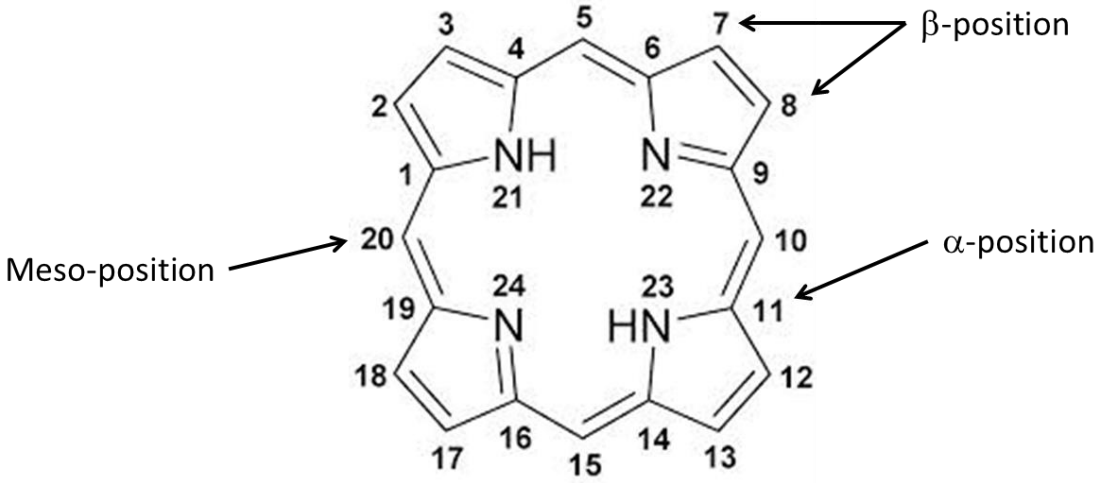

Figure 3.3.- The structure of the porphyrin. The position 5,10,15 and 20 are called meso-position, the position 2, 3, 7, 8, 12, 13, 17 and 18, called β-pyrrole positions and 1, 4, 6, 9, 11 ,14 ,16 and 19 are called α-carbons.

UV-Vis Spectra of the porphyrins

The absorption bands in the UV-visible spectra of porphyrins are due to their highly conjugated π-electron system. An example is shown in figure 3.4 for an ethanolic solution of TMPyP. It has been widely studied that changes in the conjugation pathway and symmetry of a porphyrin can affect its UV/Vis absorption spectrum[74, 76-80].

Martin Gouterman in the 1960s, with the "four-orbital" model, explained the absorption spectra of porphyrins by the discussion of the importance of the charge localization on spectroscopic properties [76, 81].

The electronic absorption spectrum of a typical porphyrin consists of two distinct regions: a strong transition to the second excited state ($S_0 \rightarrow S_2$) between 380-500 nm (Soret band or B-band), and a weak transition to the first excited state ($S_0 \rightarrow S_1$)

between 500-750 nm (Q bands). The Q bands of free-base porphyrins (without metal central atom) are a set of four absorptions arising from HOMO to LUMO transition. Of these, the first set of two lines is x-component of Q bands while the second set is its y-component. Both these, Q_x and Q_y components are composed of two types of vibrational excitations too, the lower energy one is Q(0,0) and the higher energy one Q(1,0). Thus the four lines in the set are $Q_x(0,0)$, $Q_x(1,0)$, $Q_y(0,0)$ and $Q_y(1,0)$ in the increasing order of energy.

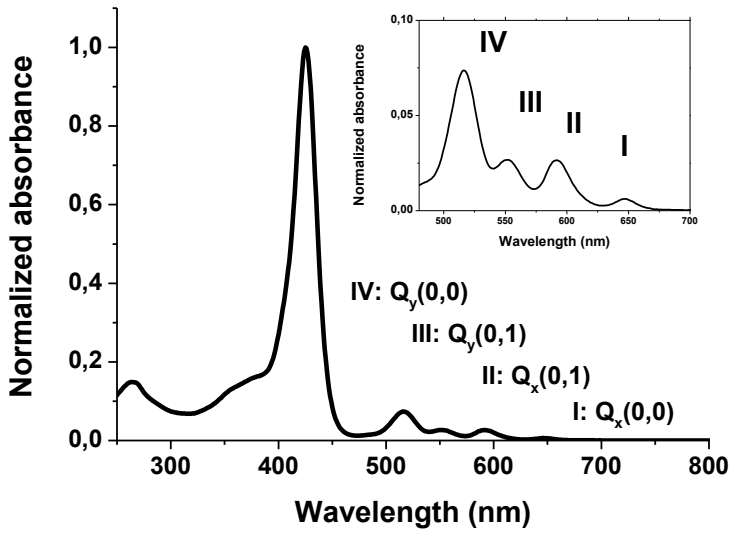

Figure 3.4.- UV-Vis spectrum of a solution of porphyrin (TMPyP) in ethanol with in inset the enlargement of Q-bands region between 480-700 nm.

These spaectra of porphyrins can be exploited to monitor of guest-binding processes to a matrix by UV-visible [82-85] [86, 87] or fluorescence spectroscopy [88, 89].

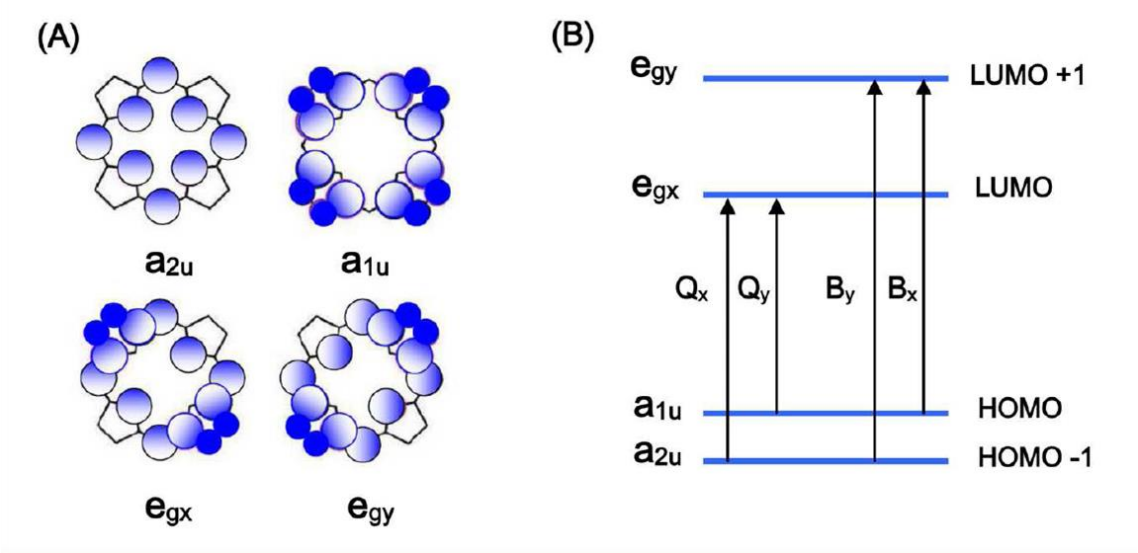

Figure 3.5.- Porphyrin HOMOs and LUMOs. (A) Representation of the four Gouterman orbitals in porphyrins. (B) Drawing of the energy levels of the four Gouterman orbitals upon symmetry lowering from D4h to C2V. The set of e_g orbitals gives rise to Q and B bands.

The variation in the UV-Vis absorption or fluorescence spectra depend strongly on the type of substituent. Variations of the peripheral substituents on the porphyrin ring cause minor changes to the intensity and wavelength of the absorption features, however, protonation of two of the inner nitrogen atoms into the macrocycle usually strongly change the visible absorption spectrum.

The structure of protonated porphyrin molecule, i. e. where the free nitrogen from the inner of the ring have two H^+, is called diacid. When porphyrin macrocycle is protonated the molecule is in a more symmetrical situation than in the porphyrin free base and this produces a reduction of the Q bands: : the initially four are reduced to two bands.

In the case of meso- substituted porphyrins, the protonated state leads to a structural deformation of the molecule consisting in a rotation of the phenyl rings are rotated between 21-33° from the plane of the porphyrin, and the pyrrole rings adopt a saddled configuration in which alternate rings are tilted up and down between 28-33°. The saddled nature of porphyrin diacids is an important factor to consider during the study of porphyrin aggregation and its organization on substrates.

Fluorescence of the pophyrins

Steady state and time resolved fluorescence spectroscopy have been widely used in the field of biological sciences. Fluorescence detection is highly sensitive, cheap, and easier to handle in comparison with radioactive tracers used in most biochemical measurements.

Figure 3.6 shows an energy level diagram that describes the emission from most aromatic molecules with singlet ground states like the porphyrins. Excitation from the ground state S_0 to any singlet excited state S_x leads to very fast radiationless decay to the lowest excited singlet S_1. From S_1 the molecule can emit fluorescence radiation $S_1 \rightarrow S_0$ at the rate k_f, thus, only the relaxation process from S_1 to S_0 with rate k_f can emit fluorescent radiation.[90]

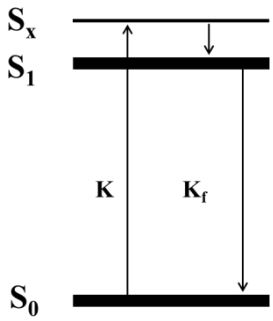

Figure 3.6.- Fluorescent radiation.

Fluorescence excitation energy of porphyrins is, in general, close to the absorption maxima, both in the Soret and the longer wavelength regions. Porphyrins fluorescence is located in the red region (600-800 nm) of the visible spectrum and is relatively free from interferences due to emissions from other compounds present in biological specimens. It consists of two strong emission bands called Q(0,0) and Q (0,1) located around 600 to 670 nn and another less intense peak between 640 to 800 nm, respectively. Figure 3.7 shows absorption, excitation and emission spectra of a free-base porphyrin.

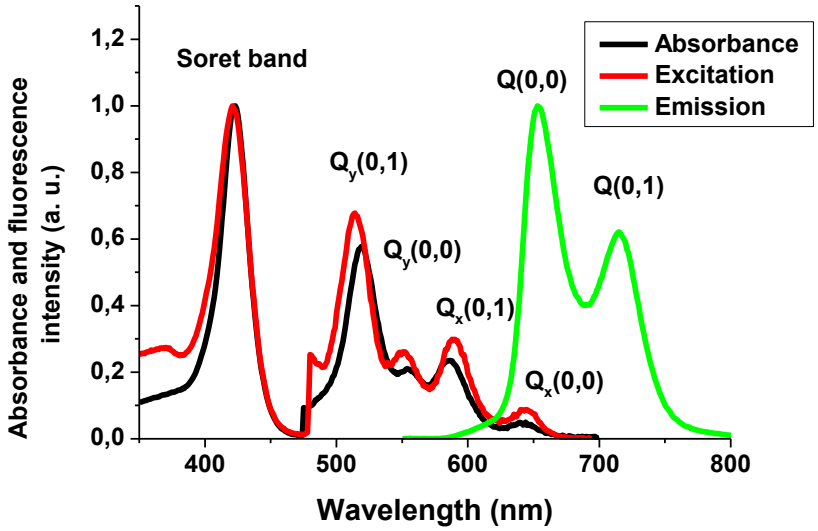

Figure 3.7.- Normalized absorption (black), excitation (red) and emission (green) spectra for TMPyP. It is indicated the name of the bands of each spectrum.

A number of processes can lead to a reduction in fluorescence intensity, i.e., quenching. Quenching it is used to refer to a process which decreases the fluorescence intensity of a substance. There are mainly two types of quenching processes: collisional (dynamic) and static (complex formation) quenching

Collisional quenching occurs when the excited fluorophore experiences contact with an atom or molecule that can facilitate non-radiative transitions to the ground state. For example, oxygen is a common quencher in fluorescent dye or, in general, the presence of heavy metal ions in porphyrins.

In some cases, the fluorophore can form a stable complex with another molecule. If this ground-state is non-fluorescent then we say that the fluorophore has been statically quenched. The fluorescence of the sample is reduced since the quencher is essentially reducing the number of fluorophores which can emit. It is the case of the protonation of the porphyrins. For example, free porphyrins have a high fluorescent intensity and its diacid structure is not fluorescent.

On the other hand, fluorescent lifetime depends on the environment of the molecule and is proportional to the so-called quantum yield, i.e. the ration between the fluorescent emitted photons divided by the absorbed ones. The measurement of lifetime is more robust that measurement fluorescence intensity (from which the fluorescent

quantum yield is determined), because it depends neither on the intensity of excitation nor on the concentration of the fluorophores.

Aggregation of porphyrins

An increasing interest in recent years is due to supramolecular assemblies of π-conjugated systems for their potential applications in optoelectronic and photovoltaic devices[91] . Porphyrins are an interesting class of self-assemble aggregates molecular.

Self-assembly of porphyrin molecules, driven by noncovalent (e.g., hydrogen-bonding, hydrophobic, and electrostatic) intermolecular interactions, allows the development of novel class of functional materials based on theirs aggregation state with potential applications in catalysis, sensor, solar cells, and electronic devices[92-94].

The aggregation and dimerization of porphyrins and metalloporphyrins in aqueous solution have been widely investigated[95, 96] and it has been deduced that it is dependent strictly on physical-chemical characteristics, such as, ionic strength, pH and solvent composition; the combination of these factors can facilitate the aggregation processes[97, 98].

Spectroscopic techniques such as UV-visible or fluorescence spectroscopy is useful for studying aggregation processes in solution and in solid phase because the aggregates of porphyrins show peculiar spectroscopic properties[99].

The electronic configuration of porphyrin molecule with 22 π-electrons causes a strong π – π interaction[100], facilitating the formation of two structure types: “J-type” with blue shift of B band and redshift of Q band and “H-type” with bathochromic shift or red shift of B and Q bands, with respect to those of monomer.

The J-type aggregates (edge-by-edge or side-to-side assemblies) were formed for transitions polarized parallel to the long axis of the aggregate, while H-type (face-to-face stacking) for transitions polarized perpendicular to it (Figure 3.8).

J-aggregates are formed with the monomeric molecules arranged in one dimension such that the transition moment of the monomers are parallel and the angle between the transition moment and the line joining the molecular centers is zero[101]. The strong coupling of monomers results in a coherent excitation with a red-shift

relative to the monomer band. H-aggregates are again a one-dimensional arrangement of strongly coupled monomers, but the transition moments of the monomers are perpendicular (ideal case) to the line of centers. On the contrary of J-aggregates, the arrangement in H-aggregates is face-to-face. The dipolar coupling between monomers leads to a blue shift of the absorption band[102, 103]. The H-aggregates are not known to have sharp spectra like the J-aggregates; nevertheless, there are many examples where the spectroscopic blue shift, evident for formation of H-aggregates, was observed.

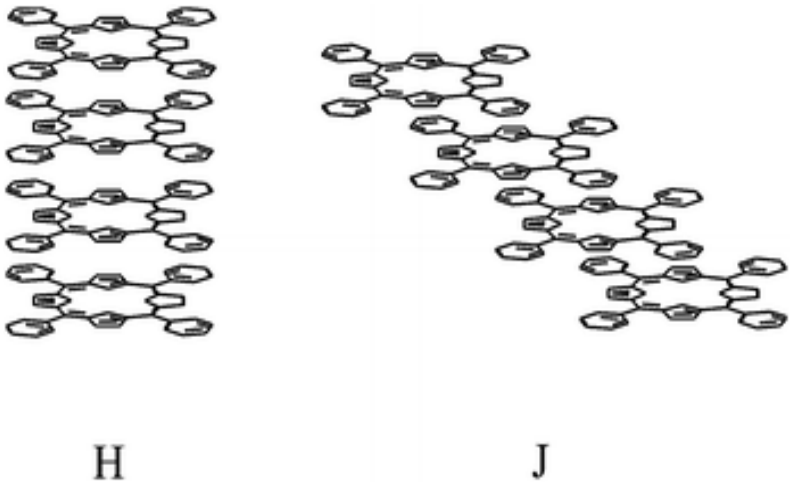

Figure 3.8.- H and J-type of pophyrin aggregates.

As a result, a wide variety of self-assembled porphyrin structures are highly desirable for practical use, which can be applied to nonlinear optical materials[85, 104-107], organic solar cells[108] and sensor devices[109].

In general, the aggregate formation of porphyrins and their physicochemical properties can be affected by the ionic strength, nature of the titrating acid, temperature, pH, peripheral substitution and presence of surfactants of ions[99, 110-112], and although much has been studied about the spectroscopic features and excitonic interactions in molecular aggregates, the detailed information of geometrical structure, especially the molecular orientation, are still the subjects of continuing interests[113].

1.4.- References

1. Tam-Chang, S.-W. and L. Huang, *Chromonic liquid crystals: properties and applications as functional materials.* Chemical Communications, 2008(17): p. 1957-1967.
2. van Esch, J.H. and B.L. Feringa, *New Functional Materials Based on Self-Assembling Organogels: From Serendipity towards Design.* Angewandte Chemie International Edition, 2000. **39**(13): p. 2263-2266.
3. Dong Liu, X., et al., *Functional Materials Derived from DNA*, in *Functional Materials and Biomaterials*. 2007, Springer Berlin Heidelberg. p. 149-178.
4. Abou Neel, E.A., et al., *Bioactive functional materials: a perspective on phosphate-based glasses.* Journal of Materials Chemistry, 2009. **19**(6): p. 690-701.
5. Bockstaller, M.R., R.A. Mickiewicz, and E.L. Thomas, *Block Copolymer Nanocomposites: Perspectives for Tailored Functional Materials.* Advanced Materials, 2005. **17**(11): p. 1331-1349.
6. Cohen, R.E., *Block copolymers as templates for functional materials.* Current Opinion in Solid State and Materials Science, 1999. **4**(6): p. 587-590.
7. Matsukawa, K., *Development of Photo-functional Materials from Organic/Inorganic Nano-Hybrids.* Journal of Photopolymer Science and Technology, 2005. **18**(2): p. 203-210.
8. Yoon, K.B., *Organization of Zeolite Microcrystals for Production of Functional Materials.* Accounts of Chemical Research, 2006. **40**(1): p. 29-40.
9. Schöllhorn, R., *Intercalation Systems as Nanostructured Functional Materials.* Chemistry of Materials, 1996. **8**(8): p. 1747-1757.
10. Fryxell, G.E., *The synthesis of functional mesoporous materials.* Inorganic Chemistry Communications, 2006. **9**(11): p. 1141-1150.
11. Yao, W.-T. and S.-H. Yu, *Synthesis of Semiconducting Functional Materials in Solution: From II-VI Semiconductor to Inorganic–Organic Hybrid Semiconductor Nanomaterials.* Advanced Functional Materials, 2008. **18**(21): p. 3357-3366.
12. Liu, P.S. and K.M. Liang, *Review Functional materials of porous metals made by P/M, electroplating and some other techniques.* Journal of Materials Science, 2001. **36**(21): p. 5059-5072.

13. Gómez-Romero, P. and C. Sanchez, *Hybrid Materials, Functional Applications.*, in *Functional Hybrid Materials*. 2005, Wiley-VCH Verlag GmbH & Co. KGaA.
14. Sanchez, C., et al., *Applications of hybrid organic-inorganic nanocomposites.* Journal of Materials Chemistry, 2005. **15**(35-36): p. 3559-3592.
15. Sanchez, C., H. Arribart, and M.M. Giraud Guille, *Biomimetism and bioinspiration as tools for the design of innovative materials and systems.* Nat Mater, 2005. **4**(4): p. 277-288.
16. Lopez, P.J., et al., *Prospects in diatom research.* Current opinion in biotechnology, 2005. **16**(2): p. 180-186.
17. Kickelbick, G., *Introduction to Hybrid Materials*, in *Hybrid Materials*. 2007, Wiley-VCH Verlag GmbH & Co. KGaA. p. 1-48.
18. Corma, A. and H. Garcia, *Silica-Bound Homogenous Catalysts as Recoverable and Reusable Catalysts in Organic Synthesis.* Advanced Synthesis & Catalysis, 2006. **348**(12-13): p. 1391-1412.
19. Taguchi, A. and F. Schüth, *Ordered mesoporous materials in catalysis.* Microporous and Mesoporous Materials, 2005. **77**(1): p. 1-45.
20. Hartmann, M., *Ordered Mesoporous Materials for Bioadsorption and Biocatalysis.* Chemistry of Materials, 2005. **17**(18): p. 4577-4593.
21. Germain, J., J.M.J. Fréchet, and F. Svec, *Nanoporous Polymers for Hydrogen Storage.* Small, 2009. **5**(10): p. 1098-1111.
22. Czaja, A.U., N. Trukhan, and U. Muller, *Industrial applications of metal-organic frameworks.* Chemical Society Reviews, 2009. **38**(5): p. 1284-1293.
23. Baskaran, S., et al., *Low Dielectric Constant Mesoporous Silica Films Through Molecularly Templated Synthesis.* Advanced Materials, 2000. **12**(4): p. 291-294.
24. Scott, B.J., G. Wirnsberger, and G.D. Stucky, *Mesoporous and Mesostructured Materials for Optical Applications.* Chemistry of Materials, 2001. **13**(10): p. 3140-3150.
25. Armelao, L., et al., *Recent trends on nanocomposites based on Cu, Ag and Au clusters: A closer look.* Coordination Chemistry Reviews, 2006. **250**(11–12): p. 1294-1314.
26. Wang, S., et al., *Organic/inorganic hybrid sensors: A review*. Sensors and Actuators B: Chemical, 2013. **182**(0): p. 467-481.
27. Andreas Mandelis, C.C., *Physics, Chemistry and Technology of Solid State Gas Sensor Devices*. 1993: Wiley.

28. Moseley, P.T.C.A.J., *Sensor materials*. 1996, Bristol; Philadelphia: Institute of Physics Pub.
29. Pearton, S.J., et al., *Recent advances in wide bandgap semiconductor biological and gas sensors.* Progress in Materials Science, 2010. **55**(1): p. 1-59.
30. Han, X. and L.P. Naeher, *A review of traffic-related air pollution exposure assessment studies in the developing world.* Environment International, 2006. **32**(1): p. 106-120.
31. Takada, T., *A new method for gas identification using a single semiconductor sensor.* Sensors and Actuators B: Chemical, 1998. **52**(1–2): p. 45-52.
32. Esposito, R., et al., *Glucose Sensing by Time-Resolved Fluorescence of Sol-Gel Immobilized Glucose Oxidase.* Sensors, 2011. **11**(4): p. 3483-3497.
33. Geckeler, K.E.R., E, *Functional Nanomaterials*. 2006: American Scientific Publishers.
34. Mandayo, G.G., et al., *Strategies to enhance the carbon monoxide sensitivity of tin oxide thin films.* Sensors and Actuators B: Chemical, 2003. **95**(1–3): p. 90-96.
35. Allen, M.G., *Diode laser absorption sensors for gas-dynamic and combustion flows.* Meas Sci Technol, 1998. **9**(4): p. 545-62.
36. Laj, P., et al., *Measuring atmospheric composition change.* Atmospheric Environment, 2009. **43**(33): p. 5351-5414.
37. Smith, D. and P. Spanel, *The challenge of breath analysis for clinical diagnosis and therapeutic monitoring.* Analyst, 2007. **132**(5): p. 390-6.
38. P. T. Moseley, B.C.T., *Solid state gas sensors*. Solid state gas sensors. 1987.
39. Bakker, E. and M. Telting-Diaz, *Electrochemical sensors.* Anal Chem, 2002. **74**(12): p. 2781-800.
40. Capone, S., et al., *Solid state gas sensors: state of the art and future activities.* Journal of Optoelectronics and Advanced Materials, 2003. **5**(5): p. 1335-1348.
41. Moos, R., et al., *Solid State Gas Sensor Research in Germany – a Status Report.* Sensors, 2009. **9**(6): p. 4323-4365.
42. Korotcenkov, G., *Metal oxides for solid-state gas sensors: What determines our choice?* Materials Science and Engineering: B, 2007. **139**(1): p. 1-23.
43. Lackner, M., *tunable diode laser absorption spectroscopy (tdlas) in the process industries – a review*, in *Reviews in Chemical Engineering*. 2007. p. 65.

44. Wark, M., et al., *Optical gas sensing by semiconductor nanoparticles or organic dye molecules hosted in the pores of mesoporous siliceous MCM-41*. Physical Chemistry Chemical Physics, 2003. **5**(23): p. 5188-5194.
45. MacCraith, B.D., et al., *Fibre optic oxygen sensor based on fluorescence quenching of evanescent-wave excited ruthenium complexes in sol-gel derived porous coatings.* Analyst, 1993. **118**(4): p. 385-388.
46. Baron, M.G., R. Narayanaswamy, and S.C. Thorpe, *A kineto-optical method for the determination of chlorine gas.* Sensors and Actuators B: Chemical, 1995. **29**(1–3): p. 358-362.
47. F. Baldini, A.N.C., J. Homola, S. Martellucci, *Optical Chemical Sensors*. 2006: Springer. 520.
48. Elosua, C., et al., *Volatile Organic Compound Optical Fiber Sensors: A Review*. Sensors, 2006. **6**(11): p. 1440-1465.
49. Germain, M.E. and M.J. Knapp, *Optical explosives detection: from color changes to fluorescence turn-on.* Chemical Society Reviews, 2009. **38**(9): p. 2543-2555.
50. Sasaki, D.Y., et al., *Fluorescence detection of nitrogen dioxide with perylene/PMMA thin films.* Sensors and Actuators B: Chemical, 2001. **72**(1): p. 51-55.
51. Ohyama, T., et al., *Fluorescence-intensity changes in organic dyes impregnated in porous glass on exposure to NO2.* Sensors and Actuators B: Chemical, 1999. **59**(1): p. 16-20.
52. Stevens, N. and D.L. Akins, *Dye-doped inorganic/organic composite films as fluorescence sensors for methanol vapor.* Sensors and Actuators B: Chemical, 2007. **123**(1): p. 59-64.
53. Yutaka, A., *Probes and Polymers for Optical Sensing of Oxygen.* Microchimica Acta 2003. **143**(1): p. 1.
54. West, A.R., *Solid State Chemistry and its Applications*. 2003, Singapore: John Wiley & Sons.
55. Chopra, K.L., *Thin Film Phenomena*. Science. Vol. 169. 1969, New York, : McGraw-Hill. 850.
56. Albella, J.M., *Láminas delgadas y recubrimientos: preparación, propiedades y applicaciones*. 2003, Madrid: CSIC.

57. Seshan, K., *Handbook of thin film deposition processes and technique*. Vol. 2. 2002, Santa Clara, California: Intel Corporation.
58. Kundt, A., *Ueber Doppelbrechung des Lichtes in Metallschichten, welche durch Zerstäuben einer Kathode hergestellt sind.* Annalen der Physik, 1886. **263**(1): p. 59-71.
59. Kaempf, F., *Größe und Ursache der Doppelbrechung in Kundtschen Spiegeln und Erzeugung von Doppelbrechung in Metallspiegeln durch Zug.* Annalen der Physik, 1905. **321**(2): p. 308-333.
60. Maurain, C., *Dichroism, birefringence and conductibility of thin metallic laminas obtained by cathodic pulverization.* Comptes Rendus Hebdomadaires Des Seances De L Academie Des Sciences, 1906. **142**(870).
61. Helwig, H.K.a.G., *Über die Struktur schräg aufgedampfter Schichten und ihr Einfluß auf die Entwicklung submikroskopischer Oberflächenrauhigkeiten.* Optik, 1950. **6**: p. 111-124.
62. Evans, J.W., *Solc Birefringent Filter*. Journal of the Optical Society of America, 1958. **48**(3): p. 142-143.
63. Young, N.O. and J. Kowal, *Optically Active Fluorite Films.* Nature, 1959. **183**(4654): p. 104-105.
64. Smith, D.O., M.S. Cohen, and G.P. Weiss, *Oblique-Incidence Anisotropy in Evaporated Permalloy Films.* Journal of Applied Physics, 1960. **31**(10): p. 1755-1762.
65. Robbie, K., et al., *Fabrication of thin films with highly porous microstructures.* Journal of Vacuum Science & Technology A, 1995. **13**(3): p. 1032-1035.
66. Robbie, K., M.J. Brett, and A. Lakhtakia, *First thin film realization of a helicoidal bianisotropic medium.* Journal of Vacuum Science & Technology A, 1995. **13**(6): p. 2991-2993.
67. Steele, J. and M. Brett, *Nanostructure engineering in porous columnar thin films: recent advances.* Journal of Materials Science: Materials in Electronics, 2007. **18**(4): p. 367-379.
68. Hawkeye, M.M. and M.J. Brett, *Glancing angle deposition: Fabrication, properties, and applications of micro- and nanostructured thin films.* Journal of Vacuum Science & Technology A, 2007. **25**(5): p. 1317-1335.
69. Messier, R., et al., *Engineered sculptured nematic thin films.* Journal of Vacuum Science & Technology A, 1997. **15**(4): p. 2148-2152.

70. Sit, J.C., et al., *Thin Film Microstructure Control Using Glancing Angle Deposition by Sputtering.* Journal of Materials Research, 1999. **14**(04): p. 1197-1199.
71. Liu, F., et al., *The magnetic properties of cobalt films produced by glancing angle deposition.* Magnetics, IEEE Transactions on, 2000. **36**(5): p. 2939-2941.
72. Sing, S.J.G.a.K.S.W., *Adsorption, surface area and porosity*. Academic Press. 1982.
73. Harper, D.B., Drew Carey, *def: porphyrins.* The Online Etymology Dictionary, 2014.
74. Dolphin, D., *The Porphyrins*. 1978, Academic, New York.
75. Milgrom, L.R., *The Colours of Life*. 1997, OUP, Oxford.
76. Gouterman, M., *Spectra of porphyrins.* Journal of Molecular Spectroscopy, 1961. **6**(0): p. 138-163.
77. Nappa, M. and J.S. Valentine, *The influence of axial ligands on metalloporphyrin visible absorption spectra. Complexes of tetraphenylporphinatozinc.* Journal of the American Chemical Society, 1978. **100**(16): p. 5075-5080.
78. Rubio, M., et al., *Theoretical study of the electronic spectrum of magnesium-porphyrin.* The Journal of Chemical Physics, 1999. **110**(15): p. 7202-7209.
79. Wang, M.Y.R. and B.M. Hoffman, *Systematic trends in metalloporphyrin optical spectra.* Journal of the American Chemical Society, 1984. **106**(15): p. 4235-4240.
80. Whitten, D.G., I.G. Lopp, and P.D. Wildes, *Fluorescence of zinc and magnesium etioporphyrin. I. Quenching and wavelength shifts due to complex formation.* Journal of the American Chemical Society, 1968. **90**(26): p. 7196-7200.
81. Gouterman, M., *Study of the Effects of Substitution on the Absorption Spectra of Porphin.* The Journal of Chemical Physics, 1959. **30**(5): p. 1139-1161.
82. Di Natale, C., R. Paolesse, and A. D'Amico, *Metalloporphyrins based artificial olfactory receptors.* Sensors and Actuators B: Chemical, 2007. **121**(1): p. 238-246.
83. Di Natale, C., et al., *Porphyrins-based opto-electronic nose for volatile compounds detection.* Sensors and Actuators B: Chemical, 2000. **65**(1–3): p. 220-226.

84. Gulino, A., et al., *Optical pH Meter by Means of a Porphyrin Monolayer Covalently Assembled on a Molecularly Engineered Silica Surface.* Chemistry of Materials, 2005. **17**(16): p. 4043-4045.

85. Yang, R., et al., *A Selective Optode Membrane for Histidine Based on Fluorescence Enhancement of Meso−Meso-Linked Porphyrin Dimer.* Analytical Chemistry, 2002. **74**(5): p. 1088-1096.

86. Shundo, A., et al., *Nuclear Magnetic Resonance Signaling of Molecular Chiral Information Using an Achiral Reagent.* Journal of the American Chemical Society, 2009. **131**(27): p. 9494-9495.

87. Tong, Y., et al., *Sn(IV) Porphyrins as NMR Shift Reagents and Supramolecular Protecting Groups: Preparation of a Carboxylate−Catenane Porphyrin Complex.* Organic Letters, 1999. **1**(9): p. 1343-1346.

88. Zhang, Y., et al., *Fluorescent Sensor for Imidazole Derivatives Based on Monomer−Dimer Equilibrium of a Zinc Porphyrin Complex in a Polymeric Film.* Analytical Chemistry, 2004. **76**(24): p. 7336-7345.

89. Zhou, H., et al., *Pattern Recognition of Proteins Based on an Array of Functionalized Porphyrins.* Journal of the American Chemical Society, 2006. **128**(7): p. 2421-2425.

90. Zheng, W., et al., *UV–visible, fluorescence and EPR properties of porphyrins and metalloporphyrins.* Dyes and Pigments, 2008. **77**(1): p. 153-157.

91. Schenning, A.P.H.J. and E.W. Meijer, *Supramolecular electronics; nanowires from self-assembled [small pi]-conjugated systems.* Chemical Communications, 2005(26): p. 3245-3258.

92. Lidzey, D.G., et al., *Photon-Mediated Hybridization of Frenkel Excitons in Organic Semiconductor Microcavities.* Science, 2000. **288**(5471): p. 1620-1623.

93. van der Boom, T., et al., *Charge Transport in Photofunctional Nanoparticles Self-Assembled from Zinc 5,10,15,20-Tetrakis(perylenediimide)porphyrin Building Blocks.* Journal of the American Chemical Society, 2002. **124**(32): p. 9582-9590.

94. Medforth, C.J., et al., *Self-assembled porphyrin nanostructures.* Chemical Communications, 2009(47): p. 7261-7277.

95. Pasternack, R.F., et al., *Molecular complexes of nucleosides and nucleotides with a monomeric cationic porphyrin and some of its metal derivatives.* Journal of the American Chemical Society, 1985. **107**(26): p. 8179-8186.

96. Borissevitch, I.E. and S.C.M. Gandini, *Photophysical studies of excited-state characteristics of meso-tetrakis(4-N-methyl-pyridiniumyl) porphyrin bound to DNA.* Journal of Photochemistry and Photobiology B: Biology, 1998. **43**(2): p. 112-120.

97. Giovannetti, R., L. Alibabaei, and F. Pucciarelli, *Spectral and kinetic investigation on oxidation and reduction of water soluble porphyrin–manganese(III) complex.* Inorganica Chimica Acta, 2010. **363**(7): p. 1561-1567.

98. Castillero, P., et al., *Active and optically transparent tetracationic porphyrin/TiO(2) composite thin films.* ACS Appl Mater Interfaces, 2010. **2**(3): p. 712-21.

99. Ohno, O., Y. Kaizu, and H. Kobayashi, *J-aggregate formation of a water-soluble porphyrin in acidic aqueous media.* The Journal of Chemical Physics, 1993. **99**(5): p. 4128-4139.

100. van de Craats, A.M. and J.M. Warman, *The Core-Size Effect on the Mobility of Charge in Discotic Liquid Crystalline Materials.* Advanced Materials, 2001. **13**(2): p. 130-133.

101. Bohn, P.W., *Aspects of Structure and Energy Transport in Artificial Molecular Assemblies.* Annual Review of Physical Chemistry, 1993. **44**(1): p. 37-60.

102. Nüesch, F. and M. Grätzel, *H-aggregation and correlated absorption and emission of a merocyanine dye in solution, at the surface and in the solid state. A link between crystal structure and photophysical properties.* Chemical Physics, 1995. **193**(1–2): p. 1-17.

103. Czikklely, V., H.D. Forsterling, and H. Kuhn, *Extended dipole model for aggregates of dye molecules.* Chemical Physics Letters, 1970. **6**(3): p. 207-210.

104. Terazima, M., H. Shimizu, and A. Osuka, *The third-order nonlinear optical properties of porphyrin oligomers.* Journal of Applied Physics, 1997. **81**(7): p. 2946-2951.

105. Collini, E., et al., *Large third-order nonlinear optical response of porphyrin J-aggregates oriented in self-assembled thin films.* Journal of Materials Chemistry, 2006. **16**(16): p. 1573-1578.

106. Liu, Z.-B., et al., *Nonlinear Absorption and Nonlinear Refraction of Self-Assembled Porphyrins.* The Journal of Physical Chemistry B, 2006. **110**(31): p. 15140-15145.

107. Matsuzaki, Y., et al., *A Theoretical Study on the Third-Order Nonlinear Optical Properties of π-Conjugated Linear Porphyrin Arrays.* The Journal of Physical Chemistry A, 2006. **110**(14): p. 4888-4899.

108. Hasobe, T., et al., *Nanostructured assembly of porphyrin clusters for light energy conversion.* Journal of Materials Chemistry, 2003. **13**(10): p. 2515-2520.

109. Fujii, Y., et al., *pH-Dependent reversible transformation of TPPS4 anchored on mesoporous TiO2 film between monomers and J-aggregates.* Chemical Communications, 2005(24): p. 3065-3067.

110. Choi, M.-S., et al., *Fullerene-Terminated Dendritic Multiporphyrin Arrays: "Dendrimer Effects" on Photoinduced Charge Separation.* Angewandte Chemie International Edition, 2003. **42**(34): p. 4060-4063.

111. De Napoli, M., et al., *Hierarchical Porphyrin Self-Assembly in Aqueous Solution.* Journal of the American Chemical Society, 2004. **126**(19): p. 5934-5935.

112. Šišková, K., B. Vlčková, and P. Mojzeš, *Spectral detection of J-aggregates of cationic porphyrin and investigation of conditions of their formation.* Journal of Molecular Structure, 2005. **744–747**(0): p. 265-272.

113. Nikiforov, M.P., et al., *The Effect of Molecular Orientation on the Potential of Porphyrin−Metal Contacts.* Nano Letters, 2007. **8**(1): p. 110-113.

Chapter 2

Experimental set up

2.1.- Electron beam evaporation

The deposition system for the fabrication of films by Electron Beam Physical Vapour Deposition (EBPVD) was designed and assembled in the Materials Science Institute of Seville. Figure 2.1 shows a picture and a scheme of the chamber. It consists on a steel cylinder of 70 cm of height with a diameter of 55 cm. The chamber is capable of working under high vacuum conditions. At the bottom, there is an electron-bombardment evaporator system "Multihearth electron beam source", EV M-5 model, supplied by Advanced Products & Technologies GmbH (AP & T). The electron source is a tungsten filament coil which is heated by passing a electric current through it. The electrons leave the tungsten filament when their thermal energy is higher than the work function according to the principles of thermionic emission. These electrons are then accelerated by an electric field at high voltage (5 kV) and directed through a magnetic field to a crucible containing therein the material to be evaporated (target). The multihearth system has four crucibles allowing the evaporation of different materials (one by one) and their change in vacuum by using a motor.

The power source (HVP4 model) provides a maximum power of 4 kW, generating a constant voltage that produce a constant acceleration for the electron and providing a variable current to the filament. It also allows to position the beam and to focus it to sweep different areas of the crucible. These parameters permit to control the deposition rate of the evaporated material, which is monitored by a quartz crystal microbalance (QCM) calibrated for each material.

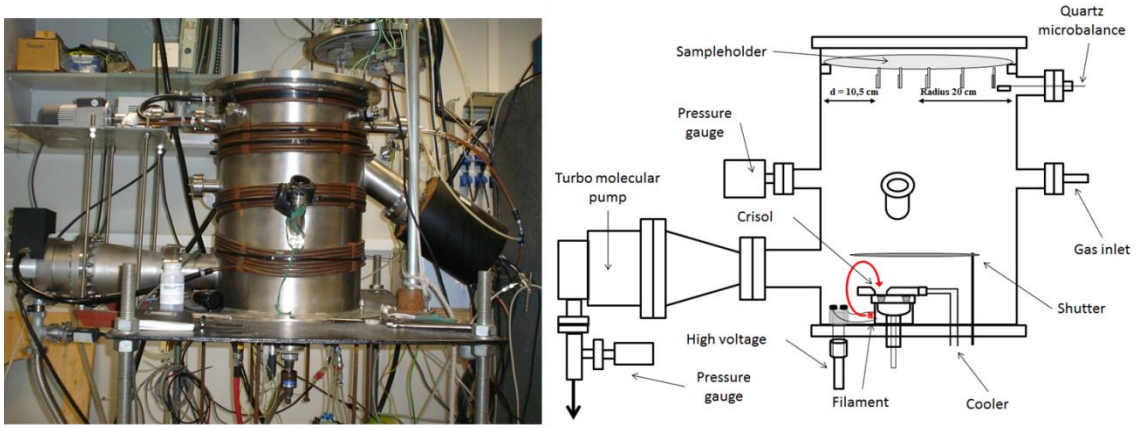

Figure 2.1.- Deposition (left) and scheme (right) of the electron-beam evaporation system.

The chamber is connected to a vacuum system comprising a rotary pump with a capacity of 6000 l/h and a turbomolecular pump of 210 l/s. These vacuum pumps are connected in series to achieve a residual vacuum pressure below 10^{-6} Torr after several hours of evacuation. A leak valve attached to the chamber permits to dose gases during the deposition. Furthermore, pressure is monitored by two different gauges that can measure a broad range from atmospheric pressure to 10^{-8} Torr.

The sample holder is placed on top of the chamber and allows the simultaneous deposition of numerous substrates. The substrates are placed vertically on a frame forming semicircles around the normal of the crucible position. A picture of the holder and a scheme is shown in figure 2.2, where the basic geometric parameters are indicated. As can be observed in the figure, the position of the samples in the holder determines the deposition angle or zenithal angle (α). This is the angle between the direction of flow of evaporated material from the crucible and the normal to the substrate surface. The sample holder allows the simultaneous deposition of a large number of samples with different deposition angles: 60º, 70º, 80º, 85º and 90º.

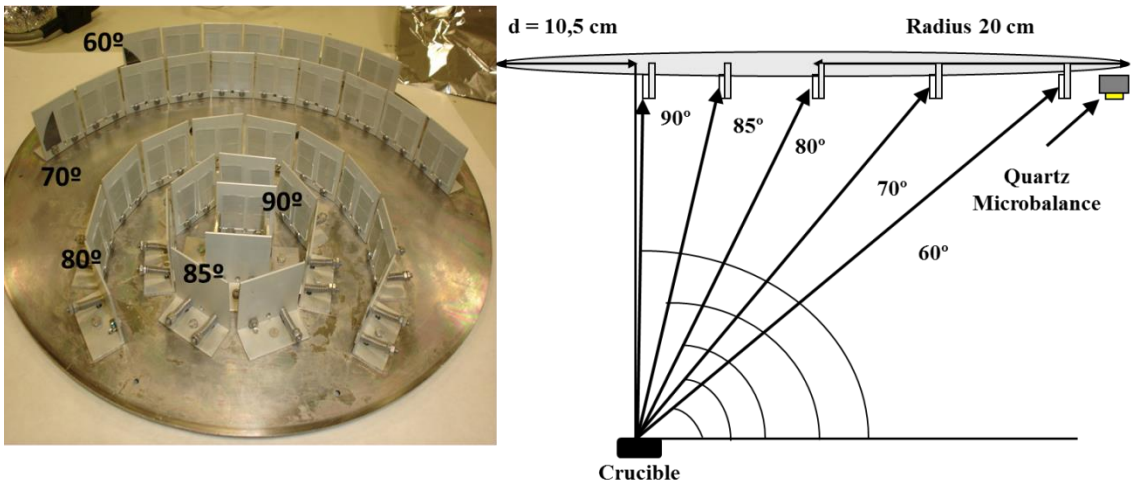

Figure 2.2.- (right) Picture of the sample holder. Quartz and silicon substrates are placed in it. (left) geometric scheme indicating the different deposition angles.

For the purpose of the present thesis, TiO_2 thin films have been fabricated in this system by using TiO as precursor material. The temperature of the substrates was lower than 373K (this upper limit is caused by the radiation from the evaporator) during the deposition under a constant flow of O_2 at the working pressure, $P_{work} = 10^{-4}$ mbar to ensure the full oxidation of the precursor. Under these conditions, amorphous and stoichiometric TiO_2 was obtained. The films growth is controlled by a Quartz Crystal

Monitor (QCM) calibrated to TiO_2. With this instrument the deposition rate was controlled between 0.5 and 1.5 Angstroms per second for a QCM thickness of 300 nm (the real thickness also depends on the zenithal angle).

The microstructure of the TiO_2 thin films deposited on silicon wafers were examined by Field Emission Scanning Electron Microscopy (FESEM), in figure 2.3 it can see top and cross sectional views micrograph of TiO_2 thin films fabricated under the conditions described before. From the images it can be observed a very open and tilted columnar morphology.

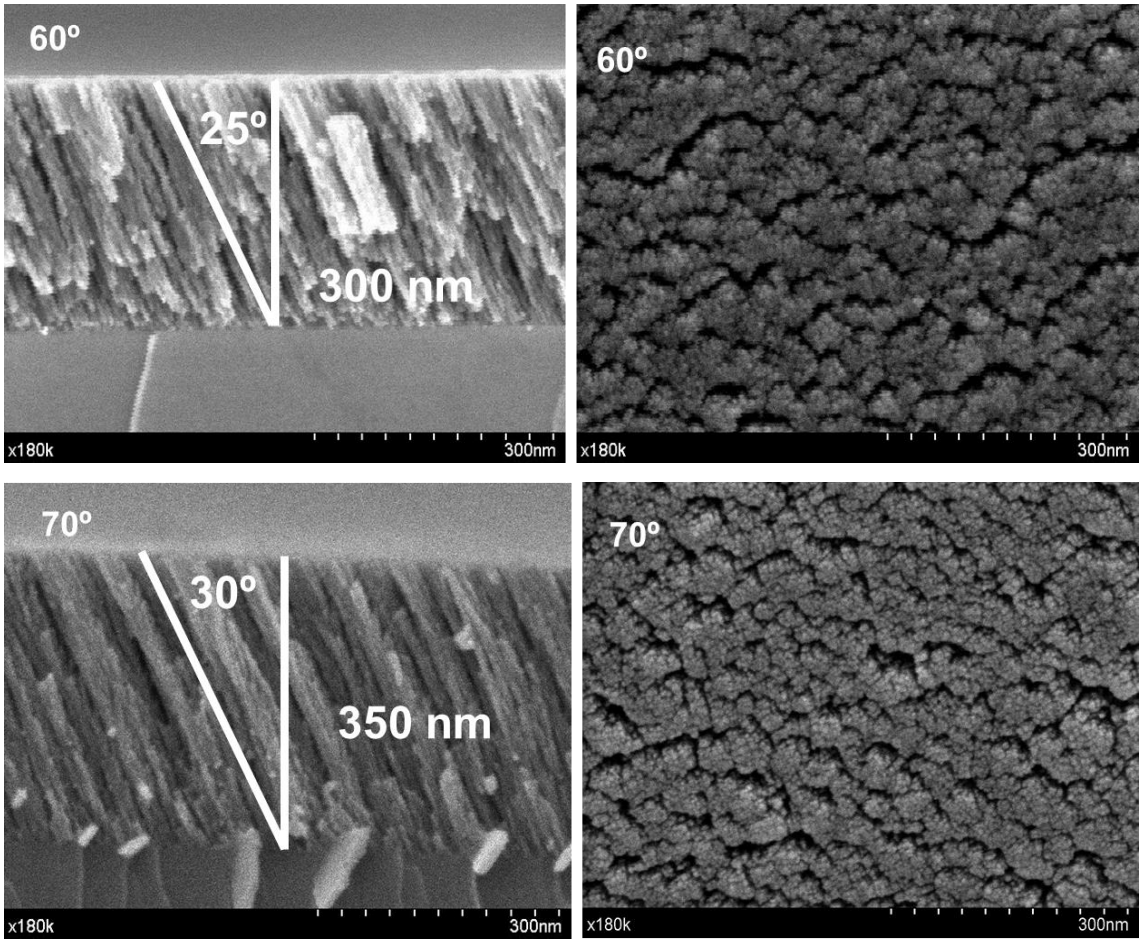

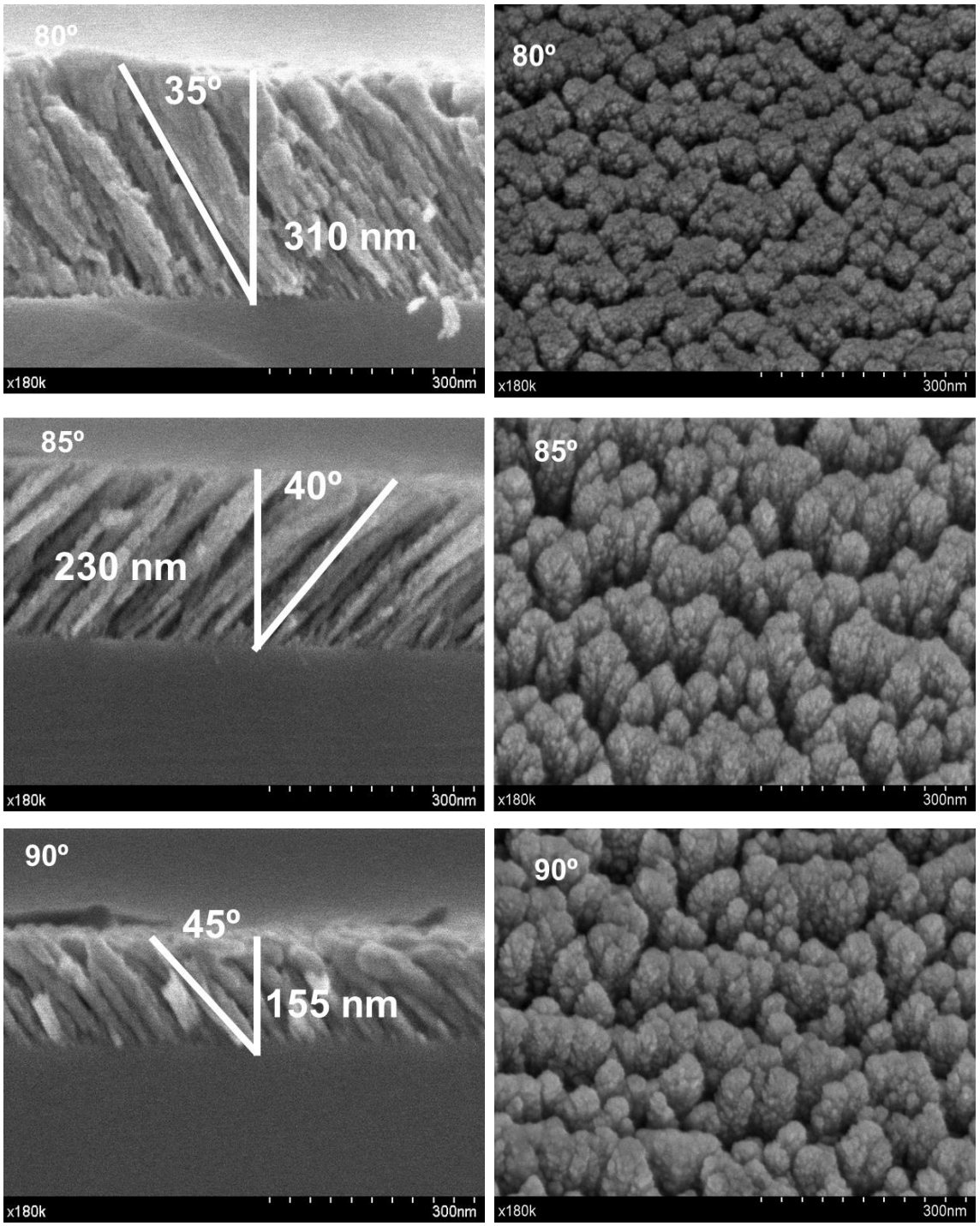

Figure 2.3.- Cross view(left) and top view (right) micrograph from the SEM of TiO_2 thin films for the indident angle of 60º, 70º, 80º, 85º and 90º.

The TiO_2 thin films deposited on glass present the transmittance spectra shown in figure 2.4. Transmittance spectrum of glass substrate is included to compare and to verify the high transparency of the films.

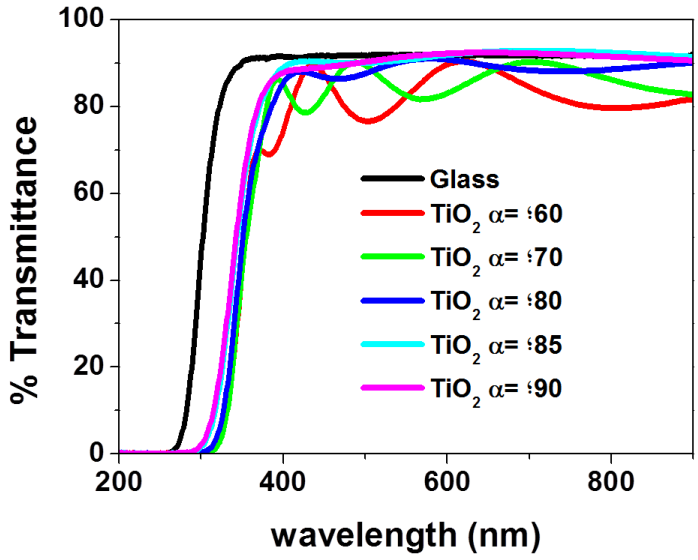

Figure 2.4.- UV Vis transmittance spectra of TiO_2 thin films for the incident angle 60º, 70º, 80º, 85º and 90º. UV Vis transmittance spectrum of glass (black line) is included to compare.

Refractive indices (n) were determined by UV-vis transmittance spectroscopy and simulated with a software analysis package based on the Sellmeier's equation. A detailed description of these experiments can be found in previous works[1, 2]. The Sellmeier's equation is a further development of the work of Cauchy and indicates the relationship between the refractive index and wavelength in the ultraviolet, visible and infrared regions for a transparent material.

$$n^2(\lambda) = 1 + \frac{(n_0^2 - 1)\lambda^2}{\lambda^2 - \lambda_o^2} \qquad \text{Sellmeier's equation}$$

Where λ_0 is the wavelength in vacuum corresponding to the natural frequency and $(n_0^2 - 1)$ is a constant proportional to the number of electrons per cubic centimeter.

The relationship between the refractive index and the porosity of the layer can be obtained from the Lorentz's relationship:

$$\frac{n_0'^2 - 1}{n_0'^2 + 2} = \frac{n_0^2 - 1}{n_0^2 + 2}(1 - P) \qquad \text{Lorentz's relationship}$$

where n_0' is the measured refractive index, n_0 is the theoretical refractive index and P is the porosity.

Table 1 show a summary of the optical characterization for the different TiO_2 thin films. It can be observed the good concordances between the simulation calculations of the thicknesses and their values from the micrographs.

		Simulation		SEM	
Incidence angle (º)	Tilt angle (º)	Thickness (nm)	Index of refraction	Thickness (nm)	**Porosity (%)**
60	65	320	1,95	300	**24**
70	60	400	1,81	350	**32**
80	55	300	1,63	310	**43**
85	50	220	1,56	230	**67**
90	45	130	1,55	150	**68**
Bulk anatase			2,49		

Table 1.- Summary of optical characterization of TiO_2 thin films for the incident angle of 60º, 70º, 80º, 85º and 90º.

The research group has a significant expertise in the fabrication of thin films using this technique. Different metal oxides, such as SiO_2, ITO and Ta_2O_5 or metals such as Ag or Cu have been successfully deposited at different angles of incidence. Further information about the characterization of these films and the ones used as host during this thesis can be found in previous works[3-6].

2.2.- Magnetron Sputtering

The deposition system employed for the fabrication of the thin films by MS technique was designed and assembled in the Materials Science Institute of Seville. Figure 2.6 displays a picture (left) and a scheme (right) of the system. The chamber consists in a steel horizontal cylinder of 40 cm of height with a diameter of 30 cm prepared to work under high vacuum conditions. On the top, there are two circular unbalanced MS heads from the company Gencoa Ltd, for a target of 50 mm of diameter. A pulsed-DC PinnaclePlus® power supply unit from Advanced Energy is connected to the MS circular heads.

The sample holder is electrically isolated and attached to an ultrahigh vacuum transfer bar, which can be placed below the MS head during the deposition or keep it away from the deposition area during the pre-sputtering. This allows to achieve a better control of the thin films. The sample holder is generally placed at a distance of 5 cm from the target and is prepared to allocate several substrates that can be deposited simultaneously. The transfer bar permits to turn the sample holder at the desirable deposition angle (α).

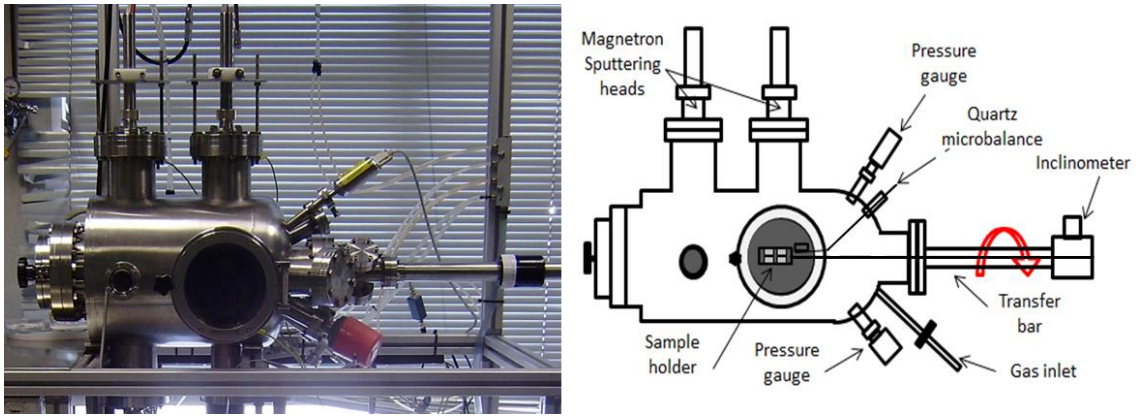

Figure 2.6.- Magnetron Sputtering deposition system. A picture (left) and scheme (right).

The chamber is connected to a vacuum system comprising a rotatory pump with a capacity of 6000 l/h and a turbomolecular pump of 210 l/s. These vacuum pumps are connected in series to achieve a residual vacuum pressure of 10^{-6} mbar after several hours of evacuation. The reactor is provided with a digital mass flow controller, IB-32 from the company Iberfluid, for each gas. The working pressure and the composition of the gas during the deposition are controlled through the mass flow controller. The

pressure of the chamber is measured by two pressure gauges that a broad range from atmospheric pressure to 10^{-8} Torr.

WO_3 and WO_3/SiO_2 thin films have been fabricated using this deposition system. WO_3 thin films have been prepared using a tungsten target of 50 mm of diameter (Goodfellow, 99.999%), the power applied was 100 watts with a pulsed frequency of 150 kHz and an off-time of 2.5 μs. WO_3/SiO_2 thin films have been prepared using a silicon target of 50 mm of diameter (Testbourne Ltd, 99.999%). On which a series of tungsten stripes (Goodfellow, 99.999%) with a width of 1.5mm and a thickness of 0.25 mm have been arranged axially as reported in the figure 2.7. The power applied was 125 watts with a pulsed frequency of 80 kHz

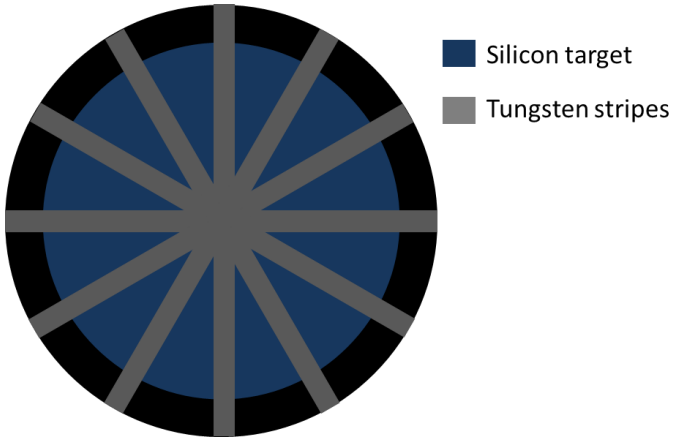

Figure 2.7.- Scheme of the stripes of tungsten over the silicon target used for WO_3/SiO_2 films.

The temperature of the substrates was always lower than 373K and the deposition was performed a constant flow of 20 sccm of Argon and 5 sccm of oxygen for WO_3 films and 40 sccm of Argon and 5 sccm of oxygen for WO_3/SiO_2 films. In both cases, the working pressure was set to 5×10^{-3} mbar. Under these evaporation conditions, amorphous and stoichiometric WO_3 and WO_3/SiO_2 thin films were obtained. Films-growth is controlled by a QCM calibrated to the density of WO_3 in the preparation of WO_3 films, or to the density parameters of SiO_2 for WO_3/SiO_2 films. The films were deposited under a deposition angle of 80º between the direction of flow of material from the target and the normal to the substrate surface achieving deposition rates between 2 and 3 angstroms per second.

The columnar WO_3 and WO_3/SiO_2 thin films were deposited on a silicon wafer and examined by Field Emission Scanning Electron Microscopy (FESEM). In figure 2.8 it can be seem top and cross sectional views of WO_3 and WO_3/SiO_2 thin films fabricated

under the conditions described before. It can be observed from the images the very open and tilted columnar morphology.

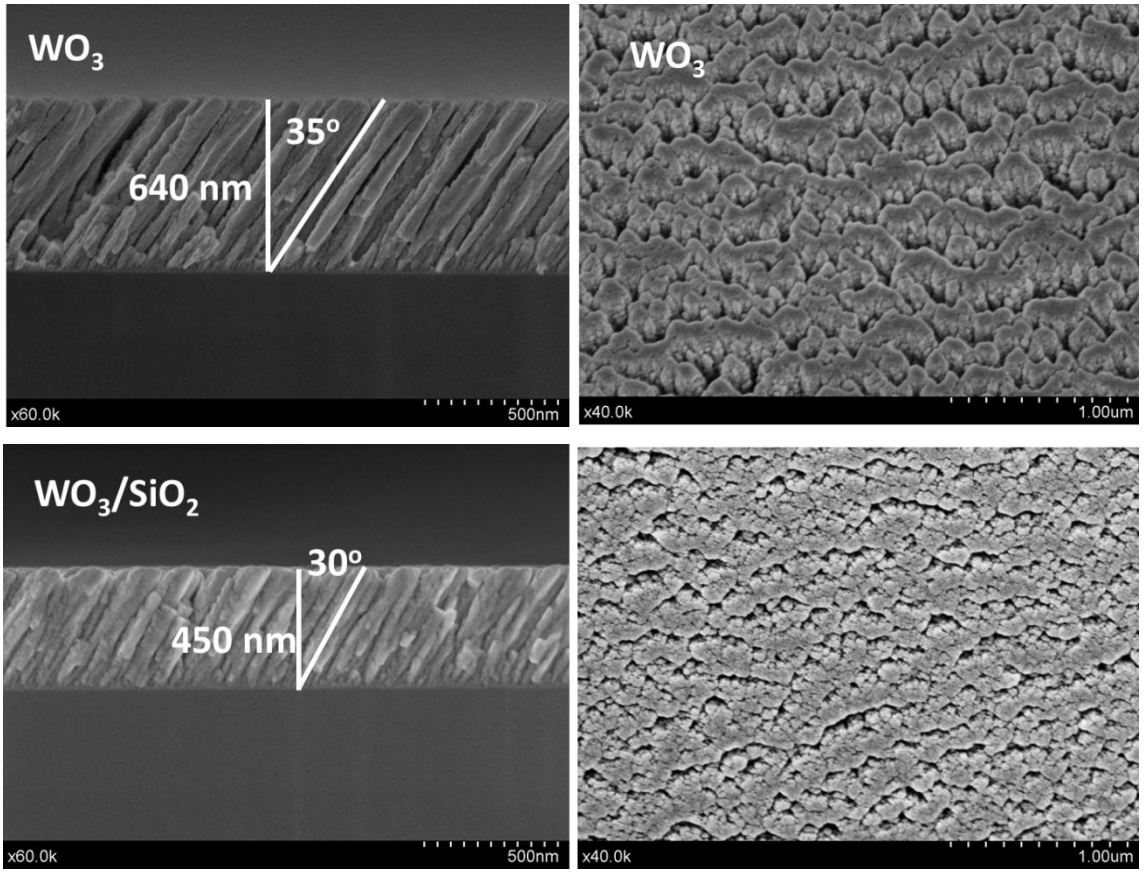

Figure 2.8.- Cross view(left) and top view (right) micrograph from the SEM of WO_3 and WO_3/SiO_2 thin films for the incident angle of 80º.

The WO_3 and WO_3/SiO_2 thin films deposited on glass present the transmittance spectra shown in figure 2.9. Transmittance spectrum of the glass substrate is included to compare and to verify the high transparency of the films.

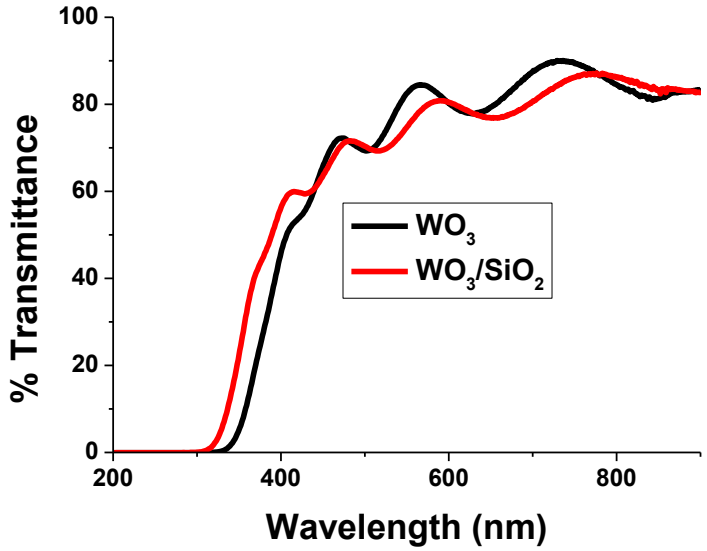

Figure 2.9.- UV Vis transmittance spectra of WO_3 and WO_3/SiO_2 thin films for the incident angle of 80º

Refractive indices (n) were determined by UV-vis transmittance spectroscopy and simulated with a software analysis package based on the Sellmeier's equation, as it has been commented before.

Table 2 is shown a summary of the optical characterization for the different WO_3 and WO_3/SiO_2 thin films. It can be observed the good concordances between the simulation calculations of the thicknesses and their values from the micrographs.

		Simulation		SEM	
Sample	Tilt angle (º)	Thickness (nm)	Index of refraction	Thickness (nm)	Porosity (%)
WO_3 porous	35	610	1,718	640	34
WO_3 bulk			2,334		
WO_3/SiO_2 porous	30	490	1,504	450	35
WO_3/SiO_2 bulk			1,867		

Table 2.- Summary of optical characterization of WO_3 and WO_3/SiO_2 thin films for the incident angle of 80º.

The group possess a big expertise in the fabrication of thin films by this technique. In fact, different metal oxides such as SiO_2, TiO_2, Cu_2O, CuO, FeO, Fe_2O_3, MoO_3 or CoO or mix metal oxides such as $Cu_xSi_yO_z$, $Ni_xSi_yO_z$, $Fe_xSi_yO_z$, $Co_xSi_yO_z$ or $Mo_xSi_yO_z$ have been deposited with different angles of incidence and different thicknesses. Futher information can be found on the characterization of these films our

previous works[7-9] and the patents “P201230048 13/01/2012” and “P201300896 30/9/2013”.

2.3.-Gas sensing system

The system to detect gases was designed and assembled in the Materials Science Institute of Seville. Figure 2.5 and 2.6 show pictures of the inner and the outer views of the sensing chamber. The chamber is a disc-shaped stainless steel of 12 cm of diameter and 2 cm of width. The chamber can reach 10^{-2} mbar with a rotatory pump to achieve a sufficiently clean atmosphere. The gas inlet is controlled by several digital mass flow controllers, from the company Bronkhorst High-Tech. The internal side of the chamber was designed to have the lowest possible volume to fill or empty the chamber quickly.

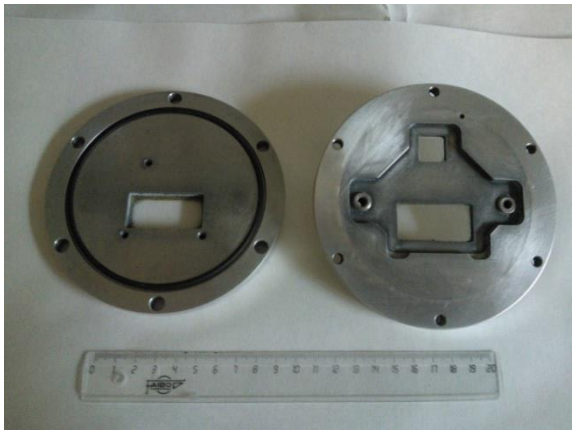

Figure 2.5.- Inner view of the gas testing chamber. Left, a window for UV-Vis spectroscopy, right, two windows for UV-Vis and Fluorescence combined spectroscopies.

Figure 2.6.- Outer view of gas testing chamber. Left, back of the chamber, right, front of the chamber. In the front of the chamber are the inlet and outlet of gases.

The chamber is held on an adjustable collimator lens holder from the company Ocean Optics and designed with two rectangular silica quart windows (one in the front and other in the back) to connect two optical fibers externally in order to measure UV-

Vis absorption spectroscopy. One of them is connected to a light source that illuminates the sample and the other one collects the light transmitted through it. Both optical fibers are connected to optical lenses to collimate the light. The samples are placed in the optical pathway, between the fibers, inside the chamber. Figure 2.7 shows how the optical fibers supported in the system. The windows for UV-Vis spectroscopy have a dimension of 4 x 2.5 cm^2 and allow to introduce two samples, one to get a reference or background and the other one to measure the UV-Vis transmittance spectrum, corrected with the reference. The chamber also has an additional square silica quartz window to measure fluorescence spectroscopy externally by an optical fiber which transports the light from the fluorimeter to the sample and, at the same time collects it to the detector. The window for fluorescence spectroscopy has a dimension of 1.5 x 1.5 cm^2 and it is placed above the rectangular windows.

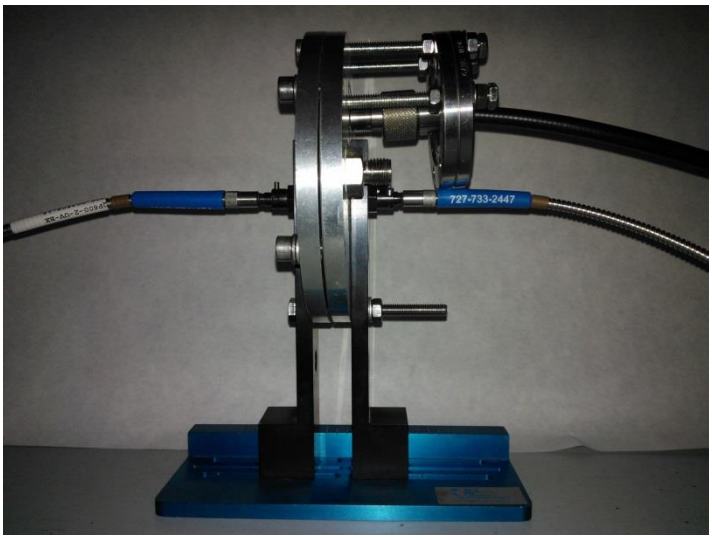

Figure 2.7.- Gas sensor chamber. The different optical fibers are placed in the chamber. The metallic and blue fibers are for UV-Vis spectroscopy and the black fiber is for fluorescence spectroscopy.

Figure 2.8 shows a picture of the samples placed inside the chamber. In the biggest window it can be observed a transparent fused silica sample (to measure the reference signal) and another sample with the composite TiO_2/porphyrin porphyrin (to measure UV-Vis transmittance). In the smallest window an additional sample with the composite TiO_2/porphyrin permits to measure fluorescence simultaneously under the same environment.

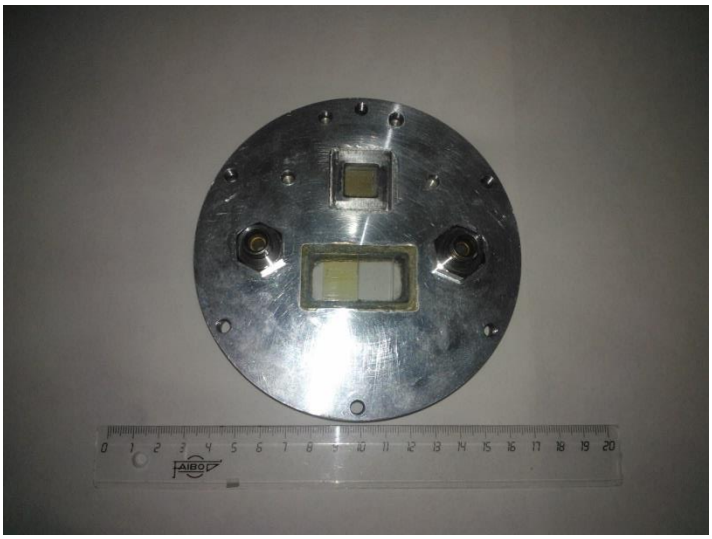

Figure 2.8.- Gas sensor chamber prepared to measure simultaneously UV-Vis transmittance and fluorescence spectroscopy. In the biggest window there are two samples, one for getting the background and the other one to UV-Vis transmittance spectroscopy of a composite of TiO_2/porphyrin. In the smallest window there is a sample of the composite TiO_2/porphyrin to measure fluorescence spectroscopy.

5.- References

1. Ana Borrás, et al., *Type of Plasmas and Microstructures of TiO2 Thin Films Prepared by Plasma Enhanced Chemical Vapor Deposition* Journal of the electrochemical society, 2007. **12**: p. 152-157.
2. Borrás, A., A. Barranco, and A.R. González-Elipe, *Design and control of porosity in oxide thin films grown by PECVD.* Journal of Materials Science, 2006. **41**(16): p. 5220-5226.
3. Rico, V., et al., *Wetting Angles on Illuminated Ta2O5 Thin Films with Controlled Nanostructure.* The Journal of Physical Chemistry C, 2009. **113**(9): p. 3775-3784.
4. Yves, G., et al., *Nanoindentation of TiO 2 thin films with different microstructures.* Journal of Physics D: Applied Physics, 2009. **42**(14): p. 145305.
5. J.R., S.-V., *Tesis doctoral: Fabricación de Láminas Delgadas Mixtas Nanoestructuradas con Funcionalidad Óptica y Fotónica*. 2010, Sevilla: US-CSIC.
6. Rico, V., *Tesis Doctoral: Láminas Delgadas de Óxidos Fotoactivos para el Aprovechamiento de Energía Solar*. 2010, Sevilla: US-CSIC.
7. Gil-Rostra, J., et al., *Electrochromic Behavior of WxSiyOz Thin Films Prepared by Reactive Magnetron Sputtering at Normal and Glancing Angles.* ACS Applied Materials & Interfaces, 2011. **4**(2): p. 628-638.
8. Garcia-Garcia, F.J.G.-R., J.; Yubero, F.; González-Elipe, A. R., *Electrochromism in WO x and W x Si y O z Thin Films Prepared by Magnetron Sputtering at Glancing Angles.* Nanoscience and Nanotechnology Letters, 2013. **5**(1): p. 89-93.
9. Gil-Rostra, J., *Tesis doctoral: Láminas Delgadas de Óxidos Mixtos con Aplicaciones Ópticas y Funcionales Obtenidas Mediante Magnetron Sputtering*. 2013, Sevilla: US-CSIC.

Chapter 3

Active and Optically Transparent Tetracationic Porphyrin/TiO_2 Composite Thin Films

Active and Optically Transparent Tetracationic Porphyrin/TiO_2 Composite Thin Films

Abstract

Fluorescent tetracationic porphyrin (TMPyP) molecules have been incorporated into optically transparent TiO_2 thin films acting as a host material. The films, with a columnar structure and open pores, were prepared by electron evaporation at glancing angles (GLAD-PVD). The open porosity of the films has been estimated by measuring a water adsorption isotherm with a quartz crystal monitor. TMPyP molecules were infiltrated in the host thin films by their immersion into water solutions at controlled values of pH.

The state of the adsorbed molecules, the infiltration efficiency, and the adsorption kinetics were assessed by analyzing the optical response of the films by UV-vis absorption and fluorescence techniques. The infiltration efficiency was directly correlated with the acidity of the medium, increasing at basic pHs as expected from simple considerations based on the concepts of the point of zero charge (PZC) developed for colloidal oxides. By a quantitative evaluation based on the analysis of the UV spectra, the infiltration process has been described by a Langmuir type adsorption isotherm and an Elovich-like kinetics. The accessibility of the infiltrated molecules in the TMPyP/TiO_2 composite films is assessed by following the changes of their optical properties when exposed to the acid vapors and their subsequent recovery with time.

Keywords:

Infiltration, TMPyP, TiO_2, GLAD-PVD, optically active composites, porous thin films.

3.1.- Introduction

Porphyrin (phy) compounds have been extensively used as active components for molecular devices such as molecular photodiodes, solar cells, and optical sensors [1-5]. Devices based on these compounds are gaining interest because of their outstanding optical and electrical properties and because of their low cost as compared with inorganic semiconductors. In particular, the direct use of this family of molecules for gas detection purposes has been recently highlighted by Rakow et al. [6] who have shown that they can be used for detecting a large variety of organic products with high selectivity and sensitivity.

Porphyrins with four positively charged pyridinium groups are interesting dyes because of their relatively low reduction potential [7], and high affinity for negatively charged solid surfaces [8]. Although in the solid state the porphyrin redox potentials maybe somewhat different from those in solution [9, 10], these two properties make these compounds suitable for the synthesis of a large variety of composite materials incorporating these molecules (e.g., as sensitizers for wide gap semiconductors, sensor devices, etc.). Fluorescent porphyrins have also been grown as monolayers films for sensing applications [11], although the design of solid-sate sensor platforms using fluorescence detection is still a challenge. In the present investigation, we have selected the fourth charged porphyrin because its incorporation into the open microstructure of TiO_2 thin films may be favored by controlling the surface charge on this oxide host by simply adjusting the pH of the medium. This approach has been previously used by us to incorporate Rhodamine molecules into this type of thin films [12, 13].

A considerable number of papers have dealt in the literature with the optical properties of the porphyrins and their incorporation into the pores of a large variety of materials, mainly in powder form [14-18]. An innovative aspect of the present work is the fact that the dye molecules are incorporated into thin films of a transparent oxide, an approach that to our knowledge has not been addressed previously in the literature. In particular, we study the incorporation of porphyrin molecules within a new type of nondispersive thin films of TiO_2 formed by a columnar microstructure with wide open voids. With respect to other dispersive solids in powder form infiltrated with dyes, the dye molecules in solution, or as monolayer films [11], we have shown that the preparation of optically transparent composite thin films provides a way for the

integration of the functional optically based properties of the porphyrin molecules into photonic structures for its direct monitoring in final fluorescence sensor devices.

The TiO_2 films used as hosts have been prepared by glancing angle physical vapor deposition (GLAD-PVD), a technique known to yield very open and porous microstructures formed by columns and, if controlled, other geometrical forms [19-23]. This method is a modification of the electron evaporator procedure used by the ophthalmic industry to cover lenses with dense optical coatings. Here the pore structure of the prepared films has been characterized by measuring water adsorption isotherms with a quartz crystal monitor, one of the few procedures available to directly measure the porosity in thin films [24].

Because of the quite open and porous microstructure of the GLAD-PVD thin films, they seem ideal for the development of photonic devices by incorporating optically active molecules or compounds. On the basis of these features, we propose here a new simple procedure for the incorporation of a tetracationic porphyrin (TMPyP) into this type of thin films and study their optical behavior as a function of the variables of the process. Within this context, we first present a phenomenological study of the adsorption equilibrium and kinetic control of the infiltration process. Second, we investigate the optical and spectroscopic properties of the TMPyP/TiO_2 composite thin films with the purpose of ascertaining the state of the molecule and the fluorescence efficiency of the films. Finally, the accessibility of the TMPyP/TiO_2 films to gaseous compounds from the environment and the possibility of following the optical changes of the films are checked by their exposure to acid vapors from a HCl solution. The fact that both the UV-vis and fluorescence spectra of the TMPyP/TiO_2 films are reversibly modified sustains that the high porosity of the composites ensures the accessibility of the infiltrated molecules to gaseous compounds from the environment and the reversibility of this process, two conditions that are necessary (although not sufficient) for the preparation of optical sensors.

3.2.-Materials and methods

Preparation of TiO_2 Thin Films.

TMPyP/TiO_2 composites were prepared by using porous TiO_2 thin films as host materials. For this purpose, transparent and amorphous films were prepared by GLAD-PVD at room temperature on quartz and silicon substrates. The glancing geometry produces films with a tilted columnar microstructure [19, 23]. A characteristic of these films is that they are very porous and, therefore, are characterized by relatively low refractive index values. For the present work the substrates were placed at an angle of 70° with respect to the evaporator source. The films had a thickness of approximately 350 nm.

TiO_2 Thin Film Characterization.

The microstructure of the TiO_2 thin films deposited on a silicon wafer was examined by field emission scanning electron microscopy (FESEM) in a Hitachi S5200 microscope. Cross-sectional views were obtained by cleaving the silicon substrates.

Refractive indices (*n*) were determined by UV-vis Absorption Spectroscopy. A detailed description of these experiments can be found in previous works [25] and additional data are gathered in the Supporting Information, Figure S1.

Because of the extraordinary small amount of material available in the prepared TiO_2 thin films, determination of porosity of this kind of materials is not straightforward by the classical BET methods based on the adsorption of gases (N_2, Kr, etc.) at their condensation temperature [26]. The commercial apparatus intended for this purpose uses glass containers which are not easily adaptable to thin films deposited on a rigid substrate, facing in addition the problem of the small amount of porous material available for the measurement. To overcome this problem, we have developed a new method based on the use of a quartz crystal monitor (QCM) and the measurement of water adsorption isotherms at room temperature [24]. A full account of the experimental method and the procedure used to extract pore size distributions can be found in this previous paper.

Infiltration of Dye Molecules into TiO_2 Porous Films.

5,10,15,20-Tetrakis(1-methyl-4-pyridyl)-21H,23H-porphyrin(TMPyP, Aldrich) was used without further purification. Unless otherwise stated, a 1 × 10-5 M solution of

the dye in water at controlled values of pH was used for these experiments. All other reagents were Merck a.g. and used as supplied. Ultrapure water from a Millipore Milli-Q-Plus system was used throughout. A scheme of the structure of the TMPyP molecule is presented in Figure 1.

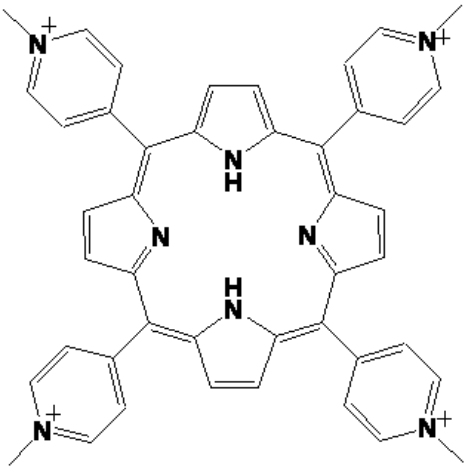

Figure 1.- *Schematic representation of the structure of the TMPyP molecular ion*

The pH of the solution was controlled between 1.9 and 10.9 by adding defined amounts of HCl or NaOH. The TiO_2 films were immersed in one of these solutions and maintained there for 1 h, except for the kinetics study. Afterward, the samples were taken out from the solution and washed with water at the same pH. With this washing, any dye molecule that is not incorporated into the thin films is removed from their surface. The films were then dried in a two steps process: first by blowing nitrogen onto their surfaces for 5 min and then by a heating at 110 °C during 1 h. After these treatments, the composite thin films presented the characteristic yellowish color of porphyrin thin films. The intensity of the color changed with the pH of the solution, a feature that pointed out that the dye adsorption degree is dependent on this parameter.

Determination of Optical Properties of the TMPyP/TiO_2 Composite Thin Films.

UV-visible spectra of the composites (TMPyP/TiO_2) films were recorded on a Cary100 Conc UV-visible spectrophotometer. Spectra are presented in absorbance after subtracting a spectrum of the TiO_2 substrate. This is an important step of the data treatment protocol to remove the interference oscillations characteristic of a thin film

with a higher refraction index than the substrate (see the Supporting Information, Figure S1). In our case, this procedure is necessary to evidence some small features of the spectra of the TMPyP molecules (i.e., the so-called Q bands, see the next section). Spectra of the films were also measured with polarized light (s and p) at 0, 30, 45, 60, and 90° of incidence angle. All the experiments were carried out at least four times.

Fluorescence spectra of the composite TMPyP/TiO_2 films were recorded in a Jobin-Yvon Fluorolog3 spectrofluorometer using grids of 2 nm for the excitation and 4 nm for emission. Depending on the samples, the fluorescence spectra were excited with radiation of 430 nm and recorded in the front-face configuration.

The amount of dye molecules incorporated into the films was assessed after desorption from the film by its prolonged stirring in a 3 M KCl aqueous solution until total film discoloration. This procedure leads to the replacement of the porphyrin molecules incorporated into the TiO_2 host thin film by K+ ions. The dye solutions resulting from this stirring were measured by optical absorption spectroscopy and the absorption intensity compared with the data of a calibration curve obtained from different reference solutions of the dye.

The amount of TMPyP incorporated into the films was expressed as an equivalent surface concentration of porphyrin (Γ). This Γ was calculated as

$$\Gamma = \frac{(Abs/\varepsilon l)V_{sol}}{Area_{film}} \qquad (1)$$

where Abs is the absorbance of the solution measured after desorption (in the maxima of Soret band at 423 nm [27], ε the extinction coefficient of the dye, l the optical pass length, V_{Sol} the volume of the 3 M KCl aqueous solution used to the desorption and $Area_{film}$ the area of the film employed.

A more straightforward way to ascertain the amount of infiltrated TMPyP molecules is the use of the Lambert-Beer law for two-dimensional systems [28]. Using this method, the surface concentration Γ can be calculated by

$$\Gamma = \frac{\int_{band} Abs_{film} d\lambda}{10^3 \int_{band} \varepsilon d\lambda} \qquad (2)$$

where Abs film is the absorbance directly measured in the composite film. In eq 2, we compare the area under the Soret band in the spectra for the composite films with that in solution. This is due to the spectral alterations (peak shifting and broadening) observed in our films that are usually induced by molecular association and/or conformation changes in the infiltrated TMPyP molecules [28-30]. Details on the validity of this method can be found in the Supporting Information, S2. It should be noted that the use of this method allow a more direct estimation of Γ avoiding the desorption procedure. The surface concentration data reported in this paper have been estimated according to eq 2 and using the desorption method as a reference.

3.3.- Results and discussion

TiO_2 Thin Film Microstructure.

Figure 2 shows FESEM normal and cross-section images corresponding to TiO_2 thin films prepared by GLAD-PVD at an angle of 70° with respect to the evaporation source. The angle formed by the columns and the substrate for the 70° as evaporation angle was approximately of 60°, as shown in the image. Films of this kind have been used as host material for the different adsorption/desorption experiments discussed in the next sections. The TiO_2 thin films are highly porous as deduced from the FESEM micrographs in Figure 2 and from the value of their refraction index, estimated as 1.79 (see the Supporting Information, Figure S1). This value is much smaller than that corresponding to the bulk material (i.e., 2.49 for TiO_2 in the form of anatase) and is a clear proof of the high porosity of the film, as previously shown for other similar nanostructures [31]. A closer inspection of Figure 2 reveals that the observed void apertures are in the form of mesopores (i.e., pores larger than 2 nm) extending from the surface up to the bottom of the film. In principle, this should facilitate the accessibility of large molecules like porphyrins during the composite preparation and improves subsequent applications that would require a fast diffusion of target molecules through the film structure.

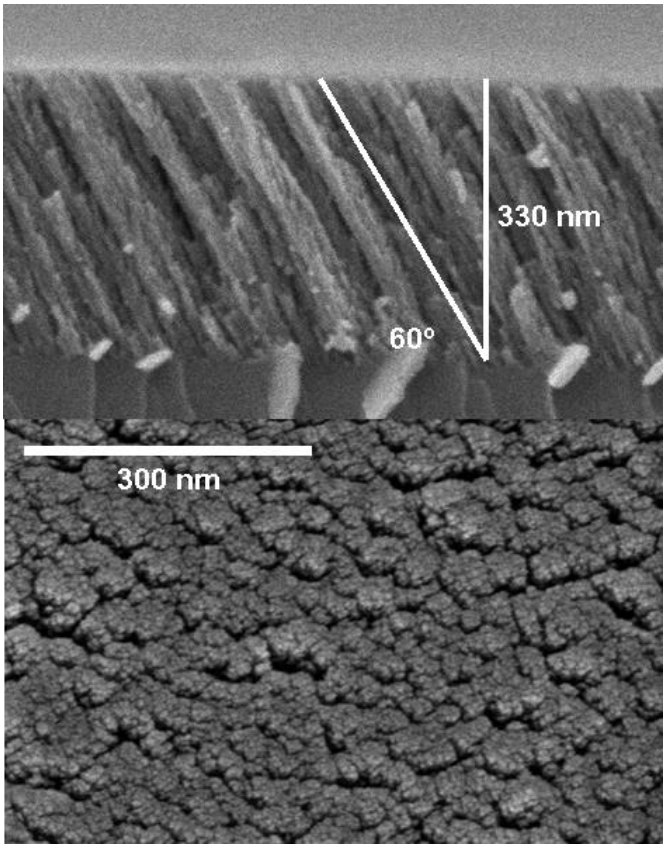

Figure.2.- *Cross section and planar views of the TiO_2 thin films used as host of TMPyP molecules.*

For a proper characterization of the films, it is important to have a direct assessment of the porosity of the films. Figure 3 (top) shows the water adsorption/desorption isotherms measured with a QCM according to the procedure described in ref 24. It is worth noting in this plot that some water incorporated in the pores of the films during the first adsorption cycle remained irreversibly adsorbed after desorption. This water is mainly filling micropores and its removal requires to heat the film at moderate temperatures (i.e., t > 110 °C). This result suggests that the pores of the TMPyP/TiO_2 composite films must be partially filled with condensed water from the atmosphere and/or residual water from the solutions where the immersion experiments were carried out. Drying either by flowing nitrogen onto the surface of the films or by heating the films at 110 °C must contribute to removal of this water.

From the analysis of these isotherms, it is also possible to extract the corresponding pore size distribution curves [24]. Figure 3 (bottom) shows the corresponding curves in the range $2r$ > 2 nm where the Kelvin equation for capillary condensation is applicable. From them, it is possible to conclude that in these GLAD-PVD thin films there is a continuous variation in the pore sizes in the whole range from

micropores (pores diameter < 2 nm) to mesopores (pore diameter > 2 nm). An evaluation based on the t-plot methodology [32] yields as a result that 30% of pores consist of micropores. The pore size distribution curves also indicate the existence of mesopores with pore diameters comprised between 2 and 6 nm. Pores as large as 14 nm are also present in the film. After evaluation of the total water adsorption, a total pore volume of 49% can be estimated for these films.

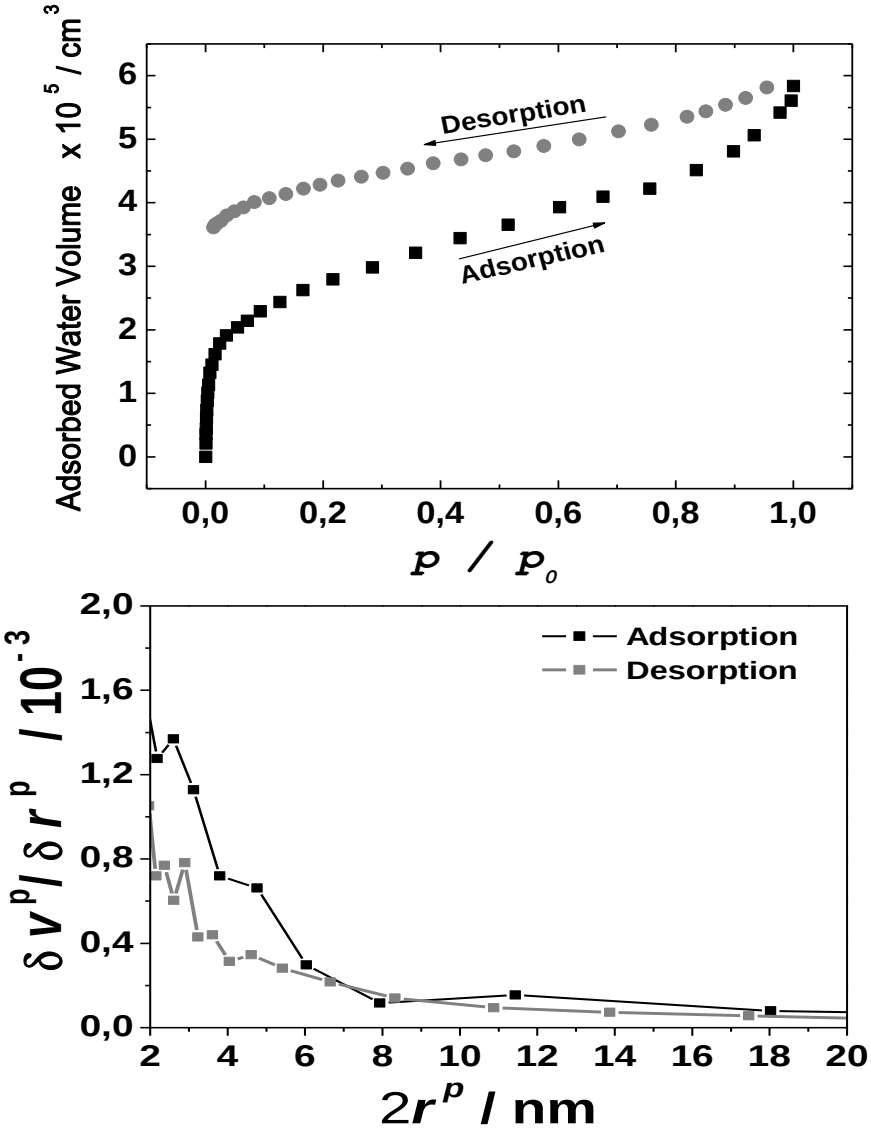

Figure 3.- *(Top) water adsorption and desorption isotherms of the films measured with a QCM. (Bottom) Pore size distribution curves derived from the adsorption isotherms.*

UV-Vis Absorption Spectra of TMPyP/TiO_2 Composite Thin Films.

Effective infiltration of the dye into the columnar microstructure of the films is achieved by controlling the pH of the solution. This can be directly deduced from Figure 4 showing the spectrum of TMPyP in water solution and of this molecule incorporated into the columnar film by infiltration at pH 6.9 and subsequent drying, first by blowing nitrogen and then by heating at 110°C. Similar results were obtained for other pHs. All the spectra exhibit the typical strong Soret band of this molecule located in the region 400-450 nm along with the four weak Q bands in the range 500-650 nm [27]. However, the maximum absorption of the TMPyP infiltrated into the transparent TiO_2 thin films is 14 nm red-shifted and broadened with respect to the water solution spectrum whose maximum appears at 423 nm. This last value for the wavelength of the *Soret* band in water solution coincides with that found by other authors [27, 33, 34]. According to Figure 4, the overall shift in the position of the Soret band in the TMPyP/TiO_2 composites occurs in two stages, following the two successive drying steps of the preparation protocol. First, after blowing nitrogen onto the sample, there is a shift of around 7 nm with respect to the position of the band for the TMPyP in water solution. A second shift by 7 nm then takes place after the samples are heated at 110 °C.

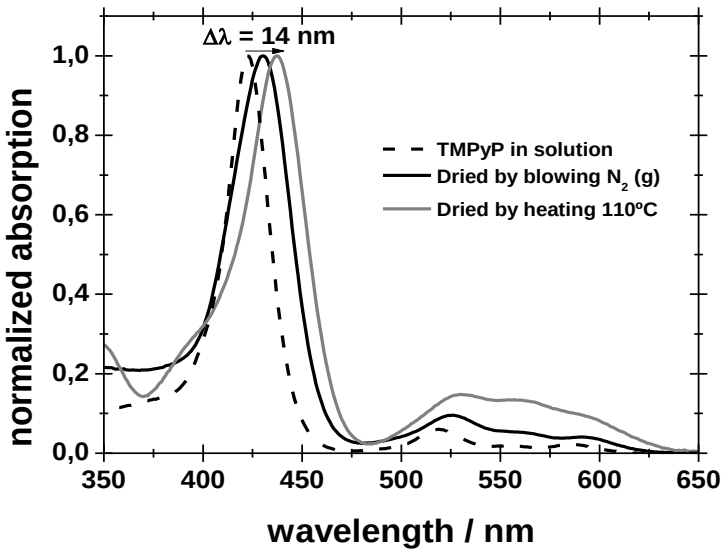

Figure 4.- *UV-visible absorption spectra recorded for the TMPyP in aqueous solution, and in the composite TMPyP-TiO_2 thin films at the different steps of the preparation protocol.*

The shifting and broadening of the Soret band is a usual phenomenon when porphyrins are incorporated into solids or, under specific conditions, in solution. In particular, a red shift has been observed for TMPyP when adsorbed in a number of host materials. This shift has been related with different physical and/or chemical changes in

the porphyrin molecular structure. Thus, Chernia et al. [29] proposed a flattening of the porphyrin molecule (through its charged peripheral methylpyridyl groups) to explain red shifts of 30 and 60 nm for the dye the adsorption and intercalation, respectively, in the clay mineral Laponite. Also, protonation of the porphyrin ring (imino nitrogens) has been suggested for soda-lime glass coated with TMPyP-doped silica solgels [35]. In this case the Soret band shifted from 423 to 435 nm, although the main changes affected the Q-band region where the original four bands turned into two bands due to the higher molecular symmetry (*D*4*h*) and the degeneration of the excited state of the protonated porphyrin. In our case, no changes in the number of Q bands are observed, suggesting the absence of significant structural modifications in the infiltrated porphyrins that should maintain their original *D*2*h* molecular symmetry.

Another possible explanation for spectral red shift of TMPyP is the formation of J-aggregates (e.g., dimers) through an appropriate compensation of the peripheral positive charges to avoid repulsion. This intermolecular interaction between the porphyrin rings has been proposed for TMPyP in aqueous solution through ion-pair interactions with four BH4 - anions [34]. Further structural details have been given for Langmuir-Blodgett (LB) films of TMPyP attached to a carboxylic calixarene matrix where a compensation of charges between the two components has been demonstrated [28]. We think that the initial shift of 7 nm with respect to the water solution can be attributed to a change in the environment of monomeric porphyrin molecules due to their anchoring onto the surface of TiO_2. The additional shift to 437 nm, found after heating at 110 °C, coincides with the elimination of the hydration water condensed in the pores (see the adsorption isotherm in Figure 3), and points to additional changes in the molecular/electronic structure related with the hydration state of the molecules. Further discussion on this point will be presented below in section 6 dealing with the fluorescence behavior of the films.

Because of the tilted microstructure of the columnar TiO_2 thin films, it might happen that the adsorbed dye molecules exhibit a preferred orientation along the tilting angle of the columns. To clarify this point, we have analyzed the samples by using UV-vis with s and p polarized light for different angles of incidence. The result of this analysis shows almost coincident spectra in all cases, indicating that the porphyrin molecules are randomly oriented in the film (see the Supporting Information, Figure S3).

pH Dependence and TMPyP Infiltration Capacity.

The amount of TMPyP molecules that can be infiltrated into the columnar TiO_2 thin film was dependent on the pH, the immersion time, and the porphyrin concentration in the solution employed to carry out the infiltration experiments. In this section, we will discuss the effect of pH in the infiltration efficiency. Figure 5 (top) shows a series of UV-vis absorption spectra recorded for thin films with a similar thickness immersed for one hour in a 1×10^{-5} M water solution of TMPyP at increasing pHs. Figure 5 (middle) shows an image taken for the composite thin films prepared at the indicated pHs and a 4×10^{-5} M water solution of this dye molecule. It is important to note that the cuvette used to keep the dye solution had a thickness of 1 mm and that the total number of molecules in the optical path was within the same order of magnitude that the number of molecules incorporated into the composite film prepared at pH 9.6. From the evolution of the intensities of these spectra, it is apparent that the adsorption efficiency is directly correlated with the acidity of the medium, increasing with the pH. Another feature that can be observed in Figure 5 (top) is the very similar shape of all spectra, indicating that there is no significant change in the adsorption and/or aggregation state of the TMPyP molecules when their amount into the film increases as an effect of the pH.

A quantitative assessment of the pH dependence of the amount of TMPyP molecules incorporated into the TiO_2 films is depicted in the Figure 5 (bottom), where the absorption intensity in the maxima of the Soret band and the surface concentration of dye molecules are plotted against the pH of the solution. The curves show that almost no infiltration occurs at pHs lower that 3.5. Some infiltration takes place in the range 3.5-5.5, whereas a sharp infiltration onset starts at pH 4.9 to reach a maximum at a pH of 10. From this value on, a slight decrease in the infiltration capacity is observed.

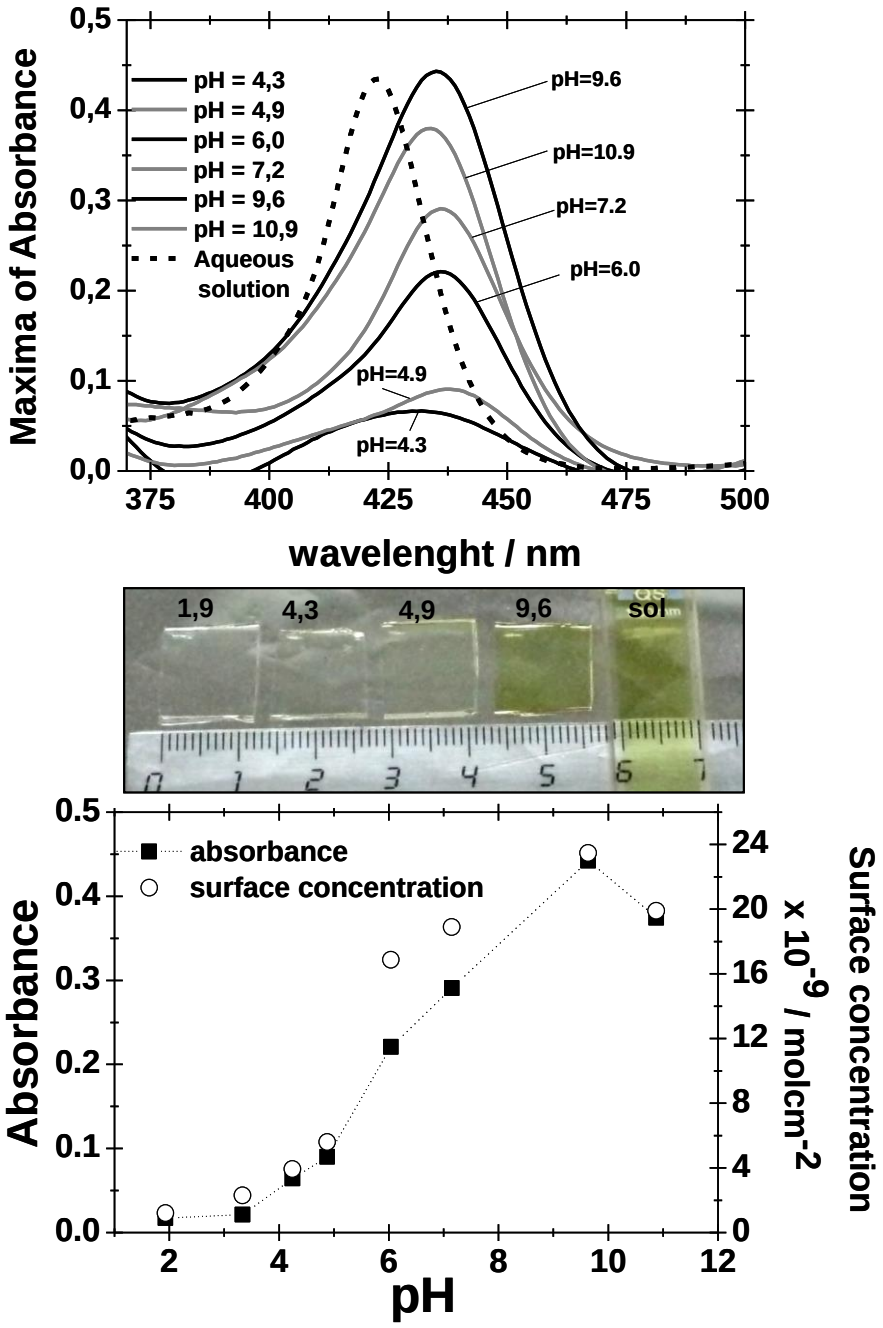

Figure 5.- *(Top) Absorption spectra for a series of composite TMPyP-TiO_2 thin films prepared by infiltration from aqueous solutions at different pHs as indicated. The figure shows the Soret Band. (Bottom) Evolution of the absorption intensity of the spectra and the amount of molecules infiltrated into the film as a function of the pH during the infiltration procedure. (Middle) Images taken for actual films prepared at the indicated pHs and a 4 ·10^{-5} M water solution.*

A similar tendency has been previously reported by us for Rhodamine-6G dye molecules incorporated into columnar TiO_2 thin films [12]. This behavior was explained

with simple considerations based on the concepts of the point of zero charge (PZC) in colloidal oxides [36, 37]. According to the point of zero charge (PZC) theory of colloids, immersion of an oxide at a pH higher than its PZC leads to the development of a negative charge on its surface by dissociation of the -OH surface groups. This charge is compensated by cations in the double layer of charge.

The fact that a significant infiltration of TMPyP molecules into the TiO_2 thin films only occurs for pHs equal or higher than 5.5 (i.e., close to its point of zero charge, PZC) [36, 37] indicates that incorporation the of dye molecules into the pores of the thin films is favored when there is an excess of negative charge distributed onto its internal surface. Such electrostatic interaction has been also claimed for other related composite systems [38]. As the pH increases, the amount of negative charges on the TiO_2 surface increases, and subsequently the amount of required positive charges (dye molecules) to compensate this negative charge invariably grows. Incorporation stops at a pH of about 11, where the amount of adsorbed TMPyP molecules slightly decreases. The observed pH dependence confirms the electrostatic nature of the TMPyP/TiO_2 interaction in the composite films.

Adsorption Equilibrium.

Besides pH, another important factor affecting the infiltration capacity of the columnar films is the concentration of the dye in the original solution. Different samples have been prepared by changing this parameter during the preparation. Figure 6 depicts, for pH 6.0 and a 1 h of infiltration time, the surface concentration (Γ) of the dye in the different films for increasing concentrations in the water solutions used for the infiltration. It is clear that the amount of incorporated porphyrin molecules increases when increasing the solution concentration. For small concentrations, the infiltration capacity is already high and sharply increases to reach a high value at a solution concentration of around 1×10^{-5} M. For more concentrated solutions, the film starts to become saturated. A similar behavior was found for other pHs in the range comprised between 5 and 10, with the saturation value following a tendency similar to that in Figure 5 corresponding to a dye concentration of 1×10^{-5} M.

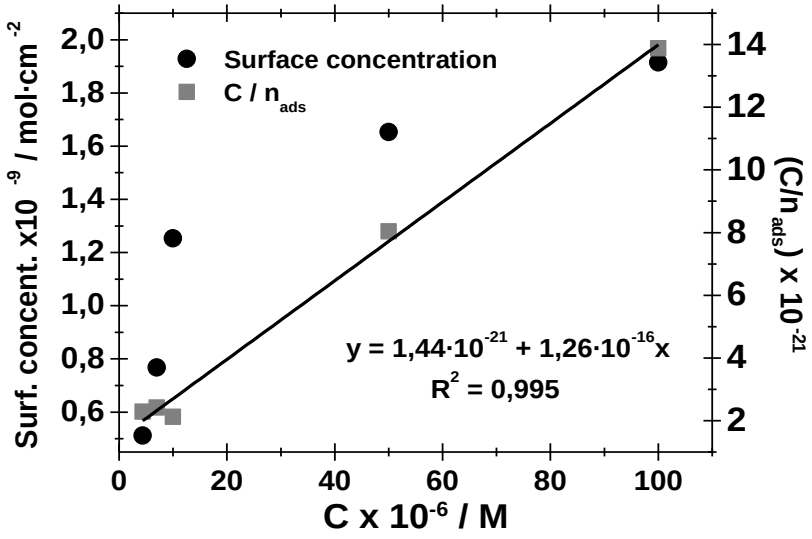

Figure 6.- *Langmuir adsorption plots for a TMPyP infiltration into TiO_2 thin films.*

A better picture for the concentration dependence of the infiltration process can be obtained by applying an isotherm model to the data points in Figure 6 [39]. The Langmuir adsorption isotherm [40] has been successfully used to account for the adsorption of different types of molecules either from gas or liquid media onto different solid materials [41-43]. The Langmuir adsorption isotherm can be expressed by

$$\frac{n_{ads}}{N_S} = \frac{\lambda c}{1+\lambda c} \qquad (3)$$

where n_{ads} is the number of the adsorbed molecules, N_S is the number of adsorption sites available on the TiO_2 surface, λ is a constant relating to the adsorption capacity of TMPyP, and c is the concentration of the dye in solution.

Rearrangement of eq 3 leads to the linear form of the Langmuir adsorption isotherm, where a plot of c/n_{ads} versus c should yield a straight line if the data points actually follow the Langmuir model. This plot has been added in Figure 6 and shows the actual number of adsorbed porphyrin molecules (n_{ads}) as a function of the dye concentration in solution. The straight line obtained indicates that a Langmuir adsorption provides a good description of the TMPyP/TiO_2 interaction during the infiltration process. According to the basic assumptions of the Langmuir model, one can conclude the following features as characteristics of the adsorption and infiltration

process: (i) the adsorption energy of all TMPyP molecules incorporated into the film is quite similar; (ii) there is a limited number of adsorption sites at a given pH; (iii) one of these sites, once occupied by a molecule, cannot contribute to an additional incorporation of TMPyP.

Adsorption Kinetics.

The infiltration of the TMPyP molecules into the columnar TiO_2 films is a time dependent process. Figure 7 shows the time evolution of the porphyrin surface concentration Γ as it becomes incorporated into a 350 nm thick TiO_2 film at a pH of the solution of 6.9 and a solution concentration of 1×10^{-5} M. The curve defined by the different data points can be divided in two parts, a first one characterized by a fast growth of the amount of infiltrated molecules followed by a much slower process where the film is approaching saturation.

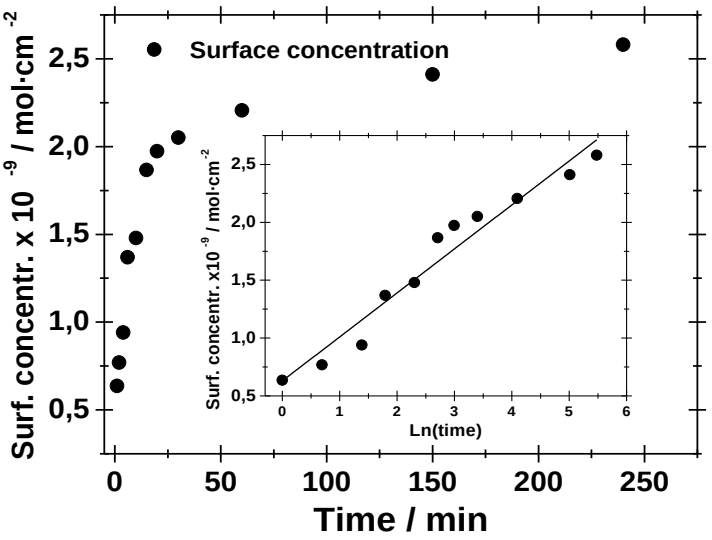

Figure 7.- *Kinetic Adsorption experiments obtained by desorption. All the experiments were carried out at least four times.*

To further characterize the infiltration process, we have tried to adjust the experimental points in Figure 7 with different kinetic models of adsorption. It was found that an Elovich kinetic model [44] fitted well the experimental points [45]. According to the integrated form of the Elovich equation, typically used in

chemisorption studies, the evolution of the surface coverage Θ as a function of time, *t*, is given by

$$\Theta = \left(\frac{1}{\beta}\right)\ln(t) + K \qquad (4)$$

where β and K are constants. Equation 4 indicates that there is an exponential decrease of the rate of the surface adsorption as the coverage of the surface increases. Using Γ as an equivalent magnitude to Θ, we have found a good fitting to the model as reported in the inset of Figure 7, where the points define an almost linear relationship over the entire range of times studied. This indicates that the probability of adsorption of a TMPyP molecule decreases exponentially with the number of occupied adsorption sites (or adsorbed TMPyP molecules) on the surface of the columnar TiO_2 structure. Moreover, the good fitting with the Elovich equation reveals that the TiO_2 columnar microstructure not only exhibits a very good infiltration capacity but also an excellent accessibility of the incoming porphyrin molecules to the active adsorption sites.

Fluorescence Behavior of TMPyP/TiO_2 Composite Films.

Figure 8 shows a representation of the normalized fluorescence spectra recorded for the films whose absorption spectra as a function of the pH are reported in Figure 5. Spectra of ethanol and aqueous TMPyP 1×10^{-5} M solutions have been included for comparison. The ethanol solution presents two well-differentiated bands corresponding to the degeneracy of the lowest singlet configuration of the TMPyP [46]. These two bands, Q(0,0) and Q(0,1), are centered approximately at 654 and 716 nm. In the water solution, the bands appear at 666 and 704 nm and are less resolved than in ethanol. This difference has been attributed to a change in the resonance interaction between the pyridinium group and the π system of the porphyrin macrocycle because of the polarity of the media [47]. For aqueous solutions, this resonance interaction increases and results in an overlapping between the two bands [27, 47].

The shape of the spectra in Figure 8 of the TMPyP/TiO_2 films as a function of the infiltration pH differs from that of the aqueous solution and is similar to that of the ethanol solution. This supports a significant change in the conformation of the molecule with respect to the aqueous solution, very likely because of its interaction with the TiO_2 surface. A closer look to these spectra reveals that the Q(0,0) band gradually shifts from 655 nm at a pH 4.3 to 660 nm at a pH 10.9, whereas the Q(0,1) band appears fixed at

719 nm for all the pHs. It is also visible that the intensity ratio of these two bands changes progressively with the infiltration pH from a value of 0.48 (pH 4.3) to 0.61 (pH 10.9). Spectral changes depicting similar tendencies can be evidenced when comparing the spectra of TMPyP in aqueous solutions or in solid media [47, 48]. These spectral changes, usually more pronounced in liquid solutions than in solids, have been related with changes in the conformation of the molecule and found to be very much dependent on the dielectric constant of the surrounding medium [47]. The fact that in our films the magnitude of the changes with the pH is relatively small suggests that the conformational changes with the pH are not very pronounced and that the TMPyP molecules, although anchored onto the surface of TiO_2, are not totally surrounded by this high dielectric constant material.

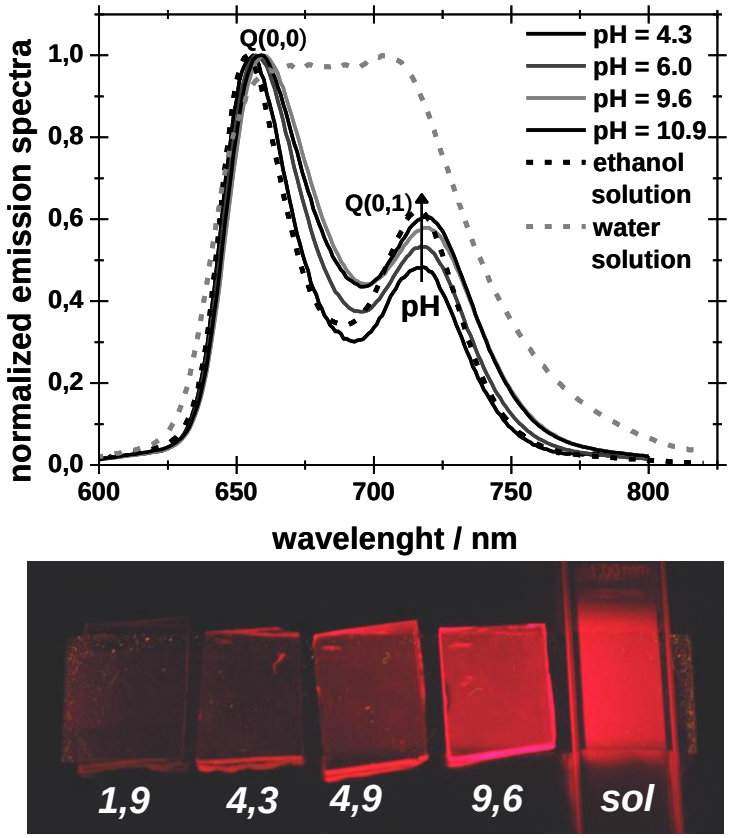

Figure 8.- *(Top) Normalized fluorescence spectra recorded for the samples whose absorption spectra is represented in Fig. 4. (Bottom) Images taken for actual films prepared at the indicated pHs and a 4 ·10^{-5} M water solution that are being illuminated with a low energy fluorescent lamp, 4 Watts, 365 nm.*

For illustration, Figure 8 (bottom) shows a photograph of the same samples than in the picture included in Figure 5, but illuminated with a low energy fluorescent lamp

of 365 nm. It is apparent that the fluorescence of the different samples increases toward the sample prepared at pH 9.6 and that the fluorescence of this composite thin film is comparable with that of the water solution.

Figure 9 shows the normalized excitation spectra of the composite films as a function of the infiltration pH and those of aqueous and ethanol solutions included for comparison. It must be mentioned that the spectra of the films, even for low loaded samples, correspond directly to the excitation bands of the molecule discarding any possible contribution due to the interference oscillations of the TiO_2 substrate (see experimental section and the Supporting Information, Figure S1). These excitation spectra, very similar in shape to the UV-vis spectra reported in Figure 5, are characterized by an intense Soret band at around 425 nm and the set of Q bands in the spectral range between 500 and 625 nm. Both the Soret and Q bands of the composite thin films are redshifted with respect to these bands in the two liquid solutions used for comparison. According to the literature, the red shift in the wavelengths of the bands can be attributed to a flattening of the molecule (i.e., a twist in the angle of the pyridinium methyl group [29, 49]) and/or to some J-aggregation [28].

Another interesting observation in the previous spectra is the appearance of a weak band at longer wavelengths (λ > 625 nm) not reported in the figure, ($Q_x(0,0)$). It is also worth noting that a comparison between the excitation and absorption spectra for the difference pHs (see such a comparison for pH 6.0 and 9.6 in the Supporting Information, Figure S4) reveals a quite good correspondence in spectral shapes. This similarity supports the absence of H dimers that might absorb light without subsequent fluorescence emission and that the excitation bands can be used for a more accurate determination of the wavelengths of the maxima. Thus, it can be established that the Soret band slightly changes from 437 to 435 nm when the pH increases from 4.3 to 9.6. Additionally, a continuous broadening of the band is apparent as the pH increases. Meanwhile, no significant change is observed in the wavelengths of the Q bands. This contrasts with the fact that their intensities increase with the infiltration pH, reaching a maximum at pH 9.6 and then decreasing for a pH of 10.9. Q bands are very sensitive to changes in the conformational structure of the molecules. In our case the increase in the Q-band intensity with the pH confirms a progressive change in the adsorption state of the molecules with this parameter [48].

Exposure of the TMPyP/TiO_2 Composite Films to HCl Vapors.

The potential use of the TMPyP/TiO_2 composite film for gas sensing applications rely on two necessary (although not sufficient) conditions: (i) the modification of the optical response of the dye molecules by their interaction with gases and (ii) the accessibility of these gases to the sensing molecules even if they are trapped into the pores of the TiO_2 films. The reversibility of the interaction process is another related condition for this purpose. To address these points with our films, we have carried out a very simple experiment consisting of the exposure of the TMPyP/TiO_2 composite thin films to the vapors of a concentrated HCl solution at 37%. The ability of the TMPyP molecule to protonate in acid solutions is a well-known property of this molecule (the p*K* of the TMPyP is around 1,5) [27] that has been proposed as pH sensor when deposited onto a glass plate [35]. The results of our experiment are shown in Figure 10, where the changes in the UV-vis absorbance (top) and the fluorescence spectra (bottom) are reported. In Figure 10 (top), it is observed that exposure of the films for less than one second to acid vapors drastically changes the shape of the whole absorption spectrum. The fact that practically no contribution of the original band remains in the spectrum supports that virtually all the TMPyP molecules have been affected by the acid exposure. To a first approximation, the spectral changes can be characterized by a shift of the Soret band by 25 nm and a drastic decrease in the intensity of the fluorescence spectrum. A quite similar shift in the Soret band has been reported by Kalimuthu et al. [50] in the above-mentioned work where these authors attributed this effect to the protonation of the molecule. Protonation is further supported in our case by the drastic decrease in the intensity of the two first Q_y bands at 522 and 560 nm and the enhancement of the intensity of the Q*x* bands at 592 and 648 nm because of a loss of the D_{2h} symmetry of the molecule [27, 30]. As shown in Figure 10 (bottom), the protonation of the TMPyP molecule produces a drastic decrease in the fluorescence intensity. Similar results has been obtained by Kalimuthu et al. [50].

The possible use of the dye/TiO_2 composite thin films as optical sensors is further sustained by the fact that, according to Figure 10, the absorption and the fluorescence spectra almost recover their initial intensity and shape by leaving the sample in air for 3 h. This recovery of the shape of the spectra indicates that the process is reversible and therefore the infiltrated molecules can undergo an exchange process with the environment. Looking at the possibility of using our films as real photonic sensors, preliminary experiments with the sample at t > 50 °C have shown that this recovery process is drastically accelerated. Further work is being carried out at present

in our group to ascertain this behavior and develop real sensor materials based on optically active porphyrin/TiO_2 composite films.

3.4.- Conclusions

In this work, we have investigated the infiltration process of TMPyP molecules within very porous but optically transparent TiO_2 thin films prepared by GLAD-PVD. The total porosity of these films and their pore size distribution has been assessed by measuring water adsorption isotherms. Because the prepared composite films did not disperse the light, they are deemed appropriate for their implementation in optical and photonic devices. In comparison with polymers and other similar matrixes, where processes like deformation and swelling may occur on exposure to certain analytes, advantages of our films are their robustness and the fact that their initial state can be recovered by pumping and/or heating at moderate temperatures.

The incorporation process of the porphyrin dye, consisting of the infiltration of the dye molecules from an aqueous solution, was highly dependent on the pH and can be explained by using the PZC concepts used to account for the evolution of the surface charge on oxide suspensions. The incorporation process can be described according to the Langmuir adsorption model, whereas the kinetics of incorporation follows an Elovich equation. This description of the equilibrium and kinetics of the adsorption discards that diffusion plays a significant role in limiting the accessibility of the TMPyP molecules to the voids of the thin film, and that the number of adsorption sites is the controlling factor of the infiltration process at each pH.

The optical properties of the composite TMPyP/TiO_2 thin films have been investigated by absorption and fluorescence spectroscopies. Although the actual state of the molecules within the films has not been unraveled yet, the assessment of these spectra confirm a tight interaction of the molecule, very likely in the form of monomer, with the surface of the TiO_2, although the formation of J-dimers cannot be excluded. The easy accessibility of gases to all dye molecules and the reversibility of the process in a preliminary experiment consisting of the exposure of the composite films to acid vapors suggests that these types of optically active thin films are potentially good materials to develop into optical gas sensors.

Acknowledgment

We thank the Ministry of Science and Education of Spain (Projects MAT 2007-65764/NAN2004- 09317 and PET2007_0363_01/_02), the Regional Government of Andalusia (Project P07-FQM-03298), and Sos Cuétara S.A. for financial support.

3.5.- Supporting information

S1.- Measured and simulated UV-vis transmission spectra for TiO_2 thin films on glass for refractive index determination

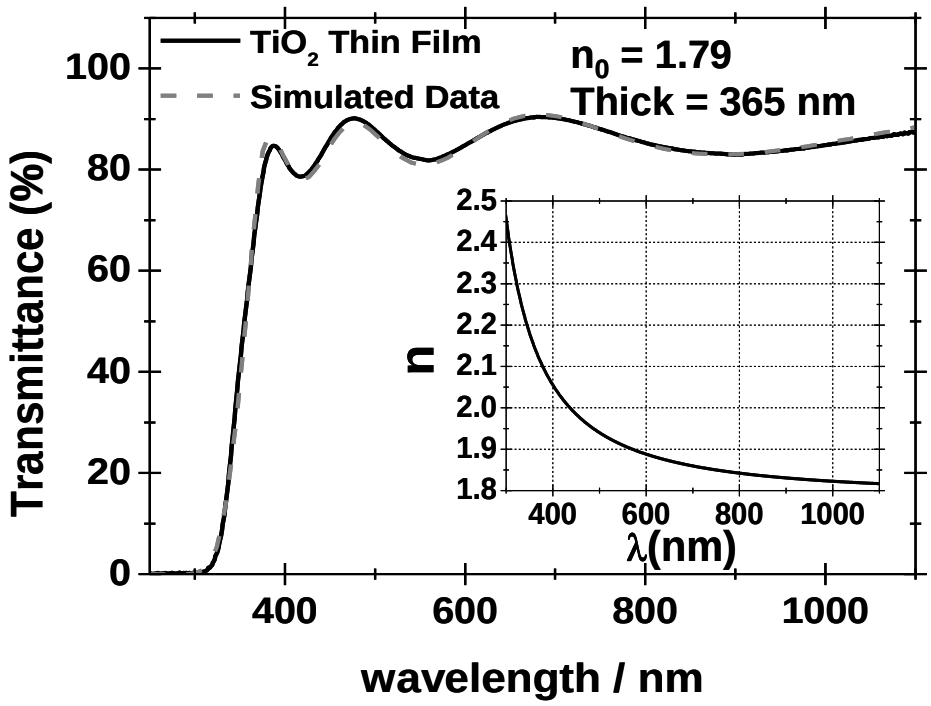

Figure S1.- UV-Vis transmission spectra recorded (solid line) and simulated (dashed line) for TiO_2 thin film deposited on glass. The simulated spectrum corresponds to a sample of 365 nm and a refractive index (n measured at 550 nm) of 1.909. The inset shows the refractive index n simulated as a function of the wavelength.

S2.- Method for the determination of the TMPyP surface concentration directly from the spectra of the films.

The Lambert-Beer law for two dimensional systems can be expressed as:

$$Abs_{film} = 10^3 \cdot \Gamma \cdot \varepsilon \qquad (1)$$

Where Abs_{film} is the absorbance of the film, Γ the surface concentration of the porphyrin in mol cm^{-2}, ε the extinction coefficient given as L mol^{-1} cm^{-1}, and 10^3 (conversion of L to cm^3) is a numerical factor. In this expression it is assumed that there is not a preferential orientation for the porphyrin molecules in the film (as demonstrated in the supporting information S3) and that the absorption is sufficiently high that reflection can be neglected.

The extinction coefficient ε can be calculated from the solution spectrum. Unfortunately, it can not be directly applied to equation (1) at a given wavelength. This is due to the observed shifting and broadening of the Soret band in the films as compared to solution. However, the oscillator strength f is directly related to the area under the absorption band and can be used as a constant parameter:[28]

$$f = \frac{4\varepsilon_0 2.303 m_e c_0}{N_A e^2} \int_{band} \varepsilon d\upsilon = 1.44 \cdot 10^{-19} \int_{band} \varepsilon d\upsilon \quad (2)$$

where ε_0 is the permittivity of a vacuum, m_e is the electron mass, e is the elementary charge, c_0 is the speed of light in vacuum, and N_A is the Avogadro's number. In equation 2, the numerical factor $1.44 \cdot 10^{-19}$ is expressed in mol cm s L^{-1}.

Finally, from equations (1) and (2), the experimental surface concentration of TMPyP can be calculated by:

$$\Gamma = \frac{\int_{band} Abs_{film} d\lambda}{10^3 \int_{band} \varepsilon d\lambda} \qquad (3)$$

Table 1 compares the values of surface concentration obtained by this method with that obtained by the desorption method for a number of TiO_2/TMPyP composite films prepared with different infiltration times. The good concordance between the two sets of values clearly validates the use of equation 3.

Infiltration time / min	***10***	***50***	***90***	***130***	***250***
$\Gamma_{deorption}$	$1.58 \cdot 10^{-9}$	$2.18 \cdot 10^{-9}$	$2.31 \cdot 10^{-9}$	$2.38 \cdot 10^{-9}$	$2.58 \cdot 10^{-9}$
$\Gamma_{integral}$	$1.48 \cdot 10^{-9}$	$2.08 \cdot 10^{-9}$	$2.27 \cdot 10^{-9}$	$2.40 \cdot 10^{-9}$	$2.60 \cdot 10^{-9}$

Table 1. *Porphyrin surface concentration values Γ (mol cm^{-2}) for TiO_2/TMPyP composite films prepared with different infiltration times. $\Gamma_{desorption}$ and $\Gamma_{integral}$ refers to the values obtained by desorption and equation 3 respectively.*

S3.- UV-vis absorbance spectra for TMPyP/TiO2 composites using unpolarized and s- and p-polarized light, for an angle of incidence of 45°

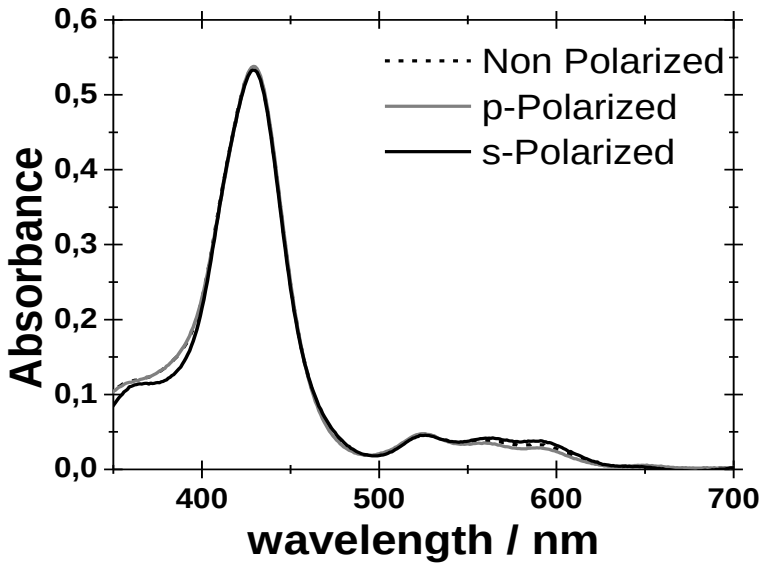

Figure S3.- Absorbance spectra of the TMPyP-TiO_2 composites recorded with unpolarized, s- and p-polarized light, for an angle of incidence of 45º. The similar shape of the spectra indicates non preferential orientation of the porphyrin molecules.

S4.- Normalized fluorescence excitation and absorbance spectra for the composites infiltrated at different pHs

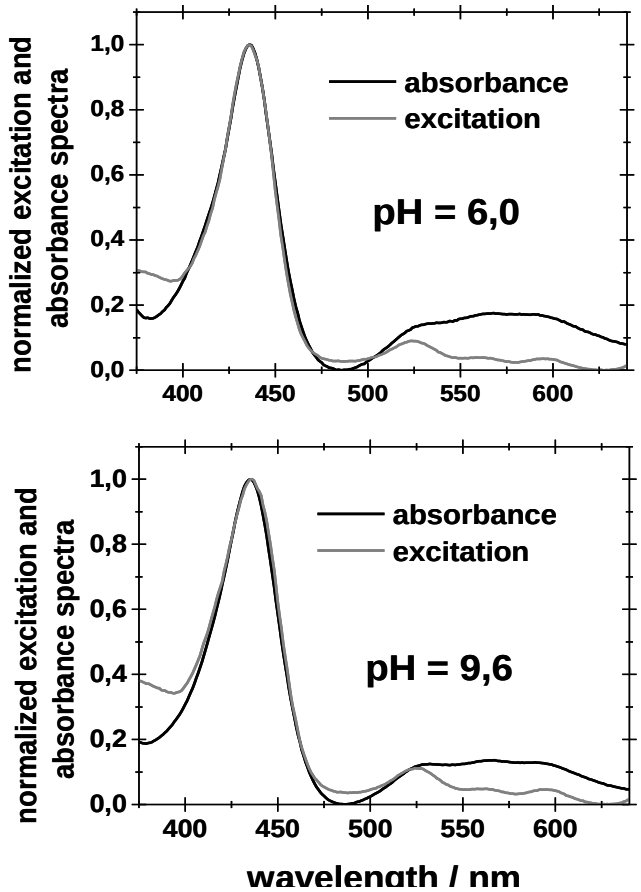

Figure S4.- Normalized fluorescence excitation and absorbance spectra at pH = 6.0 (top) and pH = 9.6 (bottom).

3.6.- References

1 Kay, A.; Gra¨tzel, M. *J. Phys. Chem.* **1993**, *97*, 6272.

2 O'Regan, B.; Gra¨tzel, M. *Nature* **1991**, *334*, 737.

3 Whitlock, J. B.; Panayotatos, P.; Sharma, G. D.; Cox, M. D.; Sauers, R. R.; Bird, G. R. *Opt. Eng.* **1993**, *32*, 1921.

4 Huijser, A.; Savenije, T. J.; Meskers, S. C. J.; Vermeulen, M. J. W.; Siebbeles, L. D. A. *J. Am. Chem. Soc.* **2008**, *130*, 12496.

5 Gupta, T.; Van der Boom, M. E. *J. Am. Chem. Soc.* **2006**, *128*, 8400.

6 Rakow, N. A.; Suslick, K. S. *Nature* **2000**, *406*, 710.

7 (a) Vergeldt, F. J.; Koehorst, R. B. M.; Schaafsma, T. J.; Lambry, J. C.; Martin, J. L.; Johnson, D. G.; Wasielewski, M. R. *Chem. Phys. Lett.* **1991**, *182*, 107.
(b) Neumann-Spallart, M.; Kalyanasundaram, K. *J. Phys. Chem.* **1982**, *86*, 5163.

8 (a) Prieto, I.; Pedrosa, J. M.; Martı´n-Romero, M. T.; Mo¨bius, D.; Camacho, L. *J. Phys. Chem. B* **2000**, *104*, 9966.
(b) Maree´, C. H. M.; Savenije, T. J.; Schaafsma, T. J.; Habraken, F. H. P. M. *Appl. Surf. Sci.* **1996**, *93*, 291.

9 (a) Gaillon, L.; Bedioui, F.; Devynck, J.; Battioni, P. *J. Electroanal. Chem.* **1993**, *347*, 435.
(b) Bettelheim, A.; Ozer, D.; Harth, R.; Murray, R. W. *J. Electroanal. Chem.* **1989**, *266*, 93.

10 Harriman, A.; Heitz, V.; Ebersole, M.; Vanwilligen, H. *J. Phys. Chem.* **1994**, *98*, 4982.

11 (a) Gulino, A.; Giuffrida, S.; Mineo, P.; Purrazzo, M.; Scamporrino, E.; Ventimiglia, G.; Van Der Boom, M. E.; Fragala`, I. *J. Phys. Chem. B* **2006**, *110*, 16781. (b) Yerushalmi, R.; Scherz, A.; Van Der Boom, M. E. *J. Am. Chem. Soc.* **2004**, *126*, 2700.

12 Sánchez-Valencia, J. R.; Borrás, A.; Barranco, A.; Rico, V. J.; Espinós, J. P.; González-Elipe, A. R. *Langmuir* **2008**, *24*, 9460.

13 Sanchez-Valencia, J. R.; Blaszczyk-Lezak, I.; Espinos, J. P.; Hamad, S.; Gonzalez-Elipe, A. R.; Barranco, A. *Langmuir* **2009**, *25*, 9140.

14 Holze, R. *Electrochim. Acta* **1988**, *33*, 1619.

15 Khanova, L. A.; Lafi, L. F. *J. Electroanal. Chem.* **1993**, *345*, 393.

16 Itoh, K.; Sugii, T.; Kim, M. *J. Phys. Chem.* **1988**, *92*, 1569.

17 Fierro, C. A.; Mohan, M.; Scherson, D. A. *Langmuir* **1990**, *6*, 1338.

18 Kim, S.; Bae, L. T.; Sandifer, M.; Ross, P. N.; Carr, R.; Woicik, J.; Antonio, M. R.; Scherson, D. A. *J. Am. Chem. Soc.* **1991**, *113*, 9063.

19 Brett, M. J.; Hawkeye, M. M. *Science* **2008**, *319*, 1192.

20 Hawkeye, M. M.; Brett, M. J. *J. Vac. Sci. Technol., A* **2007**, *25*, 1317.

21 Robbie, K.; Brett, M. J. *J. Vac. Sci. Technol., A* **1997**, *15*, 1460.

22 Wang, S.; Xia, G.; He, H.; Yi, K.; Shao, J.; Fan, Z. *J. Alloys Compd.* **2007**, *431*, 287.

23 Kiema, G.; Colgan, M. J.; Brett, M. J. *Sol. Energy Mater. Sol. Cells* **2005**, *85*, 321.

24 Borra´s, A.; Sa´nchez-Valencia, J. R.; Garrido-Molinero, J.; Barranco, A.; Gonza´lez-Elipe, A. R. *Microporous Mesoporous Mater.* **2009**, *118*, 314.

25 (a) Borrás, A.; Cotrino, J.; González-Elipe, A. R. *J. Electrochem. Soc.* **2007**, *154*, 152.

(b) Borrás, A.; Barranco, A.; Gonza´lez-Elipe, A. R. *J. Mater. Sci.* **2006**, *41*, 5220.

26 (a) Broughton, J. N.; Brett, M. J. *Electrochem. Solid-State Lett.* **2002**, *5*, A279.

(b) Harris, K. D.; Brett, M. J.; Smy, T. J.; Backhouse, C. *J. Electrochem. Soc.* **2000**, *147*, 2002.

27 Kalyanasundaram, K. *Inorg. Chem.* **1984**, *23*, 2453.

28 de Miguel, G.; Pérez-Moales, M.; Martín-Romero, M. T.; Muñoz, E.; Richardson, T. H.; Camacho, L. *Langmuir* **2007**, *23*, 3794.

29 Chernia, Z.; Gill, D. *Langmuir* **1999**, *15*, 1625–1633.

30 Dixon, D. W.; Pu, G.; Wojtowicz, H. *J. Chromatogr. A* **1998**, *802*, 367.

31 Xi, J.-Q.; Kim, J. K.; Schubert, E. F. *Nano Lett.* **2005**, *5*, 1385.

32 *Adsorption, Surface Area and Porosity*; Gregg, S. J., Sing, K. S. W., Eds.; Academic Press: London, 1982.

33 Dargiewicz, J.; Makarska, M.; Radzki, S. *Colloid Surf., A* **2002**, *208*, 159.

34 Siskova, K.; Vlckova, B.; Mojzes, P. *J. Mol. Struct.* **2005**, *744*, 265.

35 Itagaki, Y.; Deki, K.; Nakashima, S.-I.; Sadaoka, Y. *Sens. Actuators, B* **2006**, *117*, 302.

36 *Chemical Properties of Material Surfaces*; Kosmulski, M., Ed.; Marcel Dekker: New York, 2001.

37 *Principles of Colloids and Surface Chemistry*; Hiemenz, P. C., Rajagopalan, R., Eds.; Marcel Dekker: New York, 1997.

38 Savenije, T. J.; Mare´e, C. H. M.; Habraken, F. H. P. M.; Koehorst, R. B. M.; Schaafsma, T. J. *Thin Solid Films* **1995**, *265*, 84.

39 Altin, O.; Ozbelge, O.; Dogu, T. *J. Colloid Interface Sci.* **1998**, *1*, 130.

40 Langmuir, I. J. Am. Chem. Soc. 1918, 40, 1361.

41 Worsfold, O.; Dooling, C. M.; Richardson, T. H.; Vysotsky, M. O. J. Mater. Chem. 2001, 11, 399.

42 Changue, B.; Germain, J. P.; Maleysson, C.; Robert, H. Sens. Actuators 1985, 7, 199.

43 Goldberg, S. Plant Soil 1997, 193, 35.

44 Elovich, S. Y.; Zhabrova, G. M. J. Phys. Chem. 1939, 13, 1761.

45 Cabrejas, M.; Guil, J. M.; Ruiz, A. J. Chem. Soc., Faraday Trans. 1 1989, 85, 1775.

46 Spellane, P. J.; Gouterman, M.; Antipas, A.; Kim, S.; Liu, Y. C. Inorg. Chem. 1980, 19, 386.

47 Vergeldt, F. J.; Koehorst, R. B. M.; van Hoek, A.; Schaafsma, T. J. J. Phys. Chem. 1995, 99, 4397.

48 Ou, Z.-M. J. Photochem. Photobiol., A 2007, 189, 7.

49 Luca, G. D.; Romeo, A.; Scolaro, L. M. J. Phys. Chem. B 2005, 109, 7149.

50 Kalimuthu, P.; Abraham, J. S. Anal. Chim. Acta 2008, 627, 247.

This material is published in the journal *ACS Applied Materials & Interfaces* Volume: *2* Issue: *3* Pages: *712- 721* and free of charge via the Internet at http://pubs.acs.org.

Chapter 4

A transparent TMPyP/TiO_2 composite thin film as an HCl sensitive optochemical gas sensor

A transparent TMPyP/TiO_2 composite thin film as an HCl sensitive optochemical gas sensor

Abstract

Tetracationic porphyrin (TMPyP) molecules were incorporated into an optically transparent TiO_2 thin film, prepared by Glancing Angle Physical Vapour Deposition (GLAD-PVD), by simple infiltration (at pH 6.4). The preparation of optically transparent TMPyP/TiO_2 composite thin films provides a method for the integration of the porphyrin molecules into photonic devices for direct monitoring of gases. Previously, UV-visible and fluorescence spectral techniques have been used to study the reversible protonation of TMPyP in aqueous solution. The optical spectrum of TMPyP shows an intense Soret band at 423 nm with a 22 nm red shift upon protonation by HCl. The experimental conditions for monitoring the concentration of HCl gas by absorption spectroscopy have been optimized. The maximum absorbance change was observed at the Soret band wavelength. A selected temperature of 80 ºC and a 300 second recover period were found to be the optimum operating parameters (response time t_{50} = 16.8±0.7 seconds). The composite with smaller surface concentration of TMPyP (Γ = $0.3 \cdot 10^{-9}$ mol/cm2) presented the best detection limit (0.1 ppm). The response of the composite sensor was highly stable for several months.

Keywords: HCl; optical gas sensor; Tetracationic porphyrin; TMPyP/TiO_2 composite; Porous Thin Film; GLAD-PVD.

4.1.- Introduction

The need to control the emission of acidic gases in the atmosphere has increased in recent years, mainly because these compounds are hazardous to the human body and a source of acid rain. One of those acids is hydrogen chloride (HCl) gas, which now is strictly regulated in the workplaces of many countries. HCl gas is primarily produced by burning fuels that contain chloride and incinerating waste that contains plastics [1]. For this reason, HCl sensors with high sensitivity and reliability are in great demand [2-6]. Optochemical sensing of HCl gas using organic dyes is an attractive technique because it functions at room temperature to detect gas concentrations at the ppm level or less. The use of porphyrin dyes has been recently examined for the detection of HCl gas [2-4]. Different porphyrins and methods to prepare sensitive thin films were used in these studies. For example, Supriyatno et al. [2] examined a tetraphenylporphyrin dispersed in copolymers, Itagaki et al. [3] used a tetra(4-hydroxyphenyl)-porphyrin dispersed on solgel composite films, and Kalimuthu et al. [4] studied a meso-tetramesitylporphyrin deposited by direct coating onto glass. In the first two investigations, it was demonstrated that the sensitivity of the composite sensors was strongly affected by the nature of the matrices that determines the interaction between porphyrins and the analyte gases. Moreover, the third study showed a structural change from a planar to saddle conformation of the porphyrin ring upon protonation, which can result in a change in the aggregation state and may be detrimental for the interaction between the porphyrin molecule and the substrate. In turn, this effect may result in a loss of porphyrin during each exposure event, highlighting the necessity of using improved host materials to contain the sensing molecules.

In the present investigation, a new composite system is presented for HCl gas detection. The composite is based on meso-tetra(4-methylpyridinium)-porphyrin (TMPyP) as the sensing molecule and columnar optically transparent TiO_2 films, prepared by glancing angle physical vapour deposition (GLAD-PVD) [7,8], as the host material. The incorporation of the porphyrin into the open microstructure of these TiO_2 thin films is performed by simple immersion into the dye solution and has been characterized previously [7]. The main advantages of the TMPyP/TiO_2 composite thin film are its high porosity, which allows an easy diffusion of the toxic gas; a low refraction index, necessary for its use as optical sensor; a good stability with

temperature, facilitating the heating process to induce a fast recovery; and an efficient adsorption of the TMPyP by electrostatic interaction with the host medium. The exposure of the TMPyP/TiO_2 composite to HCl vapour leads to protonation of TMPyP as shown in Figure 1. The protonation of TMPyP in water solution has been studied using UV-visible and fluorescence spectroscopies. The absorbance changes at the Soret band were used to monitor the presence of HCl in gaseous phase.

4.2.- Materials and methods

5,10,15,20-Tetrakis(1-methyl-4-pyridyl)-21H,23H-porphyrin (TMPyP, Aldrich) was used without further purification. All other reagents were Merck A.G. and used as supplied. Ultrapure water from a Millipore Direct-Q system (>18 MΩ cm) was used throughout. A scheme of the reversible process with the structure of the TMPyP molecule and its protonated form is presented in Figure 1.

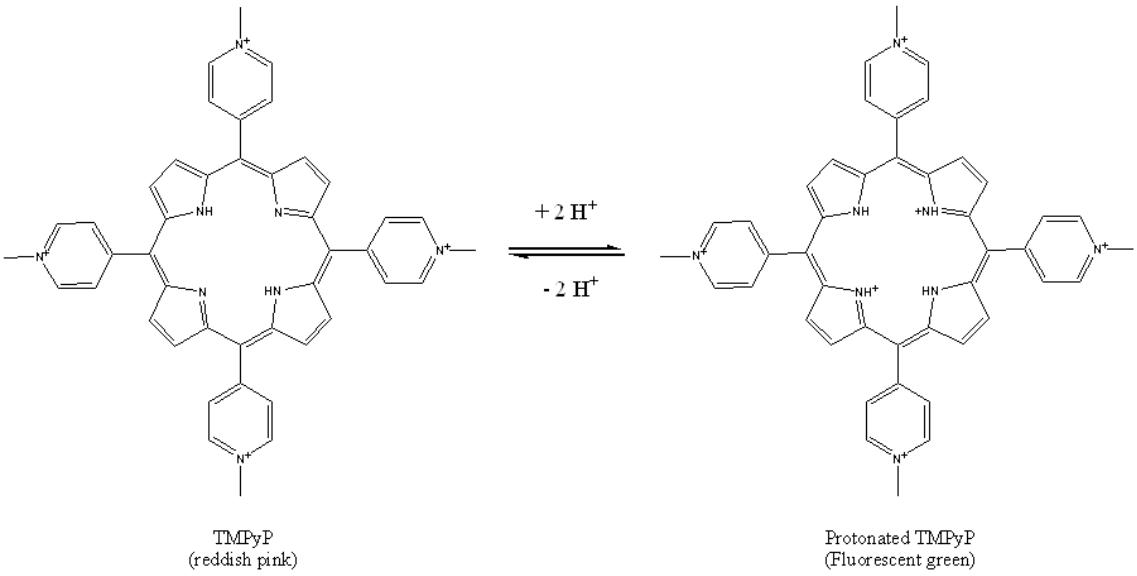

Figure 1.- Chemical structure of 5,10,15,20-Tetrakis(1-methyl-4-pyridyl)-21H,23H-porphyrin (TMPyP) and its protonated form.

The TMPyP/TiO_2 composites were prepared using porous TiO_2 thin films as host materials. For this purpose, transparent and amorphous TiO_2 films were prepared by GAPVD at room temperature on glass substrates [7,8]. A characteristic of these films is that they are very porous and possess a tilted columnar microstructure [8,9]. For the present work the substrates were placed at an angle of 70º with respect to the evaporator source. The film thickness was approximately 350 nm.

Two solutions with different concentrations of TMPyP (5 and 100 μM) in water at the original pH (6.4) were used for the preparation of the TMPyP/TiO_2 composites. The infiltration time was 24 hours in both preparations. The corresponding surface concentration Γ, was calculated by using UV-visible spectroscopy [7]. The TMPyP/TiO_2 composite was obtained by simple immersion of the TiO_2 thin films into water porphyrin solutions. A sample with a $\Gamma=0.3\cdot10^{-9}$ mol·cm^{-2} was obtained with a 5

μM TMPyP solution, whereas a $\Gamma=1.9\cdot10^{-9}$ mol·cm^{-2} was produced for a 100 μM TMPyP solution [7]. After this, the samples were taken out from the solution and washed with water at the same pH. During this washing cycle, any dye molecule which is not incorporated into the host matrix is removed from the surface. The films were then dried in a two-step process: firstly by blowing nitrogen onto their surfaces for five minutes and then by a heating at 80 ºC for one hour. After these treatments, the composite thin films presented the characteristic yellowish color of porphyrin thin films. The intensity of the color was different between the two preparations with different TMPyP surface concentrations.

UV-visible spectra of the TMPyP water solutions were recorded on a Cary 100 Conc UV-visible spectrophotometer. Fluorescence spectra of both the TMPyP in dichloromethane-ethanol mixture and the composite TMPyP/TiO_2 films were recorded in a Jobin-Yvon Fluorolog3 spectrofluorometer. The TMPyP/TiO_2 composite films were exposed to HCl gas using a specially designed gas testing chamber comprising two Tylan FC-260 mass flow controllers, which deliver a mixture of pure N_2 and standard dry HCl gas (5 ppm) for the exposure stage, followed by pure N_2 for the recovery stage. The delivery of these gases was controlled and automated using a program developed using Labview software. For the exposure of the composite sensor films to higher concentrations of the acid, pure N_2 was pumped through a closed bottle containing HCl solution (see design [10]). The temperature of the HCl solution was maintained at 0 °C by submerging the bottle in iced water, therefore mixing the N_2 gas with the analyte at a known vapor pressure. The resultant mixture was then mixed again with a second supply of N_2 controlled with another Tylan FC-260 mass flow controller and then fed into the test chamber. The effect of the humidity was also controlled. To minimize the slight contribution of the water vapour to the composite sensor signal, a similar level of humidity was incorporated into the pure N_2 (recovery) as the HCl vapour (exposure). Before starting the measurement, the %RH level of the HCl vapour was evaluated and this information was used to regulate the pure N_2 humidity to this level.

The TMPyP-TiO_2 composite films to be tested were introduced in a test chamber [10] onto a Peltier heating stage capable of controlling the film temperature in the range 20-80 °C. The Peltier heating device contains an aperture in its center to allow in situ UVvisible spectroscopy. The composite film spectra over the range of 350-850 nm (tungsten light source) were continually monitored during exposure and recovery using a World Precision Instruments “Spectromate” spectrometer. The spectra of the

composite are presented in absorbance after subtracting the spectrum of the TiO_2 substrate.

All the experiments were carried out at least four times.

4.3.- Results and discussion

Study of the TMPyP protonation in solution.

UV-visible and fluorescence spectroscopic techniques were used to study the reversible protonation of the TMPyP. Figure 2 shows the absorption spectra of the TMPyP in water during the exposure to different concentrations of HCl. The Soret band at 423 nm (Figure 2a) and the four Q bands at 518, 555, 584 and 634 nm (Figure 2b) showed the expected intensities [11]. With this original D_{2h} molecular symmetry, the $Q_y(0,0)$ band at 518 nm appears as the most intense band and the $Q_x(0,0)$ band at 634 nm is the least intense one in the TMPyP molecule. The ability of the TMPyP molecule to become protonated in acid solutions is a well known property of this molecule (the pK of TMPyP is around 1.5 [11]) and it leads to a protonation of tertiary nitrogen resulting in changes in the Soret and Q bands [3]. In this case the Soret band featured a red shift of 22 nm, from 423 to 445 nm. This shift is bigger than that obtained for mesotetramesitylporphyrin by Kalimuthu et al. [4], indicating that TMPyP shows a more sensitive behaviour for HCl detection than the previous porphyrin. Moreover, the Q band region featured an important change since the original four bands turned into two bands due to the higher molecular symmetry (D_{4h}) and the degeneration of the excited state of the protonated porphyrin. All these changes in the spectrum resulted in the modification of the color of the solution. After the protonation of TMPyP, the $Q_x(0,0)$ band at 634 nm became the most intense band with a 7 nm red shift (Figure 3b) and the $Q_y(0,0)$ band at 518 nm became the least intense one. The $Q_x(0,0)$ band at 634 nm has been attributed to the formation of a dication [12]. The appearance of an isosbestic point at 432 nm in Figure 3a clearly confirms the protonation of TMPyP. Addition of ammonia to the protonated TMPyP solution results in deprotonation, and therefore the change of the colour of the solution from fluorescent green to reddish pink.

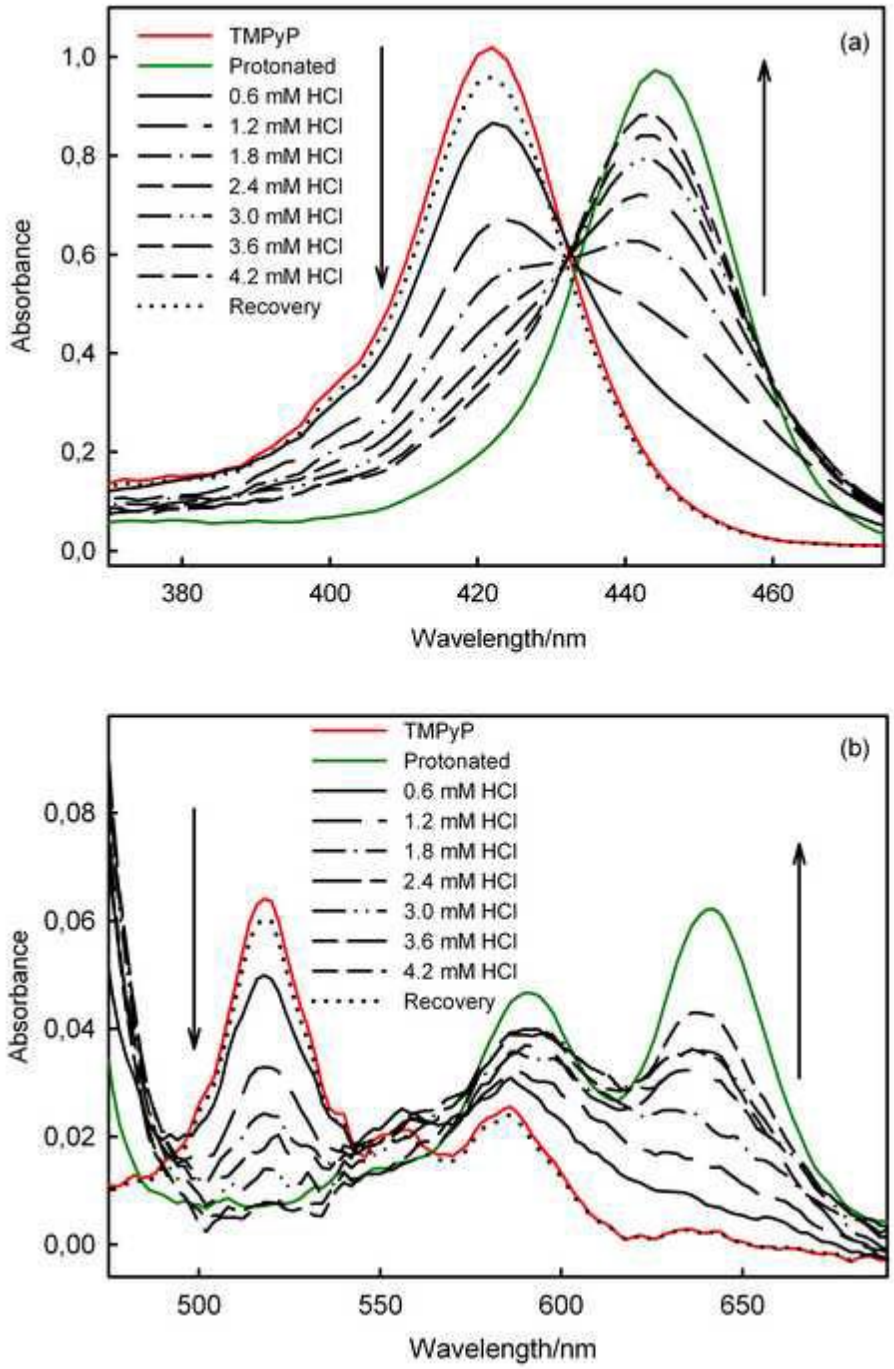

Figure 2.- Absorbance spectra of 1.5μM TMPyP in water containing of 0, 0.6, 1.2, 1.8, 2.4, 3, 3.6, 4.2mM of HCl, completely protonated with excess of HCl, and the recovered spectrum after addition of excess of ammonia to the sample with 4.2mMof HCl. (a) In the Soret band region and (b) in the Q band region.

Figure 3 shows a representation of the fluorescence spectra recorded for the TMPyP in dichloromethane-ethanol mixture solution against addition of HCl aqueous solution. The excitation of TMPyP at 423 nm results in two well differentiated bands

corresponding to the degeneracy of the lowest singlet configuration of the TMPyP [13]. These two bands, Q(0,0) and Q(0,1), are centred approximately at 654 and 716 nm respectively. In water solution, the bands appear at 666 and 704 nm and are less resolved than in ethanol. This difference has been attributed to a change in the resonance interaction between the pyridinium group and the π system of the porphyrin macrocycle due to the polarity of the media [14]. For aqueous solution, this resonance interaction increases and results in an overlapping between the two bands [11,14]. The exposure to HCl changes the shape of the whole emission spectrum and with a drastic decrease in the intensity of the fluorescence spectrum. Similar results have been obtained by Kalimuthu et al. [4]. This is mainly due to the loss of planarity of the porphyrin ring thereby increasing conjugation with the methyl pyridinium groups in solution.

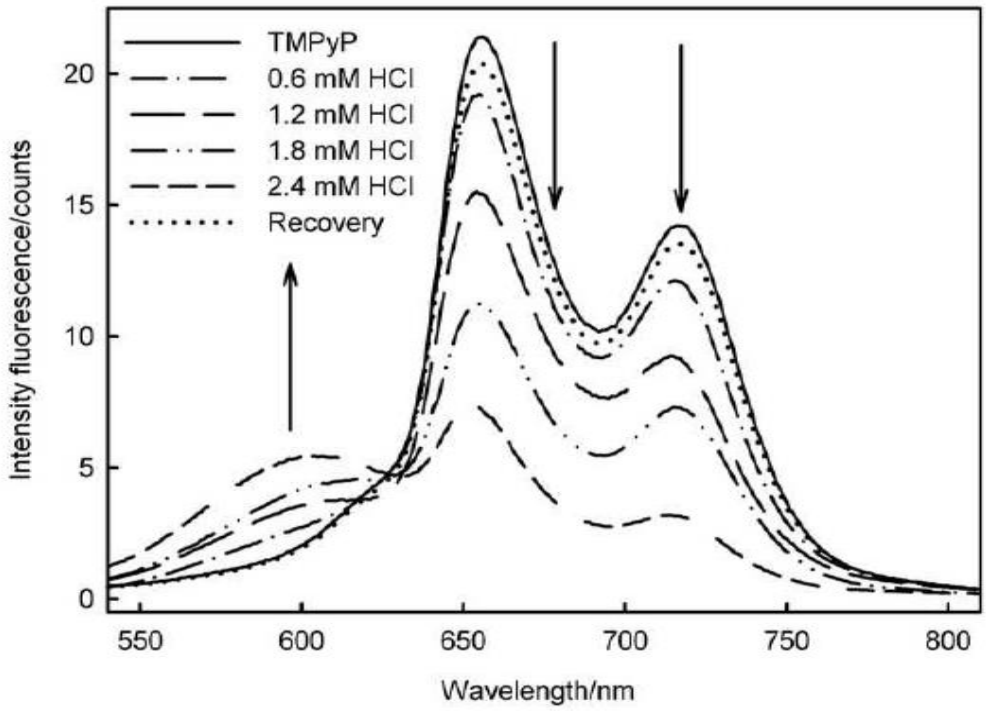

Figure 3.- Fluorescence spectra of 1.5 μM TMPyP in dichloromethane-ethanol mixture (excitation wavelength = 423 nm) containing of 0, 0.6, 1.2, 1.8, 2.4mM of HCl, and addition of excess ammonia to the sample with 2.4mM of HCl (Recovery).

The use of the TMPyP to develop a composite film as optical sensor is further justified by the fact that, according to Figure 2 and 3, the absorption and fluorescence spectra almost recover fully their initial intensity and shape by addition of excess

ammonia. This recovery of the shape of the spectra indicates that the process is reversible.

Detection of HCl gas by the composite TMPyP/TiO_2.

The TMPyP molecules were infiltrated into the host TiO_2 thin films by their immersion in water solutions at controlled pH values. The TMPyP/TiO_2 composite film has been characterized in a previous work [7]. In order to address the interaction process within the composite films, the UV-visible spectrum has been recorded and the corresponding response in the presence of ~250 ppm HCl gas is shown in Figure 4. The inset pictures show the colour difference between the composite film in the absence and presence of HCl gas. The wavelength of the Soret band (437 nm) appears red-shifted with respect to that in water solution [7] and was selected to monitor the absorbance change with respect to the concentration of the toxic gas.

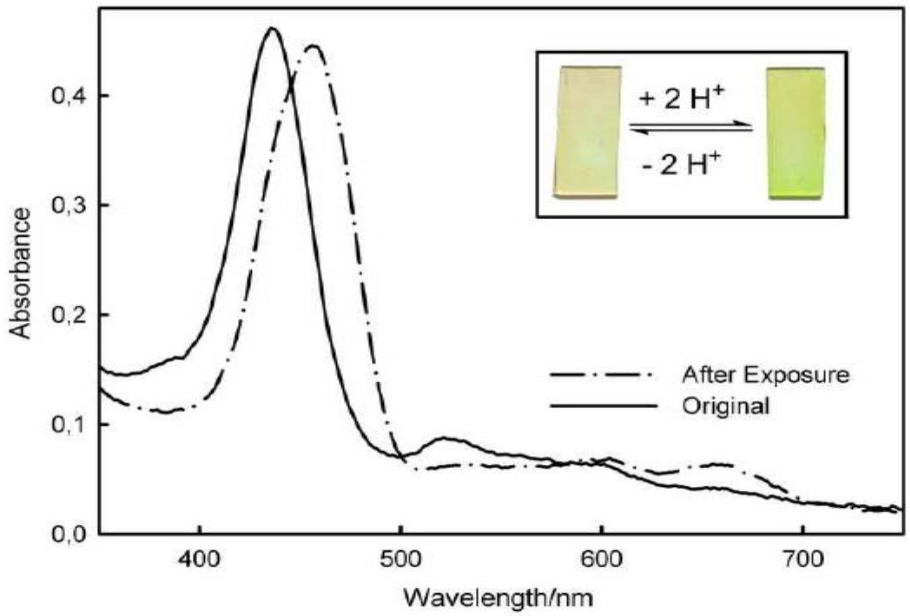

Figure 4.- (Top) Absorbance spectra for the TMPyP/TiO_2 composite thin film in the absence and presence of ~250ppm HCl vapour. $\Gamma = 0.3\times10^{-9}$ mol cm^{-2}. (Inset) Images taken for the film at each stage.

Several parameters were tested in the gas testing chamber during the cycles of exposure and recovery in order to improve the behavior of the HCl sensor. An important parameter is the temperature of the sensor. In this case, a Peltier heater was used to heat the films during the recovery phase. A high temperature produces a very fast recovery but it can also be detrimental for the stability of the porphyrins. Therefore, the selected

temperature for the recovery phase was 80 ºC. Other parameters to be optimized are both the exposure and the recovery time. Figure 5 shows the variation time (at 25, 50, 100, 200 and 300 seconds) of the absorption spectra of the TMPyP/TiO_2 composite during the exposure to ~250 ppm HCl gas at 20 ºC (Figure 5a), and the recovery time when exposed to N_2 (g) at 80 ºC (Figure 5b). An exposure time of 300 seconds was found to be sufficient when the HCl gas concentration is lower than 1000 ppm.

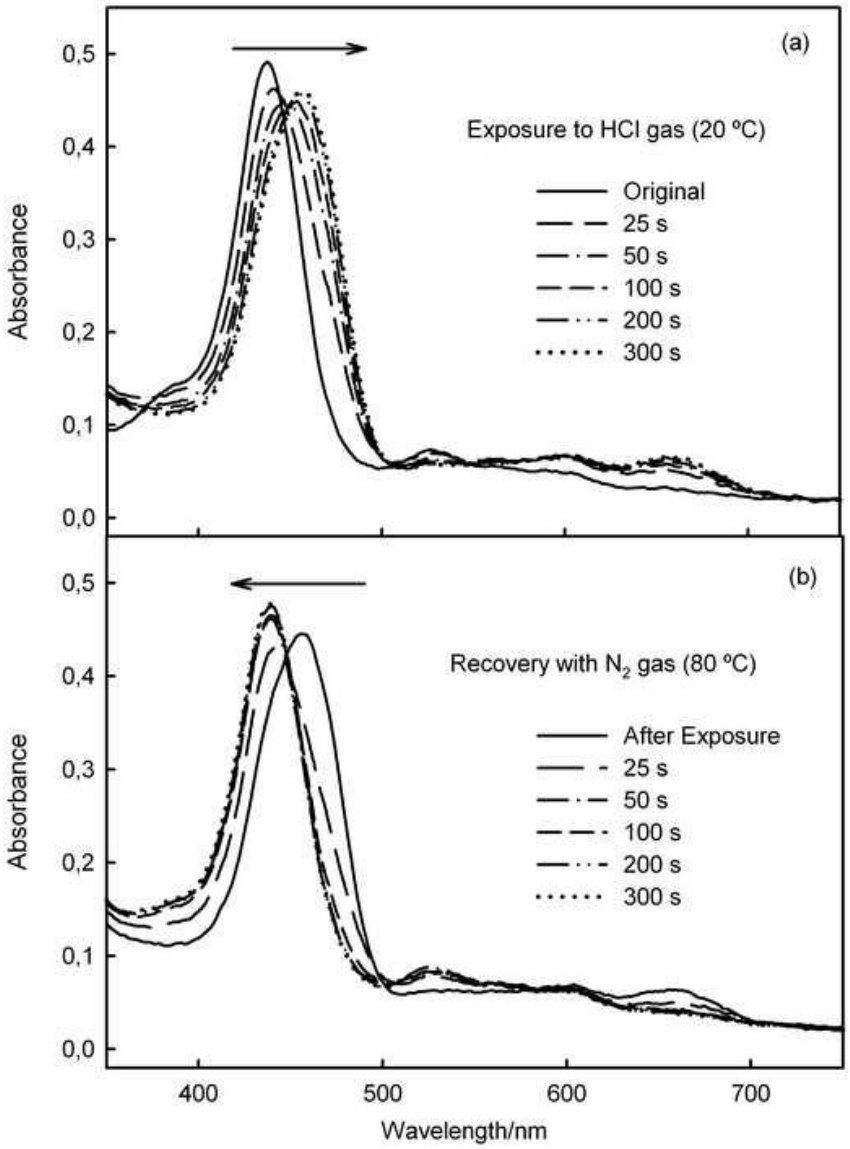

Figure. 5.- (a) Temporal evolution of the absorbance spectrum of a TMPyP/TiO_2 composite film (25, 50, 100, 200 and 300 s) during the exposure to ~250ppm HCl vapour at 20 ◦C. (b) Absorbance spectra of the TMPyP/TiO_2 composite during the recovery phase (25, 50, 100, 200 and 300 s), exposed to N_2 (g) at 80 ºC. $\Gamma = 0.3\times10^{-9}$ mol cm^{-2}

Typical sensor responses of the TMPyP/TiO_2 composite at 437 nm for three different concentrations of HCl gas are shown in Figure 6. The composite film shows a fast decrease in the absorbance after exposure to 1, 3 and 5 ppm HCl gas which implies the good sensing capability of our sensor towards HCl gas. The t_{50} parameter, defined as the response time at 50% of the maximum absorbance change during the gas exposure, was used and the value obtained was 16.8 ± 0.7 seconds. When the N_2 gas stream was directed to the film at 80 ºC after reaching the equilibrium state, the absorbance increased until the original intensity was reached, suggesting the deprotonation of the TMPyP. A set of three successive exposures to HCl of the TMPyP/TiO_2 composite sensor is shown in Figure 7. The sensor shows good response at a concentration of 3 ppm, with good reversibility and reproducibility.

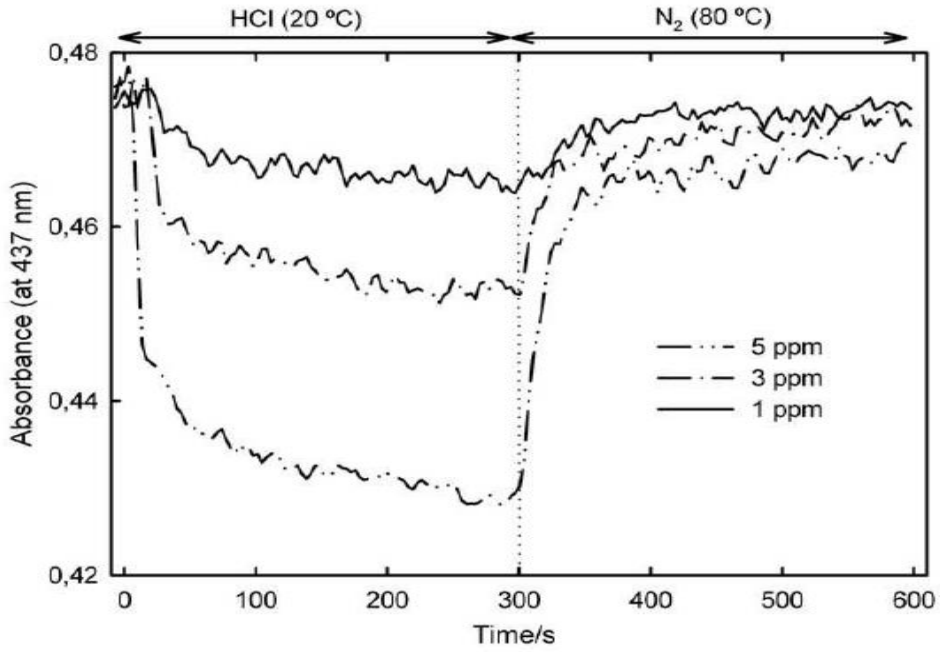

Figure 6.- Comparison of the absorbance changes at a wavelength of 437nm during three exposure (5, 3 and 1ppm HCl vapour for 300 s) and recovery (N_2 for 300 s) cycles for the TMPyP/TiO_2 composite film. $\Gamma = 0.3\times10^{-9}$ mol cm^{-2}.

The absorbance variation (ΔA) was obtained from the differences between the absorbance intensities of the composite film at 437 nm before and after the exposure to different HCl concentrations [12]. To obtain the calibration curve, the concentrations of HCl against the ΔA have been plotted. Table 1 shows the summarized analytical characteristics of two preparations with different concentration of TMPyP into the composite film. The limits of detection (LOD) were calculated according to the three signal/noise (s/n) criterion. As expected, comparing the calibration slope values

obtained, the highest sensitivity was achieved for the composite film with more surface concentration of TMPyP (Γ=1.9·10^{-9} mol·cm^{-2}). However, the best LOD was obtained for the composite film with less surface concentration of TMPyP (Γ=0.3·10^{-9} mol·cm^{-2}). A slight improvement in the regression coefficient was found in case of the less concentrated preparation.

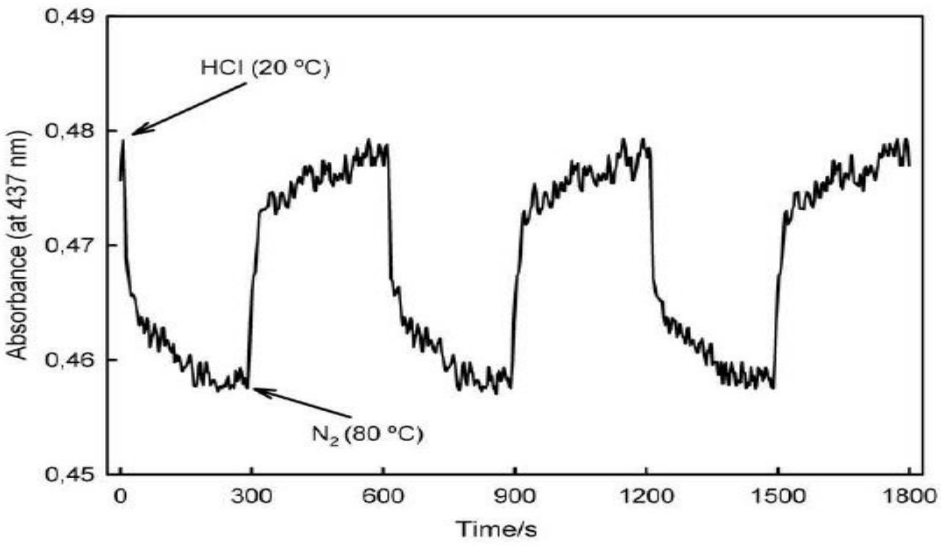

Figure 7.- Reversibility and reproducibility of the absorbance change of 437nm during three cycles of exposure to 3ppm HCl for the TMPyP/TiO$_2$ composite film. $\Gamma = 0.3\times10^{-9}$ mol cm^{-2}.

The fact that the highest slope value is obtained for the most concentrated preparation, suggests an enhancement of the sensor response with the increment of TMPyP molecules in the composite film. Nevertheless, an increment of the TMPyP yields a possible increase of the noise, and consequently a worse LOD and regression coefficient.

	Γ=1.9·10^{-9} mol·cm^{-2}	**Γ =0.3·10^{-9} mol·cm^{-2}**
Intercept (nm) (x10^{-4})	8.4 ± 2.9	8.0 ± 0.3
Slope (nm/M)	60.67 ± 3.23	35.65 ± 0.37
Regression coefficient (r)	0.9916	0.9997
Standard deviation of residuals ($S_{y/x}$)	2.8·10^{-4}	3.3·10^{-5}
LOD[a] (ppm)	0.52	0.10
R.S.D. (%)	4.4	3.7
Measurement wavelength(nm)	437	437

Table 1.- Analytical characteristics obtained from the calibration plots in the determination of HCl gas with two different TMPyP/TiO_2 composites films.

The reproducibility of the response of each composite was estimated from the response to 3 ppm HCl gas. We obtained a relative standard deviation (R.S.D.) of 3.7% for five successive determinations using the same TMPyP/TiO_2 composite. The obtained values show remarkable reproducibility (Table 1).

The stability of the sensor has been investigated by recording a weekly calibration curve for one month. After this period of time, ΔAmax becomes 84 % of its initial value, although its decrease is not significant during the first 14 days. This demonstrates that the use of the columnar TiO_2 as host material allows a good stability of the porphyrin response with the time.

The TMPyP/TiO_2 composite presents two main advantages comparing the results with the obtained for other authors. The first one is a faster response and recovery because of the high porosity and stability of the TiO_2 as host material, and the second one is the low surface concentration of TMPyP necessary to obtain a good response from the sensor.

A future HCl gas detection by a fluorescence sensor

In order to further improve the sensing capability of the TMPyP/TiO_2 composite thin film an alternative technology based on emission fluorescence is now being tested. As shown in Figure 8, the protonation of the TMPyP molecules into the TiO_2 thin film produces a drastic decrease in the fluorescence intensity. This higher change in the fluorescence intensity can improve the sensor performance in terms of sensibility, selectivity and LOD. Technical and analytical parameters such as response and recovery time, sensibility and analyte concentration dependence are been optimized and will be presented in a future publication.

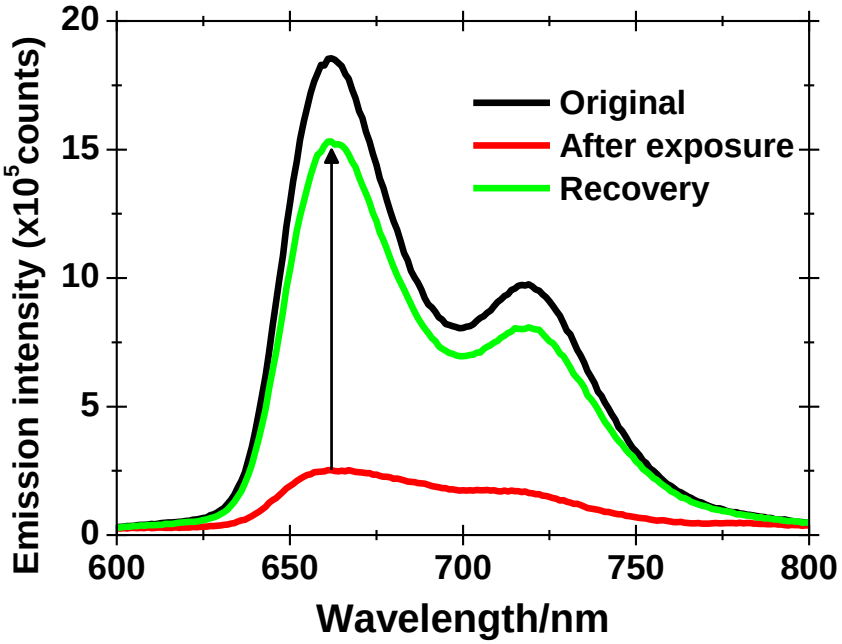

Figure 8.- Fluorescence spectra of the change and recovery under HCl exposure, recorded for the TMPyP/TiO_2 composite.

4.4.- Conclusions

The sensitivity of TMPyP to HCl vapour has been demonstrated through UV-visible spectroscopy. A new TMPyP/TiO_2 composite film has been developed for HCl gas detection. TMPyP can be used both in solution and within a composite thin film. The inclusion of the TMPyP in the composite entails a remarkable improvement in the solid state sensor, such as fast response, long-term stability and a low surface concentration of the used porphyrin compared to other previously researched systems

Acknowledgement

We thank the Ministry of Science and Education of Spain (PET2007_0363_01/_02 and project HOPE CSD2007-00007) and SOS Corporación Alimentaria S.A. for financial support.

4.5.- References

1 L.Wang, R.V. Kumar, Thick film miniaturized HCl gas sensor, Sens. and Actuators B: Chem. **98** (2004) 196-203.

2 H. Supriyatno, M. Yamashita, K. Nakagawa, Y. Sadaoka, Optochemical sensor for HCl gas based on tetraphenylporphyrin dispersed in styrene–acrylate copolymers: effect of glass transition temperature of matrix on HCl detection, Sens. And Actuators B: Chem. **85** (2002) 197–204.

3 Y. Itagaki, K. Deki, S. Nakashima, Y. Sadaoka, Development of porphyrin dispersed sol–gel films as HCl sensitive optochemical gas sensor, Sens. And Actuators B: Chem. **117** (2006) 302–307.

4 P. Kalimuthu, S.A. John, Optochemical sensing of hydrogen chloride gas using meso-tetrasitylporphyrin deposited glass plate, Anal. Chim. Acta **627** (2008) 247-253.

5 M. Matsuguchi, Y. Kadowaki, Poly(acrylamide) derivates for QCM-based HCl gas sensor applications, Sens. and Actuators B: Chem.**130** (2008) 842–847.

6 M. Matsuguchi, Y. Kadowaki, HCl gas monitoring based on a QCM using morpholine-functional styrene-co-chloromethylstyrene copolymer coatings, Sens. and Actuators B: Chem. **120** (2007) 462–466.

7 P. Castillero, J.R. Sanchez-Valencia, M. Cano, J.M. Pedrosa, J. Roales, A. Barranco, A.R. González-Elipe, Active and optically transparent tetracationic porphyrin/TiO_2 composite thin films, Appl. Mater. Interfaces **2** (2010) 712-721.

8 M.J. Brett and M.M. Hawkeye, New materials at a glance, Science **319** (2008) 1192- 1193.

9 G. Kiema, M.J. Colgan, M.J. Brett, Dye sensitized solar cells incorporating obliquely deposited titanium oxide layers, Sol. Energy Mater. Sol. Cells **85** (2005) 321.

10 A.D.F. Dunbar, T.H. Richardson, A.J. McNaughton, J.Hutchinson, C.A. Hunter, Investigation of Free Base, Mg, Sn, and Zn Substituted Porphyrin LB Films as Gas Sensors for Organic Analytes, J. Phys. Chem. B **110** (2006) 16646-16651.

11 K. Kalyanasundaram, Photochemistry of water-soluble porphyrins: comparative study of isomeric tetrapyridyl- and tetrakis(N-methylpyridiniumyl)porphyrins, Inorg. Chem. **23** (1984) 2453-2459.

12 V.N. Knyukshto, K.N. Solovyov, G.D. Egorova, Luminescence and structure of the protonated forms of meso-tetraarylporphyrins in solution, Biospectroscopy **4** (1998) 121-133.

13 P.J. Spellane, M. Gouterman, A. Antipas, S. Kim, Y.C. Liu, Porphyrins. 40. Electronic-spectra and 4-orbital energies of free-base, Zinc, Copper, and Palladium Tetrakis(perfluorophenyl) porphyrins, Inorg. Chem. **19** (1980) 386-391.

14 F.J. Vergeldt, R.B. Koehorst, A. Van Hoek, T.J. Schaafsma. Intramolecular interactions in the ground and excited-state of Tetrakis(n-methylpyridyl) porphyrins, J. Phys. Chem. **99** (1995) 4397-4405.

This material is published in the journal *Sensors and Actuators B* Volume: *B150* Issue: *2* Pages: *764-769* and free of charge via the Internet at: http://www.sciencedirect.com/science/article/pii/S0925400510006623#.

Chapter 5

Gas sensing ammonia and amines based on protonated porphyrin/TiO_2 composite thin films

Gas sensing ammonia and amines based on protonated porphyrin/TiO_2 composite thin films

Abstract

Physical Vapor Deposition in glancing angle configuration (GLAD-PVD) has been employed in the fabrication of open porous and tilted microcolumnar structures of TiO_2. These thin films with a thickness of 300nm have been used as host matrix for two different fluorescent cationic porphyrins, 5, 10, 15 triphenyl 20 mono (N-methyl 4-pyridyl) porphine tetrachloride (MMPyP) and meso – tetra (N-methyl 4-pyridyl) porphine tetrachloride (TMPyP). The porphyrins have been anchored by electrostatic force interaction to the microcolumns by self-assembly through the dip coating method. These porphyrins/TiO_2 composites have been used as a second generation amine gas sensor, it is consisted on two steps, firstly to protonate the porphyrins with chloride acid and secondly, recovery the porphyrins to its original state with ammonia or amine vapours. Absorption, emission and time-resolved spectroscopies have been used to confirm the protonation-deprotonation of the two porphyrins and follow their spectral changes in the presence of the analytes.

The sensing capabilities of both composites (MMPyP/TiO_2 and TMPyP/TiO_2) have been compared with the mono-cationic porphyrin being more sensible (up to ten times) than its tetra-cationic counterpart. This result has been attributed to the different anchoring of the two porphyrins to the TiO_2 surface and the different state of aggregation with the mono-cationic derivative being attached by its only methyl pyridyl group forming J-aggregates giving rise to a more accessible configuration for the analytes.

Finally, the decrease of the emission fluorescence intensity with the repeatability of the sensor has been studied by infrared spectroscopy with the exposition to ammonia vapour, and it has confirmed the composites, in the different cycles, retain the ammonium chloride causing a quenching in the emission fluorescence.

Keywords:

MMPyP, TMPyP, TiO_2, GLAD-PVD, optically active composites, amine gas sensing, porous thin films.

1.- Introduccion

During the last decades there has been a growing demand for the development of sensitive, portable and cost-effective gas sensors. The detection and measurement of gas concentrations using optical spectroscopy techniques is important for understanding and monitoring a variety of phenomena from industrial processes to environmental change. Volatile amines, apart from its natural origin, are present in a vast variety of areas like environmental gas analysis[1, 2], automotive industry[3-5], chemical industry[3, 6, 7], medical applications[8, 9] or, food quality indicators[10-12].

There are several types of sensors for measuring amines as described in the literature. The most frequently used techniques in commercial amines detectors are: metal-oxide gas sensors[13-15], catalytic amine detectors[16, 17], conducting polymer amine analyzers[18, 19] and optical amines detection techniques[17, 20]. In particular, the most common sensors that are manufactured for detecting ammonia vapours are without doubt metal-oxide gas sensors, mostly based on SnO_2 or WO_3[13, 21-23] where WO_3 with embedded Au nanoparticles shows a low limit detection for ammonia of 1 ppm, but it operates at an elevated temperature of more than 400 ºC[24]. An interesting alternative is the use of organic materials deposited as thin films as active elements, which can work at room temperature[25, 26]. There are two main optical approaches for the detection of amines as described in literature. Those based on a colour change in the sensor when base react with the sensing material[27], and those using changes in its absorption spectrum as the measuring parameter[28].

Gas sensors based on optical changing offer fast response (bellow 1 second are possible) and the possibility to measure in real time, which it is very important in an industrial process[29]. On the other hand, optical gas sensors offer a minimal drift and high gas specificity filling an important gap between lower cost sensors with inferior performance and high end laboratory equipment.

In this work, it has been used the host-guest method to combine an inorganic matrix or host material with a guest material, that in this case an organic molecule. The thin film composite employed in this work consist in the utilization of highly porous metal oxide thin films (host material) and the subsequent incorporation of the active material (guest) to introduce the desired functionality.

Open porous and tilted columnar microstructures of TiO_2 have been prepared by Electron Beam Physical Vapor Deposition in the configuration of Glancing Angle (GLAD-PVD). Vacuum condition ($Pressure_{work}$ = 10^{-4} mbar) is required for GLAD-PVD to avoid the contamination of the target, and keep the directionality of the sublimed material, which is mandatory to generate porous microstructures in a deposition where the material incoming are not perpendicular to the substrates.

The use of highly porous materials with the goal to enhance its accessible surface area is a common approach to enhance their functionality and can lead to a high number of applications These thin films of TiO_2 provide good optical properties (optical transparency, high porosity, low refractive index and controlled thickness, etc.) and it seem a perfect candidate to be used as the matrix of optical sensor.

Porphyrins and other dyes have been widely used in the last decades for gas-sensitive purposes[28, 30-32]. Their photochemical and photophysical properties make them ideal candidates for the optical detection of number of gaseous and volatile analytes. In particular, porphyrins have several properties which enable their use for the development of specific optical sensing systems, like their special absorption, emission, charge transfer and complexing properties as a result of their characteristic ring structure of conjugated double bonds[33]. They show strong absorptions in the UV/vis region which are changed by the coordination of the analyte thereby enabling their detection. Fluorescence gas sensor based on organic dyes are also very interesting and their use has exponentially grown in the last decade[32, 34, 35]. They are mainly based on emission changes in the presence of the analyte. The two porphyrins used in this work (MMPyP and TMPyP) have good emission properties and therefore we also report here changes in their fluorescence spectrum in the presence of volatile amines.

In early works it has been demostrated that cationic porphyrins are anchored to the negatively charged surface of TiO_2 by electrostatic interaction forces[36]. Films prepared by GLAD-PVD technique have been previously used for gas sensing purposes and have been found to enhance the sensing properties of the anchored porphyrins due to their open pores that facilitate the access of the incoming gaseous molecules[31, 36, 37].

In this work, we present a gas sensor for the detection of gaseous ammonia and amines. The sensing mechanism consists in the deprotonation by the basic analytes of the previously protonated porphyrin molecules. The analyte monitorization is based on the dramatic changes that protonation (or deprotonation) produces in the absorption and

emission spectra of porphyrins, enabling the use of UV-Vis and fluorescence spectroscopies.

2.- Materials and methods

Host material: TiO_2 thin film preparation

Porous microstructures of TiO_2 have been prepared by Physical Vapor Deposition technique in Glancing Angle configuration (GLAD-PVD) in an electron evaporation system[36, 38, 39].

The substrates, consisting of pieces of a silicon wafer or transparent silica plates, were kept at room temperature. The thin films are optically transparent and possess an open porous and tilted columnar microstructure with a thickness of 350nm exhibiting an elevated porosity (total pore volume of 49%) with void apertures on the surface in the form of mesopores (pore diameter >2 nm), that also determines a relatively low refractive index value, that was found to be 1.79[36]. The substrates are placed with a tilt angle of 70º with respect to the evaporation source. As a result, the angle between the tilted columns and the substrate surface was approximately 60º. Rico et al report further details regarding film preparation, SEM images and structural information.

Porphyrins and reagents

As it was said before, porphyrins dye is the guest material of the composite. The porphyrins 5, 10, 15 triphenyl 20 mono (N-methyl 4-pyridyl) porphine tetrachloride (MMPyP) and 5,10,15,20-Tetrakis(1-methyl-4-pyridyl)-21H,23H-porphyrin (TMPyP) were supplied by Frontier Scientific and were used without further purification. They were solved in absolute ethanol from Sigma Aldrich. Figure 1 present a scheme of the TMPyP and MMPyP porphyrins.

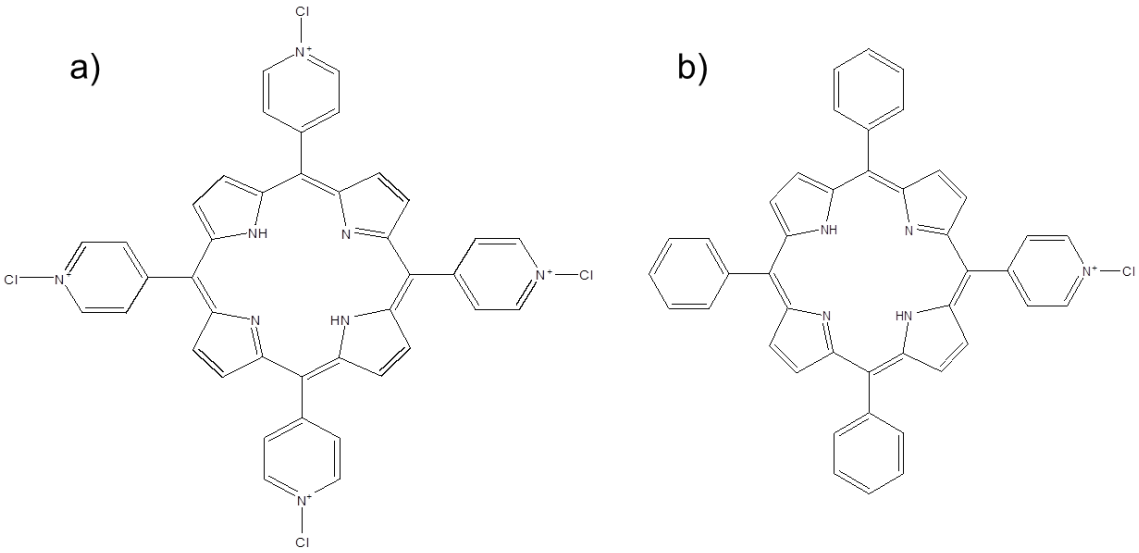

Figure 1.- Schematic representation of the structure of the porphyrins a) TMPyP and b) MMPyP.

Hydrochloric acid with a concentration of 37%, ammonia with a concentration of 33%, butylamine, ethylenediamine, cadaverine, Putresceine and Histamine were from Sigma Aldrich.

Composite thin film characterization and preparation

UV-Vis spectra were recorded on a Cary100 Conc UV-visible spectrophotometer, except the UV-visible spectra measurement in the gas chamber that they were taken with a light source DH-2000 and a QE-65000 detector. Fluorescence spectra were recorded using a Horiba Jobin-Yvon FluoroLog 3 spectrofluorometer operating in the front face mode. The emission spectra were excited with radiation of 430 nm for TMPyP and 420 nm for MMPyP using in both cases 2 and 4 nm slits for the excitation and emission monochromators, respectively. In the case of the measurement of the gas chamber with the fluorescence optical fiber it was used 4 and 8 nm slits for the excitation and emission monochromators, respectively.

Time-resolved fluorescence decays were collected using the time correlated single-photon counting (TCSPC) option of the FluoroLog 3. A NanoLED460 illuminating at 450 nm with a repetition rate of 1 MHz and a full width at half maximum of 9 ns was used to excite the sample. The signals were recorded by using an IBH Data Station Hub photon counting module, and data analysis was performed by using the commercially available DAS6 software (HORIBA Jobin-Yvon IBH). The quality of fit was assessed by minimizing the reduced chi squared function (χ_{R2}) and by visual inspection of the weighted residuals.

Two ethanol solutions with the same porphyrin concentration of 1×10^{-5} M were prepared for the infiltration. It was done by simple immersion of the TiO_2 thin film into the solution of porphyrin by dip coating technique. The infiltration time for the preparation of the porphyrins/TiO_2 composites was 1 hour. After this, the samples were taken out from the solution and washed with absolute ethanol. To remove physisorbed dye molecules which have not been anchored to the host matrix. After the washing process, the composite was dried by blowing dry nitrogen onto the film surface for 5 min.

After the infiltration process of the porphyrin into TiO_2 matrix , the composite thin films exhibit the characteristic yellowish colour of porphyrin thin films suggesting the porphyrins molecules do not suffer any type of optical or structural change.

We performed the study of the binding of the molecules in the different cycles through specular reflectance FT-IR spectroscopy using a Jasco FT/IR-6200 spectrometer.

Gas sensing system

The system to detect gases was designed and assembled in the Materials Science Institute of Seville and it consists in a disc-shaped stainless steel of 12 cm of diameter and 2 cm of width, with a gas inlet and an outlet. The gas inlet is controlled with several digital mass flow controllers, from the company Bronkhorst High-Tech The internal side of the chamber was designed to have the lowest possible volume to fill or empty the chamber quickly. The chamber it consist in two rectangular fused silica windows (one in the front and other in the back) to connect two optical fibers externally to measure UV-Vis absorption spectroscopy. One of them is connected to the light source to illuminate the sample and the other one is to collect the light transmitted through it. Both optical fibers are connected to optical lenses to collimate the light. The windows allow to introduce two samples, one to get a reference or background and the other one to measure the UV-Vis absorption spectrum, corrected with the reference. The sample is placed in the optical pathway, between the fibers, inside the chamber.

UV-Vis spectroscopy has been carried out with a light source DH-2000, an optical fiber of 50μm of diameter to deliver the light to the chamber, an optical fiber of 600μm of diameter to collect the transmittance light throught the chamber to the detector and an UV-Vis-NIR detector QE-65000, all from Ocean Optics. The fibers are held on an adjustable collimator lens holder.

The chamber also has an additional square fused silica window (placed above the rectangular windows) to measure fluorescence spectroscopy externally with an optical fiber which transport the excitation light from the fluorimeter to the sample and, at the same time collect the emission light and transport it to the detector.

Fluorescence spectroscopy in the chamber has been done with a fluorescence fiber which is held on the chamber.

So the system is designed to measure UV-Vis and fluorescence spectroscopy simultaneously in the same gaseous environment with two samples, one for each spectroscopies technique.

Figure 2 shows a scheme of the experimental set up. We obtained the gaseous volatiles by bubbling dry nitrogen through a bottle containing the desired amines volatiles at room temperature. Ultrapure water from a Millipore Milli-Q-Plus system was used to dilute amines solution. The volatiles can be calculated through its vapor pressure at the corresponding temperature.

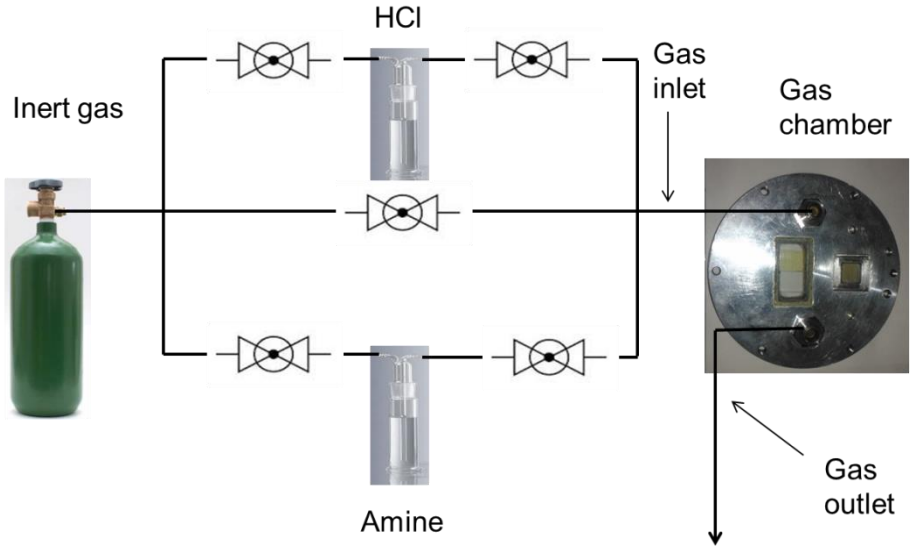

Figure 2.- Experimental setup

The initial process, before protonation, is to keep a flow of nitrogen during 30 min in order to obtain an inert atmosphere. After this, the nitrogen line is closed and the chloride line is opened until complete protonation of the porphyrin molecules. In this moment, the sample is prepared to detect amines. The line of hydrogen chloride is closed and the amine line it is opened.

3.- Results and discussion

Optical properties of steady state and protonated state of MMPyP and TMPyP porphyrins

Figure 3 shows the absorbance spectra of MMPyP and TMPyP in ethanol solution and in the TiO_2 solid films before and after protonation. The inset shows the wavelength range where the Q-bands are located (480nm to 700 nm). Table 1 shows also the position of the main peaks of the absorption spectra of the two porphyrins in solution and in the porphyrin/TiO_2 composite.

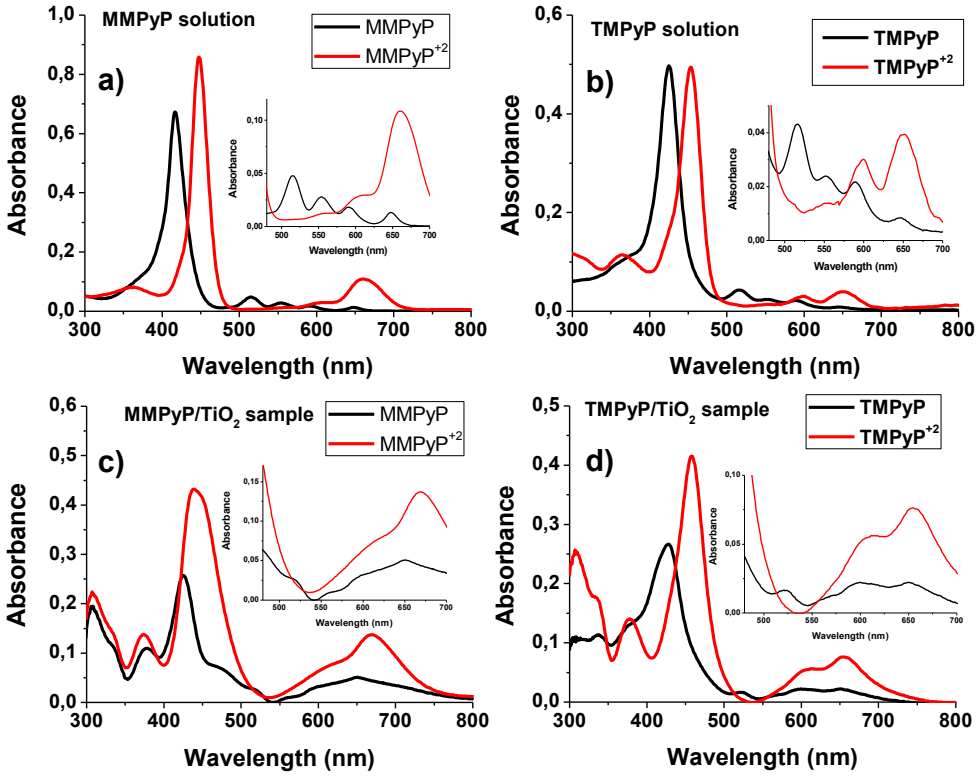

Figure 3.- Absorbance spectra of MMPyP (a and c) and TMPyP (b and d) in ethanol solution and in the TiO_2 solid films before (black line) and after protonation (red line). The inset shows the wavelength range where the Q-bands are located (480nm to 700 nm).

The UV-Vis spectra of the steady state of MMPyP and TMPyP solution (figures 3.a and 3.b, black line) it is a typical spectra of monomeric state of the dyes where in the case of MMPyP the Soret band is located in the wavelength of 417nm and its Q-bands are located in 515nm, 554nm, 591nm, and 648 nm, and in the case of TMPyP the Soret band is located in 425nm and the Q-band are located in 516 nm, 551 nm, 590 nm, and

647 nm. The UV-Vis spectra of the steady state of MMPyP and TMPyP in the TiO_2 thin films (figures 3.c and 3.d, black line) have suffered differences in the maximum of absorption of the dye infiltrated and a broadening respect to their solutions. In the case of MMPyP the Soret band (located in 426 nm) is 9 nm red-shifted while in the case of TMPyP a shoulder appear in 415 nm, which mean 10 nm blue-shifted respects to monomeric state. These results are attributed to the different aggregation state of the porphyrins molecules into the TiO_2 matrix.

There are two types of molecular organization of the dyes due to the different displacement of the dipoles. The shifting and broadening of the absorption spectra of aggregated species in thin films, relative to the monomeric spectrum in solution, has been interpreted by application of exciton models such as the point dipole model proposed by McRae and Kasha[40, 41] or the extended dipole model proposed by Kuhn and collaborators[42, 43]. Excellent discussions and comparisons between them can be found in the literature[44-46]. A J-aggregate is formed when Coulomb attraction forces between the interacting dipoles outweigh repulsion, while H-aggregates result from the stacking arrangement of porphyrin macrocycles[47].

The shift of 9 nm of the Soret band of MMPyP/TiO_2 spectrum can be attributed to J-type aggregation of the MMPyP porphyrins in the TiO_2 matrix[48]. On the other hand, the shoulder observed in the TMPyP/TiO_2 spectrum can be attributed to a partial formation of H-aggregates. I. Prieto et al. have reported how TMPyP molecules are anchored to an anionic matrix proposing an H-aggregation dimer configuration in which the parallel rings of the molecules are twisted by 45° with respect to each other[49]. This different aggregation state is due to each porphyrin are anchored according to the number of cationic radicals: MMPyP have an only cationic radical and consequently, MMPyP molecules are located in a perpendicular way to the TiO_2 surface, while the TMPyP have four cationic radicals and it is located in a parallel way to the TiO_2 surface, being more influence for the matrix. These configurations provoke different form of aggregations, in that way, the perpendicular molecules can aggregate with a certain displacement of the a ring respect to the other giving rise to J-type aggregates, on the other hand, parallel molecules only permit an aggregate where the central ring of the upper porphyrins are just located on downer porphyrins, but with a turn of 45º respect to it, where all the tetra-cationic porphyrins can interact with the negatives charges of the TiO_2 surface. This giving rise to a H-type aggregate according to Prieto et al. On the other hand, these different aggregation due to the different mechanism of

anchored have been described to mono and tetra substituted carboxyphenyl porphyrins in the same matrix of TiO_2 and it highlight the importance of the substituted in the type of anchored of the dyes to the matrix and its influence about the molecular aggregation that can be critical in its posterior functionality into the composite.

The absorbance spectra of protonated MMPyP and TMPyP in ethanol solution and in the TiO_2 can be also observed in figure 3. The structural change that occurs in a porphyrin molecule between its steady state and its protonated state is well known and basically consist in a flattering deformation. The molecule adopt a saddle type structure in which the two pyrrole rings with deprotonated nitrogens point upwards, while the other two (protonated) point downwards[50]. As a consequence, the Soret band suffers a wavelength red shift of about 30nm and, due to a higher symmetrical configuration of the protonated ring, the original four Q-bands with D_{2h} molecular symmetry turned into two Q-bands with D_{4h} molecular symmetry[37]. The absorbance spectra in figure 3 for the two porphyrins both in ethanol solution and in the TiO_2 matrix exhibit similar changes in good agreement to those described above.

Fluorescence emmision spectroscopy was measured of MMPyP and TMPyP in the TiO_2 matrix in steady state and in protonated state, as it is shown in figure 4. MMPyP and TMPyP ethanol have been included for comparison with its composites respectively. The ethanol solutions present two well-differentiated bands corresponding to the degeneracy of the lowest singlet configuration of the pophyrins[51]. For MMPyP solution these two bands, Q(0,0) and Q(0,1), are centered at 653 nm and 715 nm, while TMPyP solution are centered at 653 nm and 714 nm. The shape of the fluorescence spectrum of the porphyrins into the TiO_2 matrix is similar to its ethanol solution, indicating that the polarity of the solution is similar to the composite. MMPyP/TiO_2 composites centered at 657 nm and 718 nm, while TMPyP composites centered at 662 nm and 717 nm.

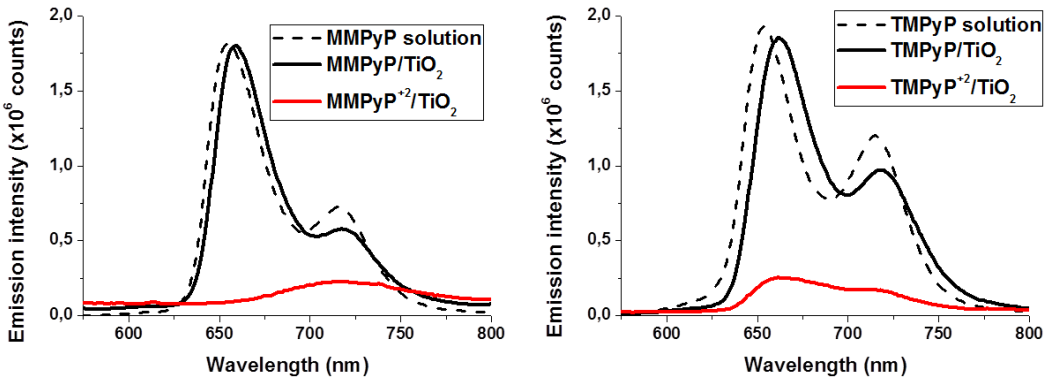

Figure 4.- MMPyP and TMPyP in ethanol solution in dash line and the composites MMPyP/TiO_2 and TMPyP/TiO_2 emission intensity spectra in solid line. Black solid line is the composite in natural state and red solid line in protonated state.

The porphyrins composites have been exposure to HCl gas to protonate them and, as it can see in figure 4 and in previous works[36, 37], the fluorescence emission suffer a drastic decrease of their intensity. Kalimuthu and John had reported that the high decrease of the emission intensity is due to the loss of the flattering of the porphyrins.

In Table 1 are indicated the position of the main peaks of the absorption spectra and the emission intensity spectra for the two porphyrins in solution and in porphyrin/TiO_2 composite in its natural state and protonated state.

		Absorbance peaks						Fluorescence peaks	
		B(0,0)	$Q_y(1,0)$	$Q_y(0,0)$	$Q_x(1,0)$	$Q_x(0,0)$	Eutectic point	Q(0,0)	Q(0,1)
a)	**MMPyP solution**	417	515	554	591	648		653	715
							434		
a)	**$MMPyP^{+2}$ solution**	448		556	608	659			
c)	**MMPyP sample**	426	518	558	596	649		657	718
							431		
c)	**$MMPyP^{+2}$ sample**	440			611	670		718	
b)	**TMPyP solution**	425	516	551	590	647		653	714
							438		
b)	**$TMPyP^{+2}$ solution**	453		551	600	652			
d)	**TMPyP sample**	427	523	560	600	651		662	717
							443		
d)	**$TMPyP^{+2}$ sample**	458			612	654		662	717

Table 1.- Position of the main peaks of the absorption spectra and the emission intensity spectra for the two porphyrins in solution and in porphyrin/TiO_2 composites in its natural state and protonated state. The eutectic points are also indicated.

TCSPC is used to determine the fluorescence lifetime of the species, e. i., it is a measurement of the time between the excitation of the sample by a pulsed laser and the arrival of the emitted photon at the detector. Figure 5 shows MMPyP and TMPyP in ethanol solution and the composites MMPyP/TiO_2 and TMPyP/TiO_2 fluorescence

intensity decay spectra in natural state and in protonate state. It is a way to confirm the state protonate of non-protonated of the porphyrins molecules. Table 2 shows the decay live time of the two porphyrins in solution and porphyrin/TiO_2 composite.

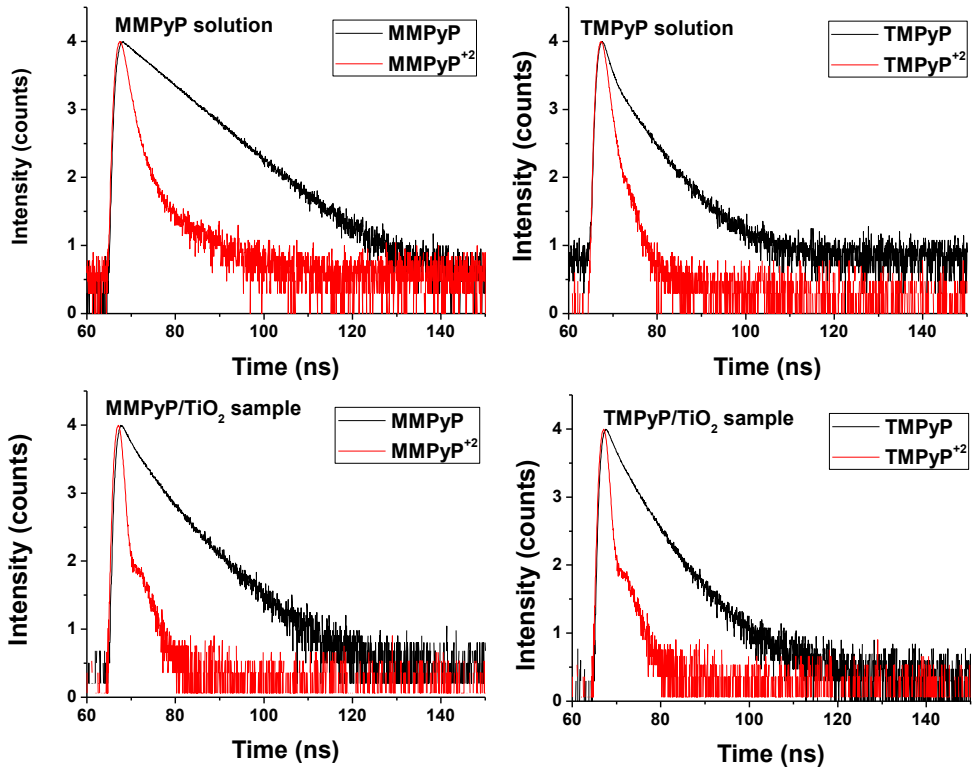

Figure 5.- MMPyP and TMPyP in ethanol solution and the composites MMPyP/TiO_2 and TMPyP/TiO_2 fluorescence intensity decay spectra in natural state (black line) and in protonate state (red line). a) shows MMPyP solution in ethanol, b) shows TMPyP solution in ethanol, c) shows MMPyP/TiO_2 composite and d) shows TMPyP/TiO_2 composite.

In Table 2 are indicated lifetime (in nanosecond) for the two porphyrins in solution and in porphyrin/TiO_2 composite in its natural state and protonated state. The decay has been fitted to one or two exponential.

MMPyP solution	MMPyP sample	TMPyP solution	TMPyP sample
7,92	1,47	1,19	1,65
	4,26	5,04	5,25
MMPyP protonated solution	MMPyP protonated sample	TMPyP protonated solution	TMPyP protonated sample
1,03	0,34	0,76	0,36

Table 2.- Lifetime of the two porphyrins in solution and in porphyrin/TiO_2 composite in its natural state and protonated state.

Response to amines

The gas sensing properties of the porphyrin/TiO_2 composite was investigated by exposing the previously protonated films to ammonia and amine vapors. During exposure to the analytes, the emission changes were recorded and expressed in the form of kinetic responses at the wavelength of the maximum change ($\lambda_{Kinetic}$ = 660 nm).

Several amines have been tested driving similar results, further information can be found in the supporting information S1. The kinetic emission of the MMPyP/TiO_2 and TMPyP/TiO_2 composites to 600 ppm of ammonia is shown in figure 6. The response has been normalized for a better comparison, so that relative changes are presented in all cases. As expected, the fluorescence emission experiences an increase as a consequence of the recovery of the steady state form of the porphyrin in the presence of the ammonia vapors. In particular, the MMPyP/TiO_2 composite shows a much faster response than that of TMPyP/TiO_2. This significant difference can be attributed to the different arrangement of the two porphyrins in the TiO_2 matrix as proposed above from the UV-vis spectra. In this way, the partial face-to-face stacking of the TMPyP derivative, with its four positive groups interacting with the TiO_2 surface, can hinder the access of the analyte molecules to the porphyrin ring, while the more open geometry of the MMPyP molecules, anchored by its only phenylpyridil group, facilitates the analyte interaction.

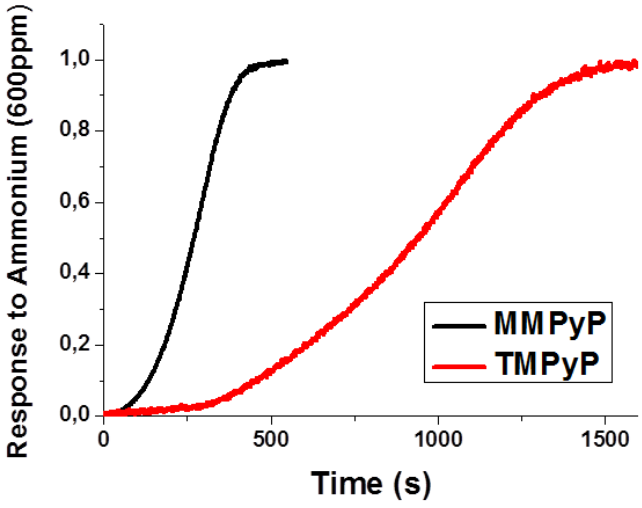

Figure 6.- Kinetic response of the MMPyP/TiO_2 (black line) and TMPyP/TiO_2 (red line) composites to 600 ppm of ammonia vapors.

The response time of a sensor can be defined as the time required for the sensor output to change from its previous state to a final settled value. There are two generally accepted ways of stating response times: the time constant t_c and the t_{10-90} . The time constant t_c is the time taken for the sensor to reach 63% of its final value while the t_{10-90} is that to traverse between 10% and 90% of its final value. Other information usually registered in the data sheet specifications is t_{50}, which is defined in the same way as t_c and t_{10-90}. The corresponding values for MMPyP/TiO_2 and TMPyP/TiO_2 are given in table 2. As can be seen, the MMPyP sensor is always more than three times faster than the tetracationic derivative, whose response times are excessively long.

	t_c (s)	t_{50} (s)	t_{10-90} (s)
MMPyP/TiO_2	301	270	247
TMPyP/TiO_2	1044	938	836

Table 2.- Response time to MMPyP/TiO_2 and TMPyP/TiO_2 composites to 600ppm of ammonia.

Figure 7 shows the sensors response to different concentrations of ammonia vapors. In all cases, the response time increases as the analyte concentration decreases. However, significant differences are observed again in the behaviour of both derivatives. While the MMPyP/TiO_2 composite gives reasonable response times to 600 and 60 ppm of NH_3, and even responds to 6 ppm of the analyte, the TMPyP/TiO_2 system shows a very slow response to 60 ppm NH_3 and gives no response to 6 ppm. The explanation of this result can be found again in the different attachment of the two porphyrins to the TiO_2 matrix. In this way, the perpendicular arrangement of the MMPyP molecules with respect to the TiO_2 keeps their ring more separated from the matrix and hence more accessible to the volatiles. On the other hand, the TMPyP molecules are placed parallel to the matrix with their central ring close to the oxide surface that inevitably hinders the analyte access.

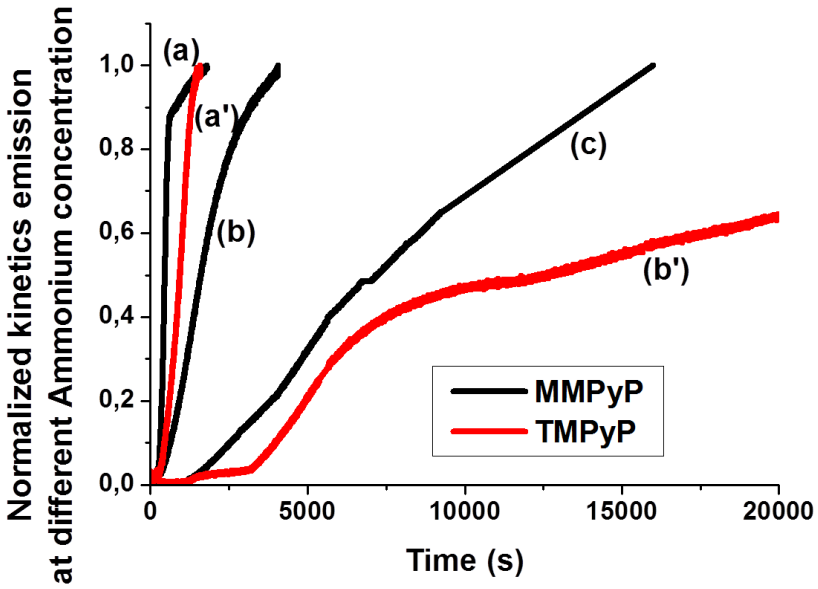

Figure 7.- Kinetics responses to different concentration of ammonia of the composites TiO_2/MMPyP ((a), (b) and (c)) and TiO_2/TMPyP ((a') and (b'). (a) and (a') correspond to 600 ppm (b) and (b') correspond to 60 ppm and (c) correspond to 6 ppm.

The limit of detection LOD was calculated for both composites under their exposure to ammonia vapors according to the corresponding signal to noise ratio (LOD=3×SNR). The corresponding values of LOD along with other analytical parameters are summarized in table 1.

	MMPyP/TiO_2	**TMPyP/TiO_2**
Intercept (cuentas) (x10^4)	1.7 ± 0.2	9.7 ± 1.2
Slope (cuentas/ppm) (x10^2)	10.4 ± 0.6	3.6 ± 0.4
Regression coefficient (r)	0.99	0.99
Standard deviation of residuals ($S_{y/x}$)	14.1	17,6
LOD (ppm)	0.05	0.16
R.S.D. (%)	2,3	3.7
Measurement wavelength (nm)	660	660

Table 2.- Summary of the analytical characteristics obtained from the calibration of MMPyP/TiO_2 composite and TMPyP/TiO_2 composite.

As can be seen, MMPyP/TiO_2 exhibits a higher slope compared to TMPyP/TiO_2 suggesting an enhancement of the sensor response (sensitivity) based again in the

different arrangement of the porphyrin molecules in the TiO_2 matrix. Another interesting parameter is the relative standard deviation (R.S.D.) of the background. For its calculation, the composites were protonated (initial point) and exposed to ammonia vapors measuring one spectrum per second during 300 seconds. In both cases, very low values were obtained with 2,3% for MMPyP/TiO_2 and 3,7% for TMPyP/TiO_2. This result indicates a reproducibility of the employed system.

Repeatability of the sensing system

To extend the applicability of the sensor different amines have been tested. It has been studied how it is the response of the composites under several cycles of protonation with HCl gas and deprotonation with amines. Figure 8 shows several cycles of protonation of MMPyP/TiO_2 with hydrogen cloride gas and deprotonation with saturated vapors of butylamine. The time period for each cycle was 600 s, with 300 s for the exposure to butylamine and 300 s for the recovery (protonation) with HCl gas. As can be observed, the intensity of the signal decreases progresively with the succesive exposure/recovery cycles. A similar behaviour was observed for the TMPyP/TiO_2 composite. The use of ammonia instead of butylamine lead to the same results with even a more dramatic decrease of intensity, (see supporting information S2). In all cases, however, the response time was similar for all cycles.

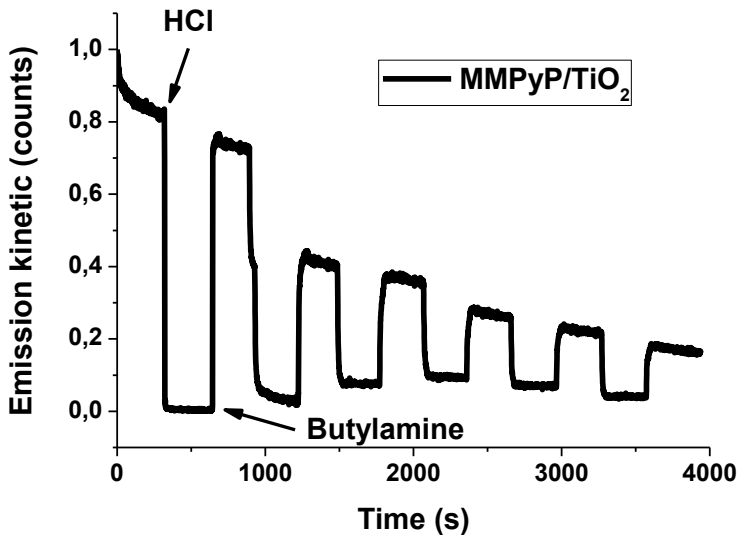

Figure 8.- Kinetic response of the composite MMPyP/TiO_2 to saturated vapour of butylamine.

In order to get better understanding of this lost of emission intensity in the successive cycles of response/recovery infrared spectroscopy was employed. Figure 9

shows a series of specular reflectance FT-IR spectra performed on both composites after alternate exposures to hydrogen chloride and ammonia vapors. The spectra in both panels were measured just after each exposure from bottom to top. In this way, the bottom spectrum in each case corresponds to the non-exposed film (deprotonated form of the porphyrin).

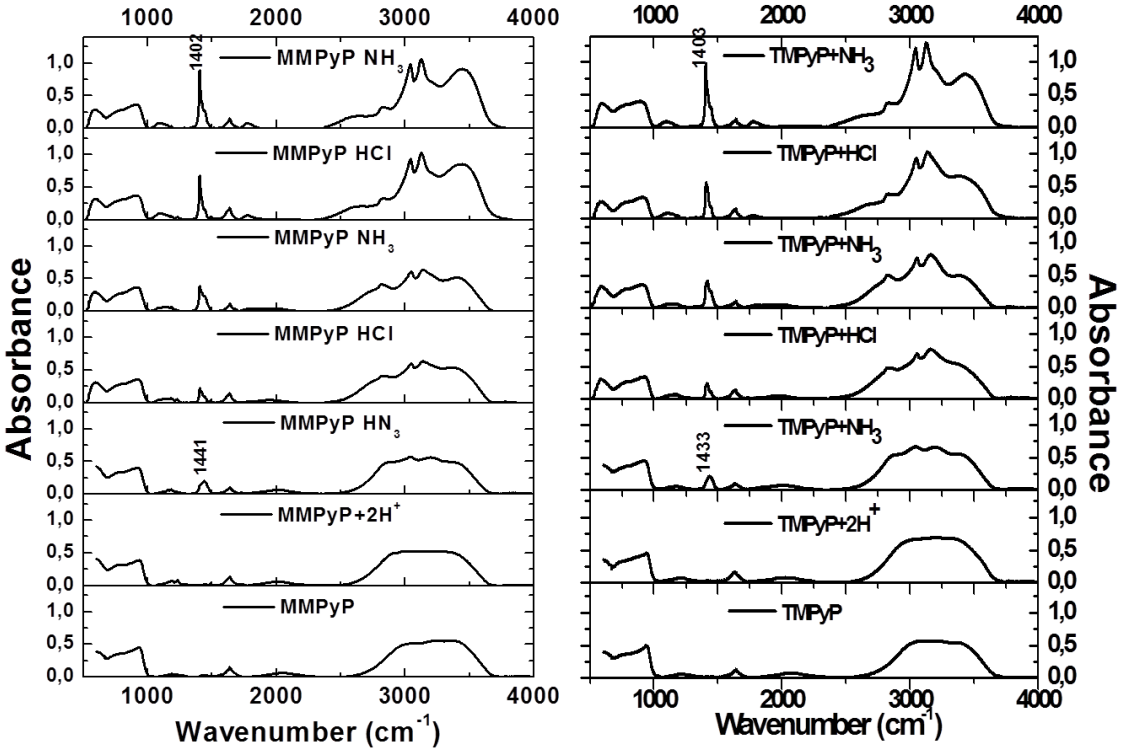

Figure 9.- Infrared spectra of the composites MMPyP/TiO_2 (left) and TMPyP/TiO_2 (right).

As can be seen, both composited show a similar behaviour with the appearance of a peak at 1441 cm^{-1} for MMPyP/TiO_2 and 1433 cm^{-1} for TMPyP/TiO_2 after the first completed cycle of exposure to HCl and NH_3 (third spectrum from bottom). Jacox et al. assigned this peak to a deformation of the ammonium ion[52], in good agreement with the National Institute of Standard and Technologies (NIST). Moreover, this peak invariably grows after each new exposure to both gases and is slightly shifted to shorter wavenumbers. In particular, , it is located at 1402 cm^{-1} for MMPyP/TiO_2 and 1403 cm^{-1} for TMPyP/TiO_2 after three completed cycles. Also, new peaks appeared in the 2500-4000 cm^{-1}range that can be also assigned to the presence of NH_4^+ ions in aqueous environment [53], In order to ensure this band assignment we also measured the spectrum of ammonium chloride as shown in the supporting information (see supporting information figure S3). This result clearly reveals the formation of ammonium chloride crystals inside the film under successive exposure to HCl and NH_3.

The initial peak with the wavenumber 1441 cm^{-1} for MMPyP/TiO_2 and 1433 cm^{-1} for TMPyP/TiO_2 present a shift respect the NIST of 1.5 cm^{-1} for MMPyP/TiO_2 and 9.5 cm^{-1} for TMPyP/TiO_2 suggest more amount of chloride to form ammonium chloride is retained in TMPyP/TiO_2 being hazardous for the sensor.

All this study can be followed with UV-Vis spectroscopies, but in the different cycles, the composites lost the base line due to the dispersion of the light induced for the ammonium chloride retained in the inner of the matrix.

4.- Conclusions

Two N-methyl 4-pyridyl cationic porphyrins have been anchored to microstructured columnar thin films of TiO_2 by electrostatic interaction and their sensing capability towards ammonia and amines has been investigated by following the emission changes of the protonated porphyrins in the presence of the gaseous analytes. Protonation of the porphyrins has been carried out by exposing the films to saturated HCl vapors with the typical changes in intensity and wavelength of the corresponding absorbance and emission spectra. Absorbance spectra of the unprotonated films also show some shifting and broadening of the Soret band with respect to solution which is indicative of intermolecular aggregation. These changes are however different for the two porphyrins with the monocationic derivative showing J-aggregation while the tetracationic exhibits some degree of H-aggregation. These differences have found to be consistent with the molecular structure of two porphyrins. In this way, MMPyP is anchored to the TiO_2 matrix with its only cationic peripheral group giving rise to a perpendicular arrangement with respect to oxide surface. On the other hand, TMPyP interacts with the matrix with its four positive charges being more probable a parallel orientation with respect to the TiO_2 surface with a second porphyrin molecule being anchored to the oxide on top of the first one. These different arrangements produce slipped aggregates (J-aggregation) in the case of MMPyP and face to face interaction (H-aggregates) in the case of TMPyP.

The two composite films were exposed to different concentrations of ammonia and butylamine vapors after previous protonation of the porphyrins. Both films showed significant emission changes in the presence of concentrated analytes, however the monocationic derivative exhibited a much faster response and lower detection limit. This behaviour has been associated to the different arrangement of the two porphyrins in the microcolumnar film. In this way, the more available ring of the monocationic derivative with its only anchoring point allows easier and faster interaction with analytes.

Finally, the repeatability of the sensor was investigated by performing consecutive exposure-recovery cycles with a significant loss of fluorescence emission intensity. Specular reflectance FT-IR revealed the formation of ammonium salts inside the films after complete cycles of exposure to HCl and analyte which has been found to

be responsible for the progressive lost of intensity in the successive cycles, mainly due to light dispersion phenomena.

Acknowledgements

We thank the Junta de Andalucía (projects: TEP8067 and FQM-2310) and the Spanish Ministry of Economy and Competitiveness (projects: MAT2013-40852-R, TEC2010-21830-C02-01, and RECUPERA 2020), and DEOLEO for financial support.

5.- Supporting information

S1.- Emission fluorescence response of MMPyP/TiO_2 composite to different volatiles of amines.

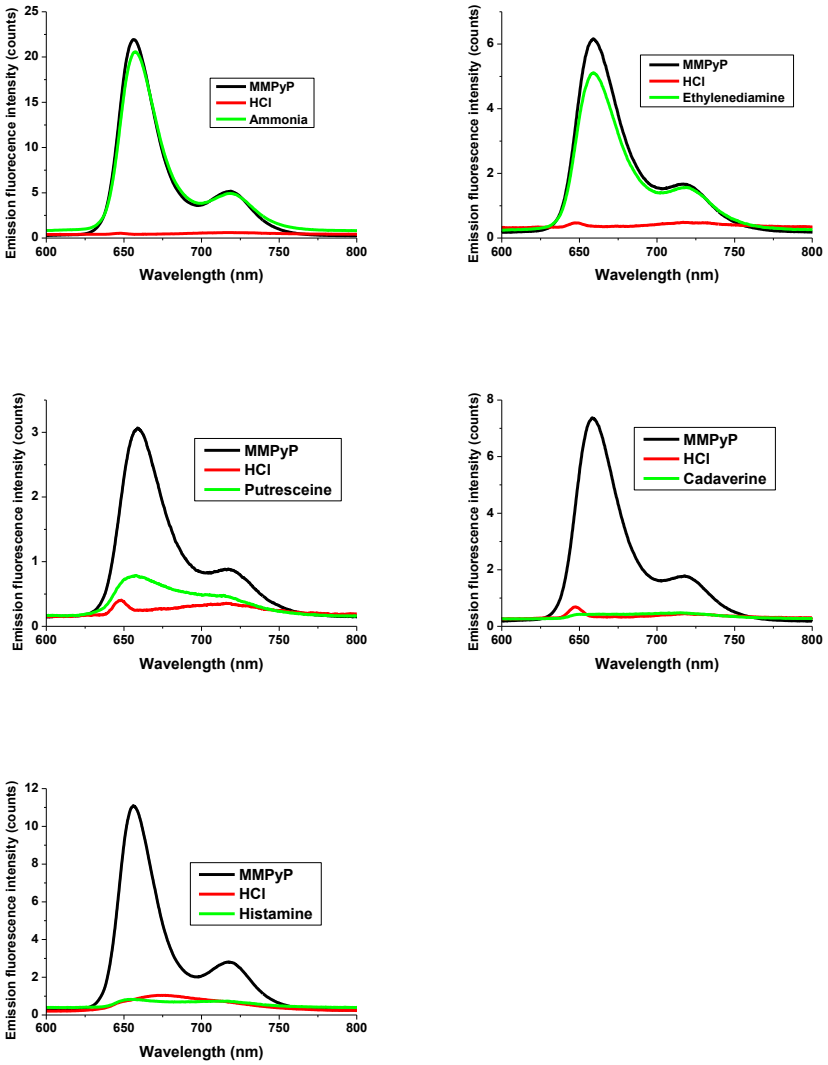

Figure S1- Emission fluorescence spectra of one cycle of protonation with HCl and detection of ammonia or amines by MMPyP/TiO_2 composite.

S2.- Response of MMPyP/TiO_2 composite to 600ppm of ammonia in Nitrogen. It can see in figure S2.1 the dramatic loser of emission fluorescent intensity with the different cycles of exposure to ammonia gas.

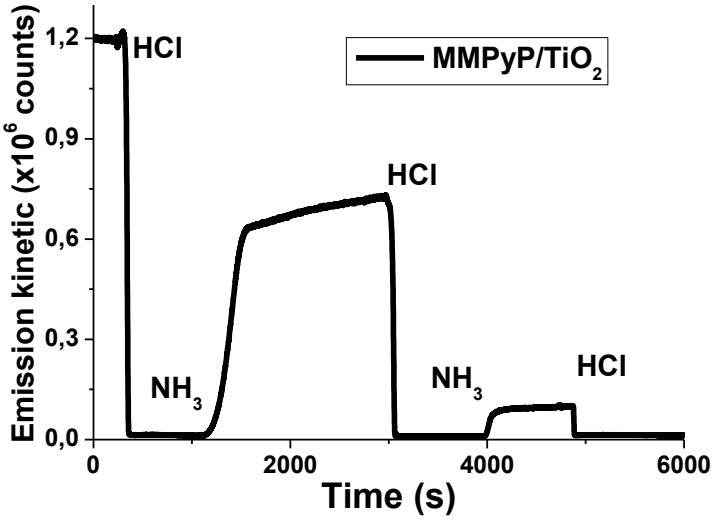

Figure S2.1- Two cycles of protonation with HCl and detection of 600 ppm of ammonia of MMPyP/TiO_2 composite.

Emission fluorescence spectra of MMPyP/TiO_2 composite measured after eight cycles of protonation and recovery with ammonia. It can see the loser of emission fluorescent intensity with the different cycles of exposure to ammonia gas in figure S2.2.

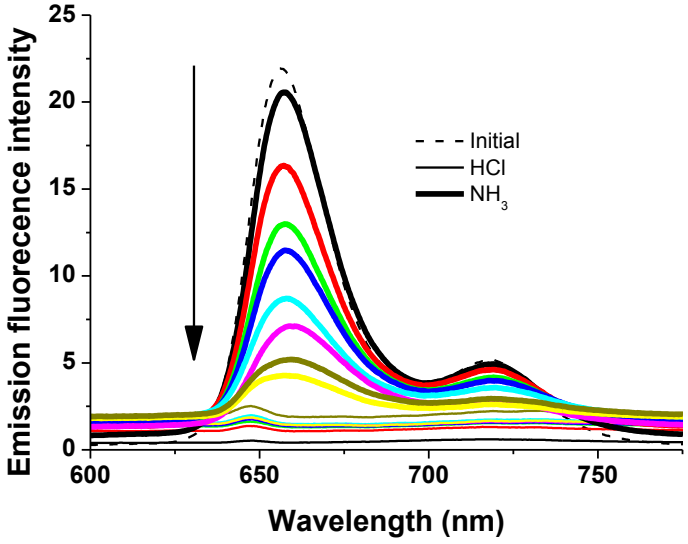

Figure S2.2.- Eight cycles of protonation with HCl and detection of ammonia of MMPyP/TiO_2 composite.

S3.- Infrared spectra of the composites after three cycles of protonation with HCl and deprotonation of the porphyrin with ammonia gas. Chloride ammonium infrared spectrum is included for comparation.

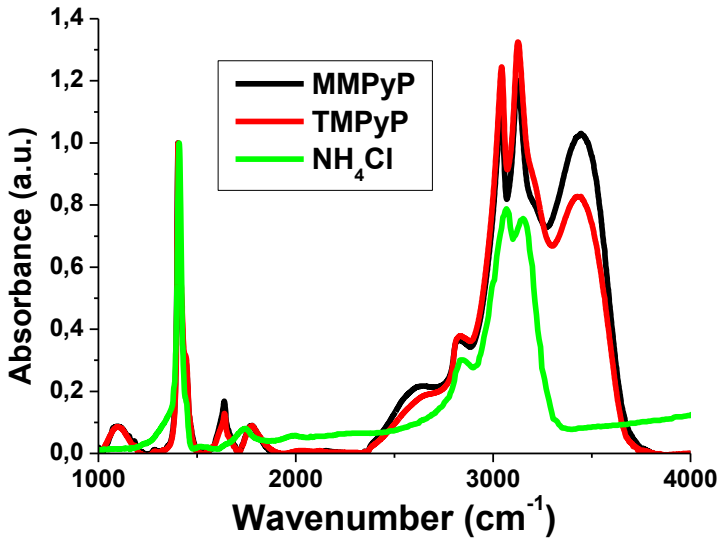

Figure S3.- Infrared spectra of MMPyP/TiO_2 (black line) and TMPyP/TiO_2 (red line) composites after three cycles of protonation with HCl and detection of ammonia, chloride ammonium infrared spectrum (green Line) is included for Comparison.

Chloride ammonium infrared spectrum is well suited to the composites. The peak in 1636 cm^{-1} corresponds to the porphyrins[54] and the peak in 3500 cm-1 corresponds to water environment[53].

REFERENCIAS

1. Erisman, J.W., et al., *Instrument development and application in studies and monitoring of ambient ammonia.* Atmospheric Environment, 2001. **35**(11): p. 1913-1922.
2. Mount, G.H., et al., *Measurement of atmospheric ammonia at a dairy using differential optical absorption spectroscopy in the mid-ultraviolet.* Atmospheric Environment, 2002. **36**(11): p. 1799-1810.
3. Close, L., F.I. Catlin, and A.M. Cohn, *ACute and chronic effects of ammonia burns of the respiratory tract.* Archives of Otolaryngology, 1980. **106**(3): p. 151-158.
4. Durbin, T.D., et al., *Estimates of the emission rates of ammonia from light-duty vehicles using standard chassis dynamometer test cycles.* Atmospheric Environment, 2002. **36**(9): p. 1475-1482.
5. Moos, R., et al., *Selective ammonia exhaust gas sensor for automotive applications.* Sensors and Actuators B: Chemical, 2002. **83**(1–3): p. 181-189.
6. de la Hoz, R.E., D.P. Schlueter, and W.N. Rom, *Chronic lung disease secondary to ammonia inhalation injury: A report on three cases.* American Journal of Industrial Medicine, 1996. **29**(2): p. 209-214.
7. Lee, S.-W., et al., *Nanoassembled Thin Film Gas Sensors. III. Sensitive Detection of Amine Odors Using TiO2/Poly(acrylic acid) Ultrathin Film Quartz Crystal Microbalance Sensors.* Analytical Chemistry, 2010. **82**(6): p. 2228-2236.
8. Ament, W., et al., *Respiratory ammonia output and blood ammonia concentration during incremental exercise.* Int J Sports Med, 1999. **20**(2): p. 71-7.
9. Kearney, D.J., T. Hubbard, and D. Putnam, *Breath ammonia measurement in Helicobacter pylori infection.* Dig Dis Sci, 2002. **47**(11): p. 2523-30.
10. A. Pacquit, K.C., D. Diamond, *Smart Packag. Technol. Fast Mov. Consum. Goods*, in *Smart Packag. Technol. Fast Mov. Consum. Goods*, P.B. J. Kerry, Editor. 2008, John Wiley & Sons Ltd. p. 75–98.
11. S. A. Hogan, J.P.K., *Smart Packag. Technol. Fast Mov. Consum. Goods*, ed. P.B. J. Kerry. 2008: John Wiley & Sons Ltd.
12. Puligundla, P., J. Jung, and S. Ko, *Carbon dioxide sensors for intelligent food packaging applications.* Food Control, 2012. **25**(1): p. 328-333.
13. Zakrzewska, K., *Mixed oxides as gas sensors.* Thin Solid Films, 2001. **391**(2): p. 229-238.
14. Kanan, S., et al., *Semiconducting Metal Oxide Based Sensors for Selective Gas Pollutant Detection.* Sensors, 2009. **9**(10): p. 8158-8196.

15. Fine, G.F., et al., *Metal Oxide Semi-Conductor Gas Sensors in Environmental Monitoring.* Sensors, 2010. **10**(6): p. 5469-5502.
16. Gao, T., E.S. Tillman, and N.S. Lewis, *Detection and Classification of Volatile Organic Amines and Carboxylic Acids Using Arrays of Carbon Black-Dendrimer Composite Vapor Detectors.* Chemistry of Materials, 2005. **17**(11): p. 2904-2911.
17. Lobnik, A., et al. *Sol-gel based optical chemical sensors*. 2011.
18. Wilson, A. and M. Baietto, *Applications and Advances in Electronic-Nose Technologies.* Sensors, 2009. **9**(7): p. 5099-5148.
19. Wang, Y., G.A. Sotzing, and R.A. Weiss, *Conductive Polymer Foams as Sensors for Volatile Amines.* Chemistry of Materials, 2002. **15**(2): p. 375-377.
20. Stumpel, J.E., et al., *An Optical Sensor for Volatile Amines Based on an Inkjet-Printed, Hydrogen-Bonded, Cholesteric Liquid Crystalline Film.* Advanced Optical Materials, 2014. **2**(5): p. 459-464.
21. Sberveglieri, G., *Recent developments in semiconducting thin-film gas sensors.* Sensors and Actuators B: Chemical, 1995. **23**(2–3): p. 103-109.
22. Imawan, C., et al., *Gas-sensing characteristics of modified-MoO3 thin films using Ti-overlayers for NH3 gas sensors.* Sensors and Actuators B: Chemical, 2000. **64**(1–3): p. 193-197.
23. Clifford, P.K. and D.T. Tuma, *Characteristics of semiconductor gas sensors I. Steady state gas response.* Sensors and Actuators, 1982. **3**(0): p. 233-254.
24. Xu, C.N., et al., *Selective detection of NH3 over NO in combustion exhausts by using Au and MoO3 doubly promoted WO3 element.* Sensors and Actuators B: Chemical, 2000. **65**(1–3): p. 163-165.
25. Pedrosa, J.M.a., et al., *The optical gas-sensing properties of an asymmetrically substituted porphyrin.* Journal of Materials Chemistry, 2002. **12**(9): p. 2659-2664.
26. Chu, C.-S., Y.-L. Lo, and T.-W. Sung, *Review on recent developments of fluorescent oxygen and carbon dioxide optical fiber sensors.* Photonic Sensors, 2011. **1**(3): p. 234-250.
27. Rakow, N.A. and K.S. Suslick, *A colorimetric sensor array for odour visualization.* Nature, 2000. **406**(6797): p. 710-713.
28. Roales, J., et al., *Anchoring effect on (tetra)carboxyphenyl porphyrin/TiO2 composite films for VOC optical detection.* RSC Advances, 2014. **4**(4): p. 1974-1981.
29. Lackner, M., *TUNABLE DIODE LASER ABSORPTION SPECTROSCOPY (TDLAS) IN THE PROCESS INDUSTRIES – A REVIEW*, in *Reviews in Chemical Engineering*. 2007. p. 65.

30. Pedrosa, J.M., et al., *Characterization and fast optical response to NO2 of porphyrin LB films.* Materials Science and Engineering: C, 2002. **22**(2): p. 433-438.
31. Roales, J., et al., *Optimization of mixed Langmuir–Blodgett films of a water insoluble porphyrin in a calixarene matrix for optical gas sensing.* Thin Solid Films, 2011. **519**(6): p. 2025-2030.
32. Nurul Huda Yusoff, M.M.S., Muhammad Yahaya *Room Temperature Fluorescence Gas Sensor Based on Coated TiO2 Nanoparticles.* Key Engineering Materials, 2013. **543**: p. 373-376.
33. Milgrom, L.R., *The Colours of Life*. 1997, OUP, Oxford.
34. Stevens, N. and D.L. Akins, *Dye-doped inorganic/organic composite films as fluorescence sensors for methanol vapor.* Sensors and Actuators B: Chemical, 2007. **123**(1): p. 59-64.
35. Germain, M.E. and M.J. Knapp, *Optical explosives detection: from color changes to fluorescence turn-on.* Chemical Society Reviews, 2009. **38**(9): p. 2543-2555.
36. Castillero, P., et al., *Active and optically transparent tetracationic porphyrin/TiO(2) composite thin films.* ACS Appl Mater Interfaces, 2010. **2**(3): p. 712-21.
37. Cano, M., et al., *A transparent TMPyP/TiO2 composite thin film as an HCl sensitive optochemical gas sensor.* Sensors and Actuators B: Chemical, 2010. **150**(2): p. 764-769.
38. Rico, V., et al., *Wetting Angles on Illuminated Ta2O5 Thin Films with Controlled Nanostructure.* The Journal of Physical Chemistry C, 2009. **113**(9): p. 3775-3784.
39. Sánchez-Valencia, J.R., et al., *Preillumination of TiO2 and Ta2O5 Photoactive Thin Films As a Tool to Tailor the Synthesis of Composite Materials.* Langmuir, 2008. **24**(17): p. 9460-9469.
40. McRae, E.G. and M. Kasha, *Enhancement of Phosphorescence Ability upon Aggregation of Dye Molecules.* The Journal of Chemical Physics, 1958. **28**(4): p. 721-722.
41. McRae, E.G. and M. Kasha, *Physical Processes in Radiation Biology*, ed. A. Press. 1958, New York.
42. Czikklely, V., H.D. Forsterling, and H. Kuhn, *Extended dipole model for aggregates of dye molecules.* Chemical Physics Letters, 1970. **6**(3): p. 207-210.
43. Hans Kuhn, H.-D.F., David H. Waldeck, *Principles of Physical Chemistry, 2nd Edition*. 2009. p. 1084.
44. Czikkely, V., H.D. Försterling, and H. Kuhn, *Light absorption and structure of aggregates of dye molecules.* Chemical Physics Letters, 1970. **6**(1): p. 11-14.

45. Evans, C.E., Q. Song, and P.W. Bohn, *Influence of molecular orientation and proximity on spectroscopic line shape in organic monolayers.* The Journal of Physical Chemistry, 1993. **97**(47): p. 12302-12308.

46. Kuhn, H., *π-Electron systems — building blocks of supramolecular machines.* Colloids and Surfaces A: Physicochemical and Engineering Aspects, 2000. **171**(1–3): p. 3-12.

47. Pedrosa, J.M., et al., *Influence of Molecular Organization of Asymmetrically Substituted Porphyrins on Their Response to NO2 Gas.* Langmuir, 2002. **18**(20): p. 7594-7601.

48. Šišková, K., B. Vlčková, and P. Mojzeš, *Spectral detection of J-aggregates of cationic porphyrin and investigation of conditions of their formation.* Journal of Molecular Structure, 2005. **744–747**(0): p. 265-272.

49. Ma Pedrosa, J., et al., *Determination of porphyrin dimer in a mixed monolayer of porphyrin/phospholipid transferred on ITO electrodes.* Electrochemistry Communications, 2000. **2**(4): p. 276-280.

50. Franco, R., S. Al-Karadaghi, and G.C. Ferreira, *Resonance Raman Spectroscopic Examination of Ferrochelatase-induced Porphyrin Distortion.* J Porphyr Phthalocyanines, 2011. **15**(5): p. 357-363.

51. Spellane, P.J., et al., *Porphyrins. 40. Electronic spectra and four-orbital energies of free-base, zinc, copper, and palladium tetrakis(perfluorophenyl)porphyrins.* Inorganic Chemistry, 1980. **19**(2): p. 386-391.

52. Jacox, M.E. and W.E. Thompson, *Infrared spectrum of the NH4-d(n)+ cation trapped in solid neon.* Phys Chem Chem Phys, 2005. **7**(5): p. 768-75.

53. Max, J.-J. and C. Chapados, *Aqueous ammonia and ammonium chloride hydrates: Principal infrared spectra.* Journal of Molecular Structure, 2013. **1046**(0): p. 124-135.

54. Craven, C.W., K.R. Reissmann, and H.I. Chinn, *Infrared Absorption Spectra of Porphyrins.* Analytical Chemistry, 1952. **24**(7): p. 1214-1215.

General conclusions

General conclusions

In this work, we have investigated the infiltration process of TMPyP molecules within very porous but optically transparent TiO_2 thin films prepared by GLAD-PVD. The total porosity of these films and their pore size distribution has been assessed by measuring water adsorption isotherms. Because the prepared composite films did not disperse the light, they are deemed appropriate for their implementation in optical and photonic devices. In comparison with polymers and other similar matrixes, where processes like deformation and swelling may occur on exposure to certain analytes, advantages of our films are their robustness and the fact that their initial state can be recovered by pumping and/or heating at moderate temperatures.

The incorporation process of the porphyrin dye, consisting of the infiltration of the dye molecules from an aqueous solution, was highly dependent on the pH and can be explained by using the PZC concepts used to account for the evolution of the surface charge on oxide suspensions. The incorporation process can be described according to the Langmuir adsorption model, whereas the kinetics of incorporation follows an Elovich equation. This description of the equilibrium and kinetics of the adsorption discards that diffusion plays a significant role in limiting the accessibility of the TMPyP molecules to the voids of the thin film, and that the number of adsorption sites is the controlling factor of the infiltration process at each pH.

The optical properties of the composite TMPyP/TiO_2 thin films have been investigated by absorption and fluorescence spectroscopies. Although the actual state of the molecules within the films has not been unraveled yet, the assessment of these spectra confirm a tight interaction of the molecule, very likely in the form of monomer, with the surface of the TiO_2, although the formation of J-dimers cannot be excluded. The easy accessibility of gases to all dye molecules and the reversibility of the process in a preliminary experiment consisting of the exposure of the composite films to acid vapors suggests that these types of optically active thin films are potentially good materials to develop into optical gas sensors.

The sensitivity of TMPyP to HCl vapour has been demonstrated through UV-visible spectroscopy. A new TMPyP/TiO_2 composite film has been developed for HCl

gas detection. TMPyP can be used both in solution and within a composite thin film. The inclusion of the TMPyP in the composite entails a remarkable improvement in the solid state sensor, such as fast response, long-term stability and a low surface concentration of the used porphyrin compared to other previously researched systems

Two N-methyl 4-pyridyl cationic porphyrins have been anchored to microstructured columnar thin films of TiO_2 by electrostatic interaction and their sensing capability towards ammonia and amines has been investigated by following the emission changes of the protonated porphyrins in the presence of the gaseous analytes. Protonation of the porphyrins has been carried out by exposing the films to saturated HCl vapors with the typical changes in intensity and wavelength of the corresponding absorbance and emission spectra. Absorbance spectra of the unprotonated films also show some shifting and broadening of the Soret band with respect to solution which is indicative of intermolecular aggregation. These changes are however different for the two porphyrins with the monocationic derivative showing J-aggregation while the tetracationic exhibits some degree of H-aggregation. These differences have found to be consistent with the molecular structure of two porphyrins. In this way, MMPyP is anchored to the TiO_2 matrix with its only cationic peripheral group giving rise to a perpendicular arrangement with respect to oxide surface. On the other hand, TMPyP interacts with the matrix with its four positive charges being more probable a parallel orientation with respect to the TiO_2 surface with a second porphyrin molecule being anchored to the oxide on top of the first one. These different arrangements produce slipped aggregates (J-aggregation) in the case of MMPyP and face to face interaction (H-aggregates) in the case of TMPyP.

The two composite films were exposed to different concentrations of ammonia and butylamine vapors after previous protonation of the porphyrins. Both films showed significant emission changes in the presence of concentrated analytes, however the monocationic derivative exhibited a much faster response and lower detection limit. This behaviour has been associated to the different arrangement of the two porphyrins in the microcolumnar film. In this way, the more available ring of the monocationic derivative with its only anchoring point allows easier and faster interaction with analytes.

Finally, the repeatability of the sensor was investigated by performing consecutive exposure-recovery cycles with a significant loss of fluorescence emission intensity. Specular reflectance FT-IR revealed the formation of ammonium salts inside the films after complete cycles of exposure to HCl and analyte which has been found to be responsible for the progressive lost of intensity in the successive cycles, mainly due to light dispersion phenomena.